Ollscoil na hÉireann, Corcaigh

National University of Ireland, Cork

Vapour-Phase Passivation of Ge(100) using Alkanethiols for Future CMOS Devices

Thesis presented by

Shane Garvey, B.Sc (Hons)

for the degree of

Doctor of Philosophy

University College Cork

School of Chemistry

Head of School: Dr. Humphrey Moynihan

Supervisors: Dr. Brenda Long & Prof. Justin D. Holmes

2021

Table of Contents

Declaration

I, Shane Garvey, certify that the work I am submitting is my own and has not been submitted for another degree, either at University College Cork or elsewhere. All external references and sources are clearly acknowledged and identified within the contents. I have read and understood the regulations of University College Cork concerning plagiarism.

_____

Shane Garvey

Abstract

The First Industrial Revolution, facilitated by the steam engine, transformed agrarian economies into ones dominated by industry and machine manufacturing. With the advent of the internal combustion engine in the late 19th century, the Second Industrial Revolution began, enabling the mass production of goods. Computers powered by microchips instigated the Third Industrial Revolution, which has been roaring since the second half of the 20th century. We now stand at the precipice of the Fourth Industrial Revolution, still powered by computers. Industry 4.0, as it is known, is characterised by automation, the internet of things, cloud computing and artificial intelligence. As the population of the world approaches 8 billion people in 2021, equipped with high-performance computers and a sense of hope, we have set our sights on the most complex problems facing humanity, problems such as climate change, pandemics, food and water shortages, drought and even interplanetary travel. The microprocessor has played a central role in the rapid development of modern technologies since it began to be widely used in the latter part of the 20th century and it will continue to play this role as we tackle the problems mentioned. Silicon has served as the bedrock of modern microprocessors and has, for many years, supported the trend known as Moore's Law. Moore's Law holds that the number of transistors in an integrated circuit (IC) doubles roughly every two years. Initially, Moore's Law was facilitated by the miniaturisation of the Si transistor. A smaller transistor footprint allowed for more to be contained in an IC, increasing the processing power. However, continued device-scaling has resulted in material and architectural limitations being reached. In an effort to keep pace with the technological demands of modernity, the use of novel materials and device architectures are being adopted to improve device

performance. Germanium has long been considered a viable candidate for use in modern processors and has seen some inclusion in the form of SiGe alloys used as the channel material in CMOS devices. With that said, before 100% Ge gains widespread industry acceptance, there are certain issues, mostly to do with its oxide, that must be overcome. This thesis aims to highlight key advancements that have been made in relation to the passivation of Ge(100) surfaces such that Ge becomes a viable material for inclusion in modern CMOS devices.

Chapter 1 serves as an introduction to the work presented in this thesis. Key concepts such as the structure and properties of Ge(100) surfaces are outlined to highlight why Ge is seriously being considered as a future channel material for CMOS devices. An in-depth review of literature on Ge passivation is included also in an effort to set the foundation for and highlight the significance of the work that follows in the coming chapters.

Chapter 2 details the characterisation methods that are used to probe the Ge(100) surfaces that are discussed in Chapters 3, 4 and 5. Since XPS is the characterisation method most used throughout this body of work, particular attention is given to it. WCA and AFM are introduced also; however, since they serve as complementary characterisation methods, only a brief introduction is presented. DFT analysis performed by Dr. Barbara Maccioni and Dr. Michael Nolan is presented in this chapter also; however, a more detailed discussion of how the DFT simulations are used to help elucidate the behaviour of Ge-SAM systems can be found in the work chapters in which they are implemented.

Chapter 3 discusses the method developed to achieve thiol-SAM passivation of Ge(100) surfaces using a novel vapour-phase approach. This method improves on

the current state-of-the-art by reducing the time required to form stable alkanethiol-SAMs on Ge(100) from 24 hours to ~200 minutes while still forming SAMs that inhibit reoxidation of the Ge for up to 1 week. Many of the vapour-phase passivation methods for Ge that are found in the literature rely on the use of high-vacuum. That is not the case for the novel process developed and documented in this chapter. Ultimately, the vapour-phase passivation method serves as the foundation for the remainder of the work presented in this thesis since it provided a reliable and reproducible method for Ge passivation. Thus, this process appears in both chapters 4 and 5 also.

Chapter 4 highlights the significant effect humidity in air has on the longevity of thiol-SAMs on Ge(100) surfaces. Although the thiol-SAM-passivated Ge surfaces that are prepared exhibit resistance to reoxidation, upon exposure to ambient conditions, reoxidation of the Ge does eventually occur. Thus, a natural progression from Chapter 1 is to determine what factors are significant in the reoxidation of Ge and the destruction of the passivating SAM. SAMs of different thiol molecules, prepared by both vapour- and liquid-phase passivation methods are prepared and exposure to various levels of humidity at constant temperature to elucidate what effect, if any, humidity in air has on the reoxidation of thiol-SAM-passivated Ge. It is found that irrespective of the passivating thiol molecule and the method used to achieve passivation, reoxidation of the Ge trends with relative humidity. DFT simulations are presented which help elucidate how water molecules interact with the SAM-Ge system and potential mechanisms for the reoxidation of the Ge and the loss of the SAM are outlined.

Chapter 5 explores what effect the length of the passivating alkanethiol molecule has on the stability of the SAM and the reoxidation of the Ge upon exposure

to ambient conditions. Only alkanethiol molecules with an even number of $-CH_2$ units in the C backbone are selected for the study to ensure parity-related effects are avoided. Thiol chain length is found to be an important factor in the stability of the SAM since long-chain thiols inhibit reoxidation of the Ge more effectively than their shorter-chain counterparts. With that said, SAMs comprised of short-chain thiol molecules, such as 1-butanethiol, still inhibit Ge reoxidation albeit less effectively than long-chain thiols such as 1-dodecanethiol.

Finally, Chapter 6 presents the conclusions made and provides an outlook on future prospects.

List of Commonly used Abbreviations

2D	Two-Dimensional
3D	Three-Dimensional
AFM	Atomic Force Microscopy
ALD	Atomic Layer Deposition
ARXPS	Angle-Resolved X-Ray Photoelectron Spectroscopy
BT	1-Butanethiol
CMOS	Complimentary Metal-Oxide-Semiconductor
CVD	Chemical Vapour Deposition
DFT	Density Functional Theory
DT/ DDT	1-Dodecanethiol
EAL	Effective Attenuation Length
EOT	Effective Oxide Thickness
ET	Ethanethiol
FET	Field-Effect Transistor
FinFET	Fin Field-Effect Transistor
GAA	Gate-All-Around
GeOI	Germanium-On-Insulator
GGA	Generalised Gradient Approximation
HCl	Hydrochloric Acid
HF	Hydrofluoric Acid
HT	1-Hexanethiol
IMFP	Inelastic Mean-Free Path

IC	Integrated Circuit
IPA	Isopropyl Alcohol
IRDS™	International Roadmap for Devices and Systems
MD	Molecular Dynamics
MEM	Microelectromechanical
MOCVD	Metal-Organic Chemical Vapour Deposition
MOS	Metal-Oxide-Semiconductor
MOSFET	Metal-Oxide-Semiconductor Field-Effect Transistor
MOVPE	Metal-Organic Vapour-Phase Epitaxy
NEM	Nanoelectromechanical
NIST	National Institute of Standards and Technology
nMOS	n-Channel MOSFET
NW	Nanowire
OT	1-Octanethiol
PBE	Perdew-Burke-Ernzerhof
pMOS	p-Channel MOSFET
PVD	Physical Vapour Deposition
RF	Radio Frequency
RH	Relative Humidity
RMS	Root Mean Square
SPM	Scanning Probe Microscopy
SAM	Self-Assembled Monolayer
sccm	Standard Cubic Centimetre per Minute
SEM	Scanning Electron Microscopy

SOI	Silicon-On-Insulator
UHV	Ultra-High Vacuum
ULSI	Ultra Large-Scale Integration
UV	Ultraviolet
VASP	Vienna Ab Initio Software Package
vdW	van der Waals
VLSI	Very Large-Scale Integration
WCA	Water Contact Analysis
XPS	X-Ray Photoelectron Spectroscopy

Acknowledgements

My PhD was not confined to one part of the UCC campus or the Tyndall National Institute. In fact, for a time, before I bought my bike, I thought I should devote a chapter of my PhD to walking as I was always on the move from one lab or office to another. Only now, as I look back, do I realise that this aspect of my PhD is one that I am grateful for since it allowed me to meet many brilliant academics and students, to whom I must express my gratitude.

Firstly, in the Kane Building and the home of the Materials Chemistry and Analysis Group (MCAG), thank you to my supervisor Dr. Brenda Long, who believed in my ability and who gave me the creative freedom and independence to explore the ideas that interested me. Thank you to Prof. Justin Holmes, the group head, for offering his sage advice along the way over cups of coffee on campus – not one of which I pay for. Thank you to Dr. Noel Kennedy, Eadaoin Casey, Will Daly, Adria Garcia, Alex Game, Alex Lonergan, Patrick Murphy and the many others whose friendship and support were both needed and enjoyed. Thank you to the Kane building staff for facilitating students in achieving their research goals.

At the Tyndall National Institute, thank you to Dr. Nikolay Petkov, Dr. Michael Nolan and Dr. Karim Cherkaoui whose extensive experience and knowledge helped me gain a broader perspective of the field of semiconductor development. Thank you to Dr. Ray Duffy for his continued support and encouragement. To Aidan Murphy, Ger O'Sullivan, Bobby Bornemann, Tim Daly, Dr. Emmanuele Galluccio,

Dedication

This is dedicated to my family and friends without whose encouragement and support, none of this would have been possible.

Ní neart go cur le chéile.

Chapter 1
Introduction

1.1   Background & Motivations

Soon after the invention of the integrated circuit (IC) in 1959 by Jack Kilby, a trend known as Moore's law has been observed. Moore's law states that the number of transistors on an integrated circuit approximately doubles every 18-24 months.[1] The continued scaling of the MOSFET according to Moore's Law has allowed for improved chip performance, decreased cost and reduced device switching power. It is on the back of this technological progress that the modern, connected world has been built. In recent decades, Moore's Law scaling of transistors has become increasingly difficult to maintain as device features scale below 10 nm. Not only are these features incredibly difficult to fabricate, but at such small dimensions, physical phenomena, such as electron tunnelling through the gate oxide, are hindering device performance.[2] In **Figure 1**, a traditional n-channel MOSFET structure with channel length 'L' is displayed. N-channel MOSFETs consist of drain and source regions that are heavily doped n^+ and a p-type substrate. When a positive voltage is applied to the gate, the holes in the area under the gate oxide are repelled down into the substrate and electrons are attracted from the source and drain into the channel. When a voltage is applied between the source and the drain, current flows through the channel. For the successful operation of the device, it is essential that the gate oxide (orange) electrically isolates the gate from the channel; otherwise, the aforementioned tunnelling issues render the device useless.
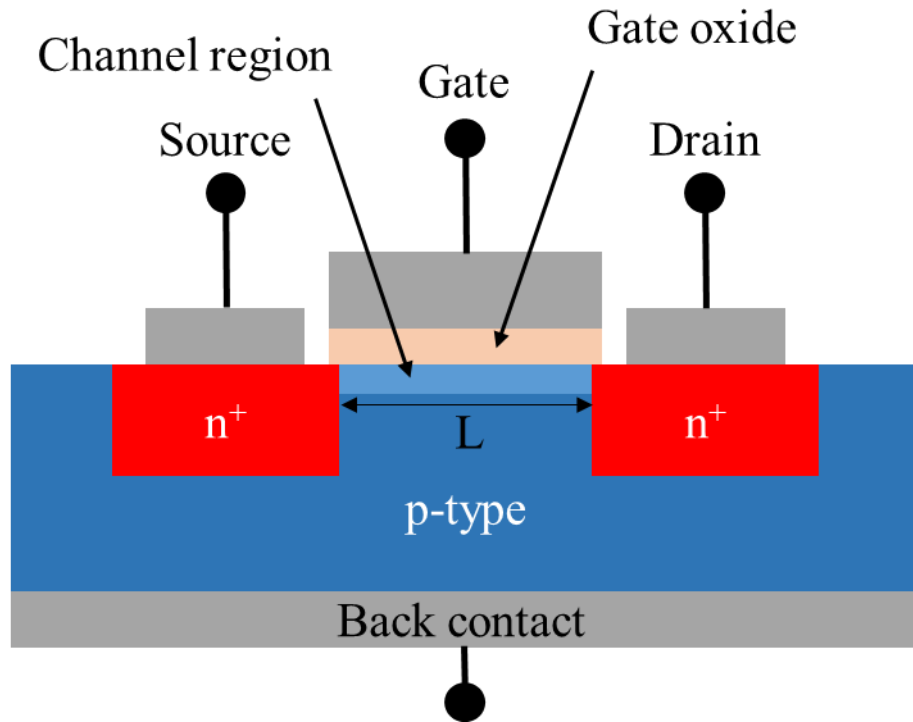
Figure 1. Traditional n-channel MOSFET structure with channel length 'L'.

Efforts to reduce the size of transistors is one that is not indefinitely possible – physical limitations exist and ultimately, we are restricted by the size of an atom. In an effort to maintain Moore's Law while circumventing the physical limitations that exist, devices with novel architectures and materials are being scrutinised. For instance, in place of planar structures, FinFET transistors [3] have been introduced and currently efforts are well underway to create the next generation of transistors using a gate-all-around (GAA) nanowire approach.[4, 5] These ingenious methods of manipulating the structure of transistors allow for 'More Moore' [6] without confronting the aforementioned issues associated with attempting to continue the miniaturisation method. The concept of 'More Moore' was first introduced in 2005 in a whitepaper released by The International Roadmap for Devices and Systems (IRDS™) committee. The term refers to the continuation of Moore's law by introducing novel materials and device architectures circumventing the issues

associated with the continued miniaturisation of devices. In 2020, the IRDS™ laid out a roadmap for the evolution of FET devices from the finFET in 2020 to lateral GAA FETs over the next decade to the 3D VLSI FET structures from 2030.
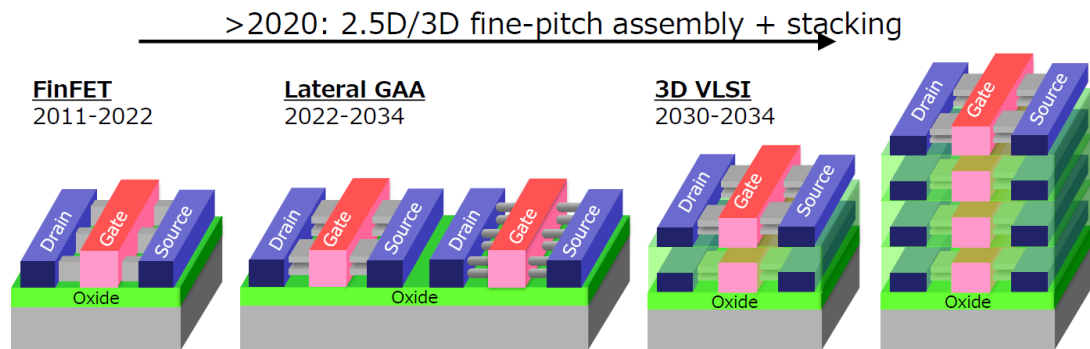
Figure 2. IRDS™ proposed evolution of FET structure.

One of the main focuses in the progression of FET architecture is to increase the amount of surface area of the channel that is in contact with the gate such that the control of the flow of charge carriers through the channel be maximised. This desire has led to taller fins, tri-gates and GAA architectures. Another motivation is to stack devices on top of each other in an effort to increase drive without also increasing the footprint of the device. In **Figure 2**, the predicted evolution of FET architecture from FinFETs to stacked lateral GAA FETs is displayed.

As well as novel architectures, new materials are being explored for next-generation complementary metal-oxide semiconductor (CMOS) devices also. To date, CMOS technology has relied on the properties of SiO_2 – its abundance,[7] mechanical strength [8] and the nature of the high quality interface between Si and SiO_2.[9] However, continued device scaling has rendered SiO_2 unfit for purpose as the gate oxide in MOSFET devices due to the current tunnelling through the dielectric.[10] The physical thickness of the gate oxide in transistors at the 65nm node and less is

lower than the limit for electron tunnelling (3nm) which results in leakage through the gate when the device is in the off-state. This renders the device useless and thus, novel materials with higher dielectric constants than that of SiO_2 have been utilised to allow for devices to be scaled beyond the 65nm node. High-κ dielectrics such as HfO_2, ZrO_2 and LaO_2 are currently being used in devices to mitigate this issue. These high-κ materials offer low equivalent oxide thickness (EOT) due to their high dielectric constant (κ) value. However, the use of high-κ dielectrics as gate oxides in Si devices is confronted with some serious issues. For one, scattering at interface charges limits the effective mobility of the transistor resulting in a low drive current, which negates having the high-κ dielectric in the first place.[11] Also, compared to SiO_2, the oxides deposited by metal organic chemical vapour deposition (MOCVD) or atomic layer deposition (ALD) are of significantly lower quality [12] and during high-κ deposition it is difficult to prevent the growth of an interfacial oxide layer between the silicon substrate and the high-κ dielectric. This switch to high-κ dielectrics has caused a shift in the current technological paradigm whereby the significance of the Si/SiO_2 interface and thus Si as the primary channel material has been negated. Over the past two decades, extensive research into alternative channel materials has been conducted.[13, 14] In **Table 1**, important material properties of semiconductors are shown. Germanium (Ge) has attracted interest as a channel material due to its high carrier mobility. Ge boasts electron (3900 $cm^2V^{-1}s^{-1}$) and hole (1900 $cm^2V^{-1}s^{-1}$) mobilities more than 2 and 4 times that of Si, respectively.[14]

Material→ Property↓	Si	Ge	GaAs	InAs	InP	InSb
Electron mobility ($cm^2V^{-1}s^{-1}$)	1400	3900	8500	40000	5400	77000
Hole mobility ($cm^2V^{-1}s^{-1}$)	450	1900	400	500	200	850
Bandgap (eV)	1.12	0.66	1.42	0.35	1.34	0.17
Lattice constant (Å)	5.431	5.658	5.653	6.058	5.869	6.749
Dielectric constant	11.7	16.2	12.9	15.2	12.5	16.8

Table 1. Properties of high mobility semiconductors.[14]

Although, from inspection of **Table 1** it may seem that other semiconductor candidates outperform Ge. For instance, InSb has an electron mobility 55 times greater than Si. However, the integration of Ge into current very large-scale integration (VLSI) lines seems more feasible than other potential channel materials such as the III-Vs since Ge can be processed in many of the same ways as Si and so many of the processes used in Si chip fabrication are also applicable to Ge. An often stated concern in relation to Ge is that its relative abundance is too low to support the semiconductor industry. Ge is less abundant than Si, which accounts for 27.7% of the Earth's crust (by weight) and is the second most common element behind only O – the only other constituent in the dielectric, SiO_2. The annual production of semiconductor Si is 7 million tonnes and the global reserves of Ge are estimated to be 2-3 thousand tonnes [15] so it is implausible to fathom a world where Ge replaces Si entirely. Nowhere in this work is it stated that Ge could or should completely replace Si as the cornerstone

of the semiconductor industry but rather a claim is made that Ge could be used in tandem with Si assisting us to maintain Moore's law to continue to meet the technological demands of modernity. Materials such as Ge-on-insulator (GeOI) provide opportunity whereby wafer-scale Ge can be processed without needing an entire Ge wafer – instead, a thin Ge film on the abundant SiO_2 is sufficient. High quality Ge films can also be grown epitaxially on Si to produce devices that are particularly useful in the field of optoelectronics.[16] Epitaxy refers to a type of crystal growth or material deposition whereby crystalline material is grown in one or more well-defined orientations with respect to the crystalline substrate the growth process is occurring on. In the case of epi-Ge, Ge is grown on Si. By introducing tensile strain when growing the films, the band gap shrinks enhancing the optoelectronic properties of Ge. Progress is constantly being made in the production of high-quality epi-Ge with fewer defects.[17] Using materials such GeOI and epi-Ge offer significant advantages over the use of bulk Ge such as reduced cost, increased mechanical strength and increased compatibility with existing Si processing equipment.

1.2   Structure of Ge

Ge, being the 32nd element on the periodic table, is in the same group as C and Si and thus exhibits many of the same properties as its Group IVA counterparts. For one, it has 4 valence electrons and so each Ge atom is fully saturated when it has 4 bonds. Thus, as is the case with Si and C (diamond), Ge is a covalent solid which crystallises into a cubic lattice structure with a lattice constant of 5.658 Å (**Figure 3(a)**).[18] If the Ge lattice is cut along a (100), (010), or (001) plane the surface atoms are left with two broken or dangling bonds. When prepared under vacuum, the crystallographic faces

of Ge that are thought to be the most industry useful (the (100) and (111) faces) reconstruct such that the surface geometry differs greatly from that of bulk material.[19] These reconstructions occur to minimise the energy of the surface. It is important to remember that the surface of any crystalline material can be thought of as a 'macro-defect' since the repeating crystallographic pattern is abruptly disrupted by the lack of more material and an interface with space or other materials is present instead. As a result of this, the properties at the surface differ greatly to the properties of the bulk. In an effort to reduce the number of dangling bonds at the surface from two to one, the Ge(100) surface reconstructs to form Ge dimers. In **Figure 3 (b)** and **(c)** asymmetric b(2x1) and c(4x2) reconstructed Ge(100) surfaces are shown and have been observed by scanning-tunnelling microscopy.[20] These dimers are often considered to be akin to a double bond containing both a σ and π bond. For Ge, the π bond is considerably weaker than that of a C=C bond found in alkenes and is buckled away from a symmetric configuration.
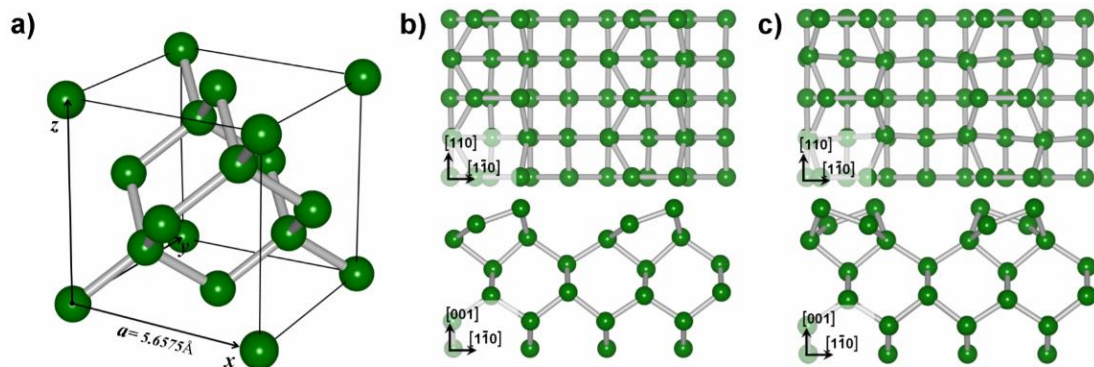
Figure 3. (a) Ball and Stick model of the Ge lattice structure. Ball and stick model of reconstructed Ge(100) with an asymmetric **(b)** b(2x1) and **(c)** c(4x2) reconstruction.[18]

1.3   Electronic Properties of Ge

Like pure Si, pure Ge is an intrinsic semiconductor with an indirect bandgap meaning the minimum energy of the conduction band has a different momentum to the maximum energy of the valence band and thus direct photon emission does not occur spontaneously. In semiconductors, the bandgap is small enough to allow electron transfer from the valence band to the conduction band upon excitation – perhaps from the sun in the case of photovoltaic cells (**Figure 4**). The excitation of the electron into the conduction band leaves a hole where the electron once was. An electron from an adjacent atom can fill that hole creating a chain-reaction of moving holes and electrons - an electric current.
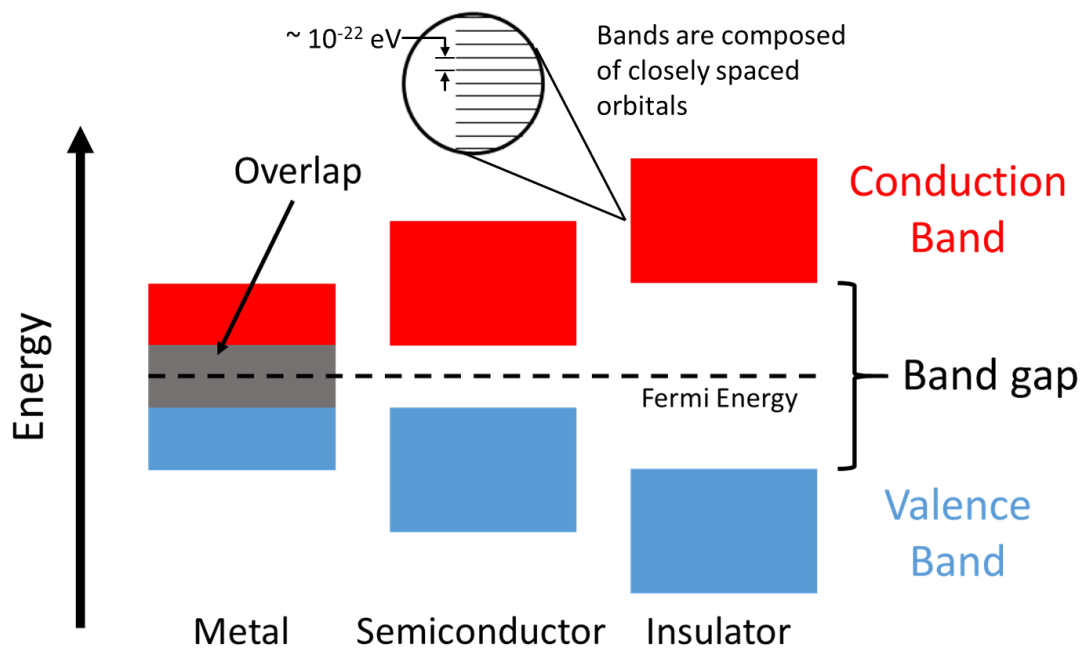
Figure 4. Band diagrams for metals, semiconductors and insulators showing difference in bandgap for each material type.

Doping is the intentional introduction of impurities into an intrinsic semiconductor with the purpose of augmenting the electrical, optical and/or structural

properties of the material. Once doped, the semiconductor is referred to as an extrinsic semiconductor. Doping semiconductors with impurity atoms can drastically increase the conductivity of the material. Ge can be doped negatively (introducing electrons) or positively (introducing holes) by incorporating impurity atoms in the Ge crystal structure. To achieve p-type Ge, the Ge crystal is doped with a trivalent element such as Ga, which increases the number of holes in the system. Doping in this way shifts the Fermi level of the material closer to the valence band. To achieve n-type Ge, the Ge crystal is doped with a pentavalent element such as P or Sb. Doping in this manor shifts the Fermi level of the material closer to the conduction band by introducing more electrons to the system. For Ge to be more widely incorporated into modern devices, some electronic issues must first be overcome. One of the issues relates to contacting n-type Ge with metals. A Schottky barrier forms when a metal and a semiconductor contact each other. Optimisation of Si transistors has made this barrier as thin as possible such that charge carriers can tunnel across it. Ge poses some interesting dilemmas when it comes to thinning the Schottky barrier since holes readily move from the metal into the Ge; however, the same is not true for electrons. The practical implication of this is that n-type Ge devices such as nFETs experience high electron resistance and heat loss. In an attempt to mitigate this issue, it has been proposed the future MOSFET devices that incorporate Ge as the channel material should be comprised of nFETs from III-V compounds and pFETs from Ge.[21]

1.4   Germanium's Native Oxide

There are some challenges facing Ge that need to be overcome before there is widespread use of Ge in integrated circuits. First and foremost, it has largely been due

to the nature of the Ge oxide that has hindered the practical use of Ge to date. Dielectrics play an essential role in CMOS devices and although high-κ dielectrics have replaced SiO_2 as the gate dielectric, SiO_2 still serves a multitude of purposes in modern IC devices. For example, SiO_2 is used to isolate one device from another, as a passivation layer to protect the junction from moisture and other atmospheric contaminants and to provide electrical isolation for the multilevel metallisation used in VLSI. Like Si-based devices, Ge-based devices would benefit from a stable native oxide. However, Ge's native oxide is less than ideal. In 1986, Schmeisser et al. used high resolution Ge 3d XPS spectra to resolve the surface oxidation states of Ge(100) and Ge(111). It was found that Ge's oxide is a complex system consisting of Ge in a range of oxidation states (+1, +2, +3 and +4).[22] The stability of the GeO (Ge^{+2}) was highlighted when Prabhakaran et al. carried out oxidation of both the Ge(100) and Ge(111) surfaces by dipping in a mixture of H_2O_2 and H_2O or HNO_2 and found that mainly GeO was produced. They also found that in situ oxidation of both surfaces produced mainly GeO.[23] Exposure of the Ge surfaces to air instigated the growth of the native oxide where Ge exists in a +4 oxidation state. This native oxide (GeO_2) has some undesirable properties from a device fabrication perspective. For example, it is water-soluble which is problematic since current processing techniques involve aqueous processing steps which pose no problem for SiO_2 but would cause oxide etching for GeO_2. Also, thermal oxide growth (an important step in the Si transistor fabrication process) is not readily achieved for Ge – oxidation of Si followed by a high-temperature anneal results in SiO_2 formation from suboxides whereas oxidation of Ge by O_2 results in the growth of Ge 1+, 2+ and 3+ oxidation states but little of the 4+ state found in GeO_2.[24]

In an attempt to mitigate the issues related to Ge's unreliable native oxide, with the knowledge that high-κ dielectrics will most likely be used as the gate oxide in modern MOSFETs and that SiO_2 will continue to serve as the bedrock for devices, efforts to remove the native Ge oxide and replace it with a more stable passivation layer have been made by many.

1.5   Reactivity of the Ge Surface

The literature on the passivation of Ge contains both vapour- and liquid-phase methods - each method confronted with specific challenges. For example, vapour-phase methods often require high vacuum and noxious, highly reactive precursors depending on the type of passivation that is required. While the liquid-phase passivation reactions often require long reaction times. There are some passivating molecules can be delivered through either liquid or vapour, depending on the specific desired outcome. A review of the literature of both vapour- and liquid-phase passivation of Ge is presented.

1.5.1 Vapour-Phase Passivation of Ge

The vapour-phase passivation of Ge and other materials is desirable for a number of reasons. As mentioned, devices with novel architectures such as GAA strained Ge pMOS devices created by Witters et al. consist of arrays of densely-packed nanostructures (9 nm diameter Ge NWs – **Figure 5**) which could be damaged by wet-chemical processing due to capillary forces and surface tension.[25]
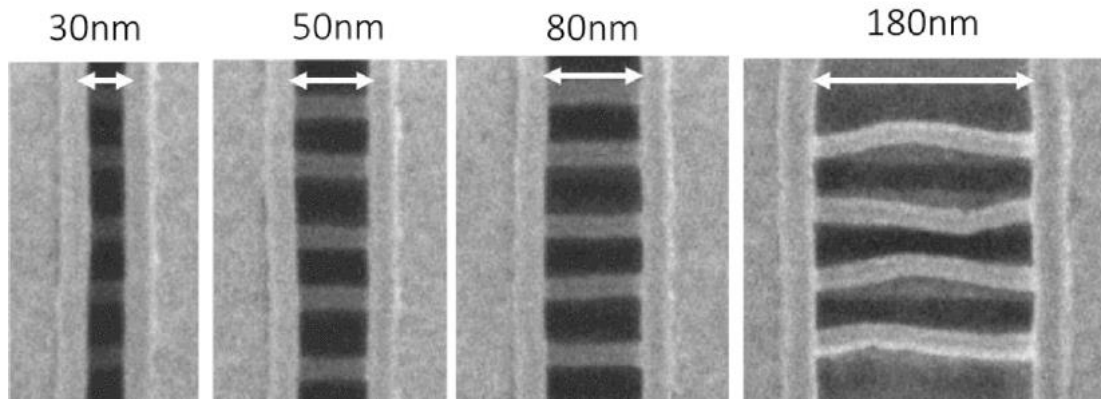
Figure 5. Top-view SEM images of free-hanging Ge NWs.[25]

Also, Tao et al. stated that contamination by insoluble residues and metallic impurities during wet-chemical processing was a motivating factor for their work on exclusively gas-phase passivation of Si surfaces for NEMS (Nano Electro-Mechanical Systems) and MEMS (Micro Electro-Mechanical Systems) devices.[26] The vapour-phase passivation of Ge has been conducted using a diverse range of chemicals including halides [27-33], sulfides [34-37], nitrides [38, 39], oxynitrides [40-43], organics [44-51], graphene [52-59], and Si.[60-64] Herein, these methods will be discussed and recent methods to passivate Ge using vaporised reagents will be focused on. First, it is important to define a vaporised reagent. Vaporisation of a reagent is dependent on temperature and pressure and so, vapour-phase reactions with Ge at ambient temperatures and pressures are discussed along with those reactions that occur under ultra-high vacuum (UHV). UHV may be necessary for a number of reasons. In an attempt to minimise the number of variables, many reactions are carried out under UHV conditions. The UHV system offers an environment where the intended chemistry can be deployed with less concern for contamination from the environment. In addition, low pressures and high temperatures encourage vaporisation of many

materials and thus allow vapour-phase chemistry to be carried out with materials that would otherwise be liquid or solid at room temperature and pressure.

1.5.1.1 Halide Passivation

Treatment of Ge with acid halides has been shown to be effective at removing the native oxide leaving a halide or H-terminated Ge surface depending on the reagent used. HF vapour etching is a common process in the preparation of Si MEMS and NEMS devices since it can be used to under etch Si, removing the underlying SiO_2, to make freestanding Si nanostructures from silicon-on-insulator (SOI). The literature on the use of HF vapour etching to remove GeO_2 and H-passivate Ge is sparse however the use of halide acids such as HCl, HBr and HI has been documented in the literature. Cullen et al. showed in 1962 that reacting the hydrated germanium oxide with heated HCl gas at 144-147°C, resulted in H_2O and $GeCl_4$, which are volatile at that temperature. Then, when exposed to a mixture of Cl_2 and HCl gas at 87-90°C, a Cl-terminated Ge surface which is reactive toward Grignard-type chemistry was formed.[27] Since then, vaporised halide-atom-containing molecules (X_2, HX where X = F, Br, Cl, I) have been used to remove native oxide on Ge and to passivate it with the halide atom or with H as in the case of HF. The structure of halide terminated Ge has been discussed by Citrin et al. They used surface extended x-ray absorption fine-structure measurements to show that Cl on annealed Ge (111)-(2x8), is the onefold-atop site which was contrary to previous photoemission studies of the system.[29] In the same year, Bachelet and Schluter at Bell Labs confirmed these results using total-energy minimisation.[28] For the most part, halide passivation of Ge has been achieved using vaporised HCl or Cl_2 gas. However, Fouchier et al. showed that native oxide removal and subsequent Ge halide passivation could be achieved using Br as

the halide atom.[30] Passivation of Ge by Br was achieved using an electrochemical AgBr cell that produced molecular Br under UHV. The Ge(111) surface was prepared by ion sputtering at 900K followed by an annealing step. Gothelid et al. reacted Ge(111) surfaces with I under UHV conditions and found that two Ge-I species are created (GeI and GeI_2) which are chemically stable when exposed to O_2.[31] Halide passivation is often used as an intermediary step towards passivation with other molecules as it effectively removes the oxide and provides surfaces that are robust enough to withstand exposure to the ambient for some time while also being reactive toward to organic molecules such as Grignard-reagents and alkanethiols.

1.5.1.2 Sulfur Passivation

Sulfur, being bivalent, has the potential to passivate the Ge(100)-2x1 surface since each Ge atom has two dangling bonds. By disassociating S from AgS_2 under UHV conditions, Weser et al. successfully passivated Ge(100) and found the S to be positioned in a bridge-like position whereby the bulk Ge structure was maintained and a 1 x 1 surface structure was observed.[34] Roche et al. used core-level photoemission spectroscopy to show that for the same system, a non-ideal surface is formed which consists of Ge in four oxidation states and that annealing at 200°C promotes the S-Ge phase which desorbs by annealing at higher temperatures resulting in etching of the surface.[37] These works relied on S passivation of Ge using atomic S under UHV conditions. Much of the work carried out in relation to vapour-phase passivation of Ge by S relies on the use of the H_2S. Cohen et al. first cleaned the Ge(100) surface by carrying out a series of annealing and sputtering steps and then passivated by exposing the oxide-free Ge(100) to H_2S under UHV conditions. They described the adsorption of H_2S on Ge(100) using temperature-programmed desorption and found that adsorbed

H$_2$S decomposes upon heating into H$_2$ and GeS, which desorb at 570 and 660 K, respectively.[35] Nelen et al. expanded on this and found that higher Ge surface temperatures, result in higher total surface coverage due to hydrogen desorption from the Ge surface which creates additional surface sites for H$_2$S decomposition.[36]

1.5.1.3 Nitride & Oxynitride Passivation

Passivation of Ge surfaces using nitrides and oxynitrides has been explored in an attempt to fabricate insulating films on Ge of sufficient interfacial quality for MOS and junction passivation applications. In the late 1980's, Hymes et al. used a vapour-phase approach where they found that an oxidation step followed by exposure to ammonia (NH$_3$) at 600°C for long periods resulted in the formation of a stable, stoichiometric oxynitride, Ge$_2$N$_2$O.[40] Paine et al. followed this work by evaluating the quality of the germanium-oxynitride interface using TEM. They found that the layers grown using the vapour-phase method outlined by Hymes et al. were uniform in thickness and are interfacially smooth.[41] Since these original vapour-phase experiments using NH$_3$ for passivation of Ge, other N-containing molecules such as N$_3$H and N$_2$H$_4$ [38] have been studied also. Tindal et al. found that HN$_3$ reacts with Ge(100) at relatively low temperatures to form Ge$_3$N$_4$ by adsorbing molecularly at temperatures below 300 K and above which, it decomposes, causing N$_2$ to desorb leaving N-H groups on the surface. At 575 K, the final hydrogen was found to desorb yielding a nitrided Ge surface.[38] Kim et al. have studied how the HfO$_2$ (high-κ dielectrics) form on nitrided Ge(100). They used a vapour-phase passivation approach using NH$_3$ at 600°C and found that they had achieved effective passivation of surface defects and that the presence of a thin GeO$_x$N$_y$ layer between the high-κ dielectric and Ge(100) substrate behaved as a diffusion barrier for metal species from the dielectric

into the Ge.[42] The deposition of high-κ dielectrics on nitrided Ge surfaces has been further studied by Dimoulas et al. In their work, Hf was evaporated using e-beam under atomic O generated by an RF plasma source to create HfO_2 layers on a thin film of GeO_xN_y on Ge. The initial vapour-phase passivation of the Ge surface by the oxynitride was deemed necessary in order to obtain MOS capacitors of acceptable electrical quality, since direct deposition of HfO_2 on Ge resulted in leaky or no MOS behaviour.[43] These results showed that improved MOS behaviour could be achieved when the native germanium oxide was removed and an interfacial layer was used to separate the high-κ dielectric and the underlying Ge.

1.5.1.4 Silicon Passivation of Ge

In an attempt to improve on the MOS capacitors created using an interfacial nitride film, Wu et al. passivated Ge using SiH_4 gas to create an interfacial Si layer between the HfO_2 and the Ge.[60] They found that their MOSFET exhibited less frequency dispersion, a narrower gate leakage current distribution, and higher peak mobility than the devices with surface nitridation. Their method for Si passivation involved exposing H-terminated Ge to SiH_4 at ambient pressure at 400°C. Following the Si passivation, the HfO_2 gate dielectric was deposited in an O_2 and N_2 environment at 400°C using hafnium tert-butoxide as the precursor. Mitard et al. expanded on this and used both SiH_4 and Si_3H_8 to grow epi-Si on Ge and illustrated that reduced Si growth temperature resulted in the introduction of negatively charged defects possibly located at the Si/SiO_2 interface.[61] Creating other Si-based layers between Ge and high-κ dielectrics has been explored also. Chen et al. deposited an ultrathin (0.8nm) SiO_2 film on a thin Ge film by physical vapour deposition (PVD) and followed that with a Ti_x $La_{1-x}O$ layer (x ∼ 0.67).[62] The vapour-phase passivation of Ge by SiO_2 was an

essential step in creating a MOSFET that worked well since had the Ge not been capped, the Ge would have been oxidised by water and air during the cleaning process and the GeO_2 layer that formed would have been dissolvable in water causing the loss of the thin Ge layer.

1.5.1.5 Passivation of Ge by Organic Molecules

Vapour-phase passivation of Ge using organic molecules has been a topic of interest since the first retro-Diels-Alder reactions between conjugated butadienes and the Ge(100)-2×1 surface carried out by Teplyakov et al. in 1998.[44] In their study, they found that Diels-Alder chemistry occurs on Ge(100)-2×1 at room temperature as readily as on Si(100)-2×1, which has been shown previously.[65, 66] The Diels-Alder reaction on Ge were carried out in a UHV chamber whereby the Ge was sputtered clean and dienes were introduced to the chamber and found to chemisorb to the Ge surface in accordance with the computational predictions for Si made by Konecny.[65] Lal et al. expanded on this by carrying out vapour-phase passivation of Ge(100) using ethylene gas. They showed that ethylene chemisorbs molecularly on the Ge(100)-(2x1) surface at room temperature. In their study, C_2H_4 and C_2D_4 were deposited onto the Ge(100) substrate at 300 K under UHV conditions.[45] Lee et al. furthered this line of research by using cyclic unsaturated hydrocarbons (cyclopentene and cyclohexene) to passivate Ge surfaces. They found that both hydrocarbons react with the surface Ge-dimer bonds to yield reaction products that are consistent with a [2+2] cycloaddition reaction.[46] Much like the other works referenced in this section, these reactions were carried out under UHV conditions; however, unlike the other works that used Ar^+ sputtering to clean the Ge surfaces, Lee et al. used an ex-situ Ge preparation procedure which involved exposure to ultraviolet generated ozone.

Vapour-phase passivation reactions of Ge using organic molecules with novel atoms has also been studied. Takenaka et al. have reacted As-containing precursors with Ge surfaces at high temperatures using a metal-organic vapour phase epitaxy (MOVPE) system to achieve gas-phase doping of Ge.[51, 67]

1.5.1.6 Graphene Passivation of Ge

Graphene, considered as a wonder material by many has garnered a lot of attention owing to its unique physical properties and truly exceptional electronic properties. It is because of these electronic properties (specifically the extraordinary carrier mobility) that graphene has long been predicted to play a role in post-Si electronics. As such, efforts have been made to grow graphene using chemical vapour deposition (CVD) on a range of substrates including Ge. Wang et al. have grown large-area graphene directly on Ge obviating the need to transfer graphene grown on a metal foil onto Ge. They found that defect-free, large area graphene growth was achieved on Ge when H_2 and CH_4 were flown at a ratio of 50:0.1 sccm into the reaction chamber at 910°C for 100 minutes and also demonstrated that Ge has an effective catalytic ability for direct fabrication of Ge.[52] Kiraly et al. have elaborated on this by exploring the electronic and mechanical properties of CVD grown graphene on Ge. They found that the crystallographic orientation of the Ge has significant impact on the atomic structure and electronic properties of the material interface.[54] One of the focuses of this thesis is develop a method to inhibit the oxidation of Ge upon exposure to the ambient. Rojas Delgado et al. have experimented with graphene as an oxidation inhibitor for oxide-free Ge surfaces and found that CVD-grown graphene effectively inhibits the growth of oxide for up to 17 weeks on Ge(100) surfaces.[58] Of all of the

methods described in this section for the growth of graphene, this is the only one that uses CVD-grown graphene to prevent the oxidation of Ge.

1.5.2 Liquid-Phase Passivation of Ge

Methods for the wet-chemical passivation of Ge have been explored also and can largely by broken into the 4 methods listed below; however, there are also some novel methods for the wet-chemical functionalisation of Ge that have recently been demonstrated. For the purposes of monolayer doping of Ge with As atoms, Kennedy et al. have demonstrated a method for the wet-chemical functionalisation of Cl-terminated Ge using arsanilic acid.[68] Aside from these niche methods, the main methods are:

1) Halide passivation

2) Grignard-chemistry

3) Hydrogermylation

4) Alkanethiol passivation

1) The halide passivation methods described in the vapour-phase passivation method section which proceeds this section have been achieved for liquid acid halides also. The wet chemical etching of Ge using acid halides is often used to remove the native oxide and replace it with a monolayer of halide atoms in the case of HCl,[69] HBr [70] and HI or H in the case of HF.[71] In the current semiconductor fabrication process, HF is used to etch SiO_2 leaving a H-terminated Si surface that has been shown to be a useful reactive precursor for further functionalisation. HF etching of Ge oxides has been explored also. The H-terminated Ge surfaces that are created after etching in an aqueous solution of HF have been shown to reoxidise rapidly upon exposure to the

ambient.[71, 72] The H-terminated Ge surface is used as a reactive precursor to additional liquid-phase organic functionalisation. Unlike with Si, HCl can be used to etch Ge oxides and yield a Cl-terminated surface which has been shown to be more stable than H-terminated Ge surfaces.[73] These Cl-terminated Ge surfaces exhibit more ambient stability than H-terminated surfaces while also being useful as reactive precursors to additional organic functionalisation.

2) Passivation using Grignard chemistry was first demonstrated by Cullen et al. in 1962 whereby an ethyl-Grignard was reacted with a Cl-terminated Ge surface forming Ge-C bonds.[27] Grignard reagents are formed by the reaction of magnesium with alkyl or alkenyl halides. They exhibit strong nucleophilic properties, reacting with electrophilic species such as the Cl-terminated Ge surface. Originally, it was thought that the formation of the Ge-C bonds was in a one-to-one ratio with the Ge surface atoms; however, the chlorination procedure implemented in Cullen's experiment has since been shown to cause etching of the Ge surface and as such, the Ge-C ratio is not clear.[24] Following on from this, different lengths of alkane chains such as have been attached to the Ge surface using Grignard reagents (ethyl-Grignard, octadecyl-Grignard).[74] These Grignard-alkylated Ge surfaces have been shown to be stable upon exposure to the ambient for 5 days or boiling water for 30 minutes.[74]

3) Hydrogermylation reactions whereby an alkene or alkyne is reacted with a Ge surface mediated by a Lewis acid, UV light, or heat resulting in a Ge-C bond like the Grignard-type passivation. With hydrosilylation (the most extensively studied wet chemical functionalisation method for Si) in mind, Choi and Buriak first achieved hydrogermylation of a H-terminated Ge(100) surface in the year 2000.[75] This route for functionalising the Ge surface is advantageous over the Grignard approach since

hydrogermylation reactions typically take between 1 and 12 hours at room temperature whereas Grignard-type reactions can take between 6 hours and 7 days at elevated temperatures.

4) Alkanethiol passivation reactions involve reacting thiol molecules with a halide- or H-terminated Ge surface resulting in the formation of Ge-S bonds. Much like the heavily-studied Au surface, alkanethiol molecules with long-chain C backbones form self-assembled monolayers (SAMs) on Ge. Since the primary focus of this body of work is to passivate Ge(100) using SAMs of 1-alkanethiol molecules, a more detailed insight into this Ge passivation method is presented in **Section 1.6**.

1.6   Alkanethiol Self-Assembled Monolayers

The concept of self-assembly is the formation of a system without the guidance of external forces but rather as a consequence of specific, local interactions among the components themselves.[76] Self-assembled monolayers are an example of the phenomenon that take place at gas-liquid, gas-solid and liquid-solid interfaces.[77] A self-assembled monolayer on a solid surface is typically formed when a single layer of molecules bond to the surface in a self-limiting fashion to yield a surface that is saturated and chemically stable. The stability of a monolayer is largely dictated by: (1) the strength of the bond that is formed between the atoms on the surface of the material and the reactive site in the molecule and (2) the intermolecular van der Waals (vdW) forces that exist between adjacent molecules in the SAM. Van der Waals forces are weak, distance-dependant forces that exist between molecules or atoms. These forces do not result in chemical bonds and are easily disturbed - in a SAM, each molecule in the monolayer stabilises adjacent SAM molecules, which increase the global stability

of the SAM. Among SAMs, the most popular are those of thiols or dithiols, which have been shown to form on a range of oxide-free metals and semiconductors.[77-82]
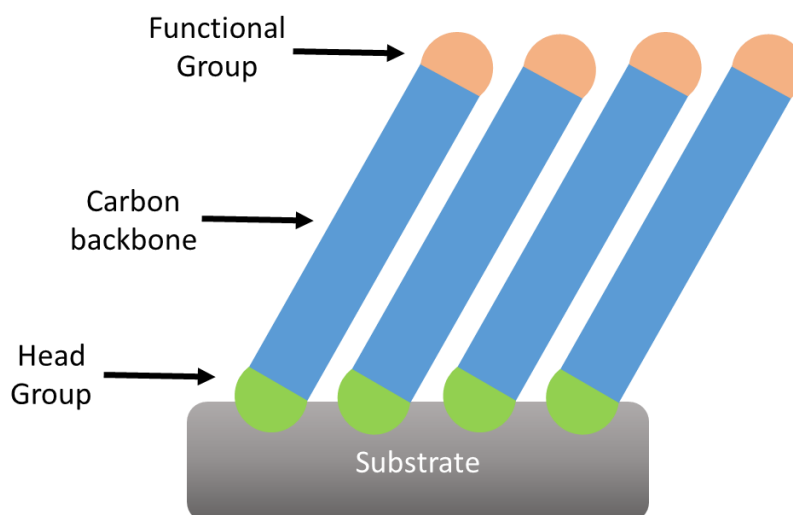
Figure 6. Schematic of thiol molecules assembled on substrate surface elucidating the 3 constituent parts of the molecule.

Alkanethiol molecules consist of a reactive S-H head group, a carbon backbone and a functional group at the tail of the molecule (**Figure 6**). The properties of the functional group at the tail of the molecule influence the characteristics of the surface. For example, the hydrophobicity of the surface can be engineered by creating a SAM whose constituent molecules have a non-polar functional group (such as CH_3) at the tail. The non-polar tail of the long thiol molecules used to create SAMs on gold cause the hydrophobicity of the surface to increase dramatically when compared to the surfaces prior to SAM formation.[83] The length of the carbon backbone also affects the properties of the functionalised surface. Studies on gold have shown that long-chain thiol molecules form ordered, stable assembles and that as the C backbone decreases in length, the SAM becomes increasingly disordered with lower packing density and coverage.[84]

Figure 7 illustrates a simple 4 step mechanism by which a thiol SAM is formed on Au from the vapour, according to Vericat et al.[82] It is a process that begins with **(i)** the physisorption of thiol molecules onto the Au surface - no covalent bonds are formed at this stage. The second phase of the process **(ii)** involves the chemisorption (bonding) of the reactive S head of the thiol molecule with the Au surface. The chemisorbed thiol molecules lie down on the Au surface. **(iii)** Further physisorption and bonding of the thiol molecules to the surface occurs such that the concentration of bonded molecules at the Au surface reaches a level whereby adjacent molecules being to stand up and align due to the weak van der Waals forces that occur between the C backbones. The final step of the process **(iv)** involves the saturation of the available surface sites and the forming an ordered array of thiol molecules on the Au surface.
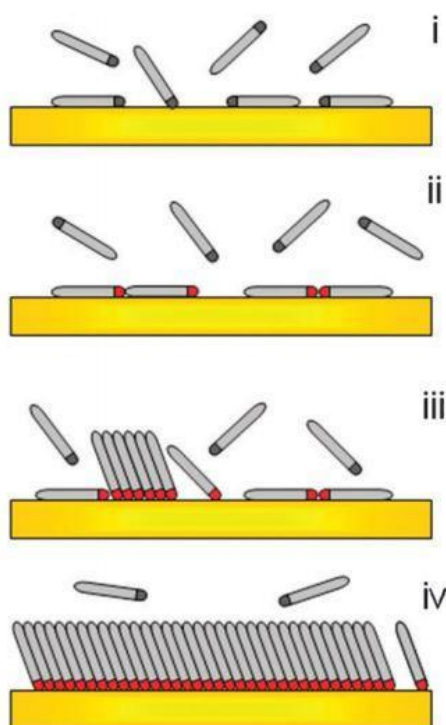
Figure 7. The 4 stages of alkanethiol SAM formation on Au(111): **(i)** physisorption, **(ii)** lying-down phase formation, **(iii)** nucleation of the standing-up phase, **(iv)** completion of the standing up phase.[82]

The relative ease at which this process can be conducted has made the process of interest to those who wish to engineer the properties of surfaces or interfaces. SAMs are used for many applications including ultrathin layers for corrosion prevention [85], friction reduction [79, 86], and as anti-stiction coatings in MEMs fabrication.[87] SAMs lend themselves especially useful for the functionalisation of nanostructures (nanoparticles, nanorods and nanowires) that are otherwise difficult to functionalise. Yuan et al. have functionalised Ge nanowires using a SAM of 1-dodecanethiol molecules for lithium-ion battery applications and found that the passivated wires outperformed non-passivated wires electrochemically. They hypothesised that the organic SAM helped maintain the structural integrity of the nanowire during the lithiation/delithiation process.[88] Collins et al. have also functionalised Ge nanowires for the purposes of oxidation prevention. They found that the SAM formed from 1-dodecanethiol molecules on the Ge nanowire offered greater oxidation resistance than Ge nanowires functionalised using Grignard chemistry.[89]

1.7 References

1. G.E., M., *Cramming More Components onto Integrated Circuits.* Electronics, 1965. **38**: p. 114-117.

2. Hirose, M., *Electron Tunneling Through Ultrathin SiO2.* Materials Science and Engineering: B, 1996. **41**(1): p. 35-38.

3. Mitard, J., L. Witters, H. Arimura, Y. Sasaki, A.P. Milenin, R. Loo, A. Hikavyy, G. Eneman, P. Lagrain, H. Mertens, S. Sioncke, C. Vrancken, H. Bender, K. Barla, N. Horiguchi, A. Mocuta, N. Collaert, and A.V.Y. Thean, *First Demonstration of 15nm-WFIN Inversion-Mode Relaxed-Germanium n-FinFETs with Si-Cap Free RMG and NiSiGe Source/Drain.* Vol. 2015. 2015. 16.5.1-16.5.4.

4. Su, C., T. Tsai, Y. Liou, Z. Lin, H. Lin, and T. Chao, *Gate-All-Around Junctionless Transistors With Heavily Doped Polysilicon Nanowire Channels.* IEEE Electron Device Letters, 2011. **32**(4): p. 521-523.

5. Witters, L., F. Sebaai, A. Hikavyy, A.P. Milenin, R. Loo, A.D. Keersgieter, G. Eneman, T. Schram, K. Wostyn, K. Devriendt, A. Schulze, R. Lieten, S. Bilodeau, E. Cooper, P. Storck, C. Vrancken, H. Arimura, P. Favia, E. Vancoille, J. Mitard, R. Langer, A. Opdebeeck, F. Holsteyns, N. Waldron, K. Barla, V.D. Heyn, D. Mocuta, and N. Collaert. *Strained Germanium Gate-All-Around PMOS Device Demonstration using Selective Wire Release Etch Prior to Replacement Metal Gate Deposition.* in *2017 Symposium on VLSI Technology.* 2017.

6. Clavelier, L., C. Deguet, L.D. Cioccio, E. Augendre, A. Brugere, P. Gueguen, Y.L. Tiec, H. Moriceau, M. Rabarot, T. Signamarcheix, J. Widiez, O. Faynot,

F. Andrieu, O. Weber, C.L. Royer, P. Batude, L. Hutin, J. Damlencourt, S. Deleonibus, and E. Defaÿ. *Engineered substrates for future More Moore and More than Moore integrated devices*. in *2010 International Electron Devices Meeting*. 2010.

7. Taylor, S.R., *Abundance of Chemical Elements in the Continental Crust: A New Table.* Geochimica et Cosmochimica Acta, 1964. **28**(8): p. 1273-1285.

8. Petersen, K.E., *Silicon as a Mechanical Material.* Proceedings of the IEEE, 1982. **70**(5): p. 420-457.

9. Pacchioni, G., L. Skuja, and D. Griscom, *Defects in SiO2 and Related Dielectrics: Science and Technology.* 2000.

10. Wilk, G.D., R.M. Wallace, and J.M. Anthony, *High-κ Gate Dielectrics: Current Status and Materials Properties Considerations.* Journal of Applied Physics, 2001. **89**(10): p. 5243-5275.

11. Hiratani, M., S.-i. Saito, Y. Shimamoto, and K. Torii, *Effective Electron Mobility Reduced by Remote Charge Scattering in High-κ Gate Stacks.* Japanese Journal of Applied Physics, 2002. **41**(Part 1, No. 7A): p. 4521-4522.

12. Haller, E.E., *Germanium: From Its Discovery to SiGe Devices.* Journal fur praktische Chemie, 1986. **34**(34): p. 45.

13. Gupta, A., T. Sakthivel, and S. Seal, *Recent Development in 2D Materials Beyond Graphene.* Progress in Materials Science, 2015. **73**: p. 44-126.

14. Satta, A., A.R. Peaker, A. Theuwis, A.N. Larsen, B. Depuydt, B. De Jaeger, C. Quaeyhaegens, C.O. Chui, C. Deguet, C. Claeys, D. Esseni, E. Simoen, E. Sangiorgi, E. Kasper, F. Letertre, I. Romandic, J. Vanhellemont, J. Coutinho, K.C. Saraswat, M. De Jonghe, M. Heyns, M. Meuris, M. Caymax, M. Houssa,

P. Clauws, P. Palestri, R. Jones, T. Akatsu, V. Markevich, and W. De Baets, *Germanium-Based Technologies. From Materials to Devices*, ed. C. Claeys and E. Simoen. 2007, Oxford: Elsevier. xiv-xvi.

15. Crowson, P., *Germanium*, in *Minerals Handbook*. 1996, Palgrave Macmillan: London.

16. Ye, H. and J. Yu, *Germanium epitaxy on silicon.* Science and Technology of Advanced Materials, 2014. **15**(2): p. 024601.

17. Brunco, D.P., B. Jaeger, G. Eneman, A. Satta, V. Terzieva, L. Souriau, F. Leys, G. Pourtois, M. Houssa, K. Opsomer, G. Nicholas, M. Meuris, and M. Heyns, *Germanium: The Past and Possibly a Future Material for Microelectronics.* ECS Transactions, 2007. **11**.

18. Vanpoucke, D., *Ab Initio Study of Pt Induced Nanowires on Ge(001)*. 2009: University of Twente, Enschede, The Netherlands.

19. Duke, C.B., *Semiconductor Surface Reconstruction: The Structural Chemistry of Two-Dimensional Surface Compounds.* Chemical Reviews, 1996. **96**(4): p. 1237-1260.

20. Zandvliet, H.J.W., *The Ge(001) Surface.* Physics Reports, 2003. **388**(1): p. 1-40.

21. Todi, R.M. and M.M. Heyns, *Germanium: The semiconductor comeback material.* IEEE Potentials, 2007. **26**(2): p. 34-38.

22. Schmeisser, D., R.D. Schnell, A. Bogen, F.J. Himpsel, D. Rieger, G. Landgren, and J.F. Morar, *Surface Oxidation States of Germanium.* Surface Science, 1986. **172**(2): p. 455-465.

23. Prabhakaran, K. and T. Ogino, *Oxidation of Ge(100) and Ge(111) Surfaces: an UPS and XPS study.* Surface Science, 1995. **325**(3): p. 263-271.

24. Loscutoff, P.W. and S.F. Bent, *Reactivity of the Germanium Surface: Chemical Passivation and Functionalization.* Annual Review of Physical Chemistry, 2006. **57**: p. 467-495.

25. Witters, L., H. Arimura, F. Sebaai, A. Hikavyy, A.P. Milenin, R. Loo, A.D. Keersgieter, G. Eneman, T. Schram, K. Wostyn, K. Devriendt, A. Schulze, R. Lieten, S. Bilodeau, E. Cooper, P. Storck, E. Chiu, C. Vrancken, P. Favia, E. Vancoille, J. Mitard, R. Langer, A. Opdebeeck, F. Holsteyns, N. Waldron, K. Barla, V.D. Heyn, D. Mocuta, and N. Collaert, *Strained Germanium Gate-All-Around pMOS Device Demonstration Using Selective Wire Release Etch Prior to Replacement Metal Gate Deposition.* IEEE Transactions on Electron Devices, 2017. **64**(11): p. 4587-4593.

26. Tao, Y., R. Hauert, and C.L. Degen, *Exclusively Gas-Phase Passivation of Native Oxide-Free Silicon(100) and Silicon(111) Surfaces.* ACS Applied Materials & Interfaces, 2016. **8**(20): p. 13157-13165.

27. Cullen, G.W., J.A. Amick, and D. Gerlich, *The Stabilization of Germanium Surfaces by Ethylation.* Journal of The Electrochemical Society, 1962. **109**(2): p. 124-127.

28. Bachelet, G.B. and M. Schlüter, *Structural Determination of Cl Chemisorption on Si[1] and Ge[1] by Total-Energy Minimization.* Physical Review B, 1983. **28**(4): p. 2302-2304.

29.   Citrin, P.H., J.E. Rowe, and P. Eisenberger, *Direct Structural Study of Cl on Si [1] and Ge [1] Surfaces: New Conclusions.* Physical Review B, 1983. **28**(4): p. 2299-2301.

30.   Fouchier, M., M.T. McEllistrem, and J.J. Boland, *Novel Adatom-Terminated Step Structure on the Ge(111)-(1×1):Br Surface.* Surface Science, 1997. **385**(1): p. l905-l910.

31.   Göthelid, M., G. LeLay, C. Wigren, M. Björkqvist, and U.O. Karlsson, *Iodine Reaction and Passivation of the Ge(111) Surface.* Surface Science, 1997. **371**(2): p. 264-276.

32.   Dharma-wardana, M.W.C., M.Z. Zgierski, D. Ritchie, J.G. Ping, and H. Ruda, *Comparison of Cluster and Slab Models of the Surface Structure of Cl-Terminated Ge(111) and GaAs(111) Surfaces.* Physical Review B, 1999. **59**(24): p. 15766-15771.

33.   Cao, S., J.C. Tang, and S.L. Shen, *Multiple-Scattering and DV-Xa Analyses of a Cl-Passivated Ge(111) Surface.* Journal of Physics: Condensed Matter, 2003. **15**(30): p. 5261-5268.

34.   Weser, T., A. Bogen, B. Konrad, R.D. Schnell, C.A. Schug, Steinmann, and W, *Photoemission Surface Core-Level Study of Sulfur Adsorption on Ge(100).* Physical Review B, 1987. **35**(15): p. 8184-8188.

35.   Cohen, S.M., Y.L. Yang, E. Rouchouze, T. Jin, and M.P. D'Evelyn, *Adsorption and Decomposition of Hydrides on Ge(100).* Journal of Vacuum Science & Technology A, 1992. **10**(4): p. 2166-2171.

36.   Nelen, L.M., K. Fuller, and C.M. Greenlief, *Adsorption and Decomposition of H2S on the Ge(100) Surface.* Applied Surface Science, 1999. **150**(1): p. 65-72.

37. Roche, J., P. Ryan, and G.J. Hughes, *Core Level Photoemission Studies of the Sulphur Terminated Ge(100) Surface.* Applied Surface Science, 2001. **174**(3): p. 271-274.

38. Tindall, C. and J.C. Hemminger, *HREELS Studies of the Chemistry of Nitrogen Hydrides on Ge(100): Formation of a Surface Nitride at Low Temperatures.* Surface Science, 1995. **330**(1): p. 67-74.

39. Maggioni, G., S. Carturan, L. Fiorese, N. Pinto, F. Caproli, D.R. Napoli, M. Giarola, and G. Mariotto, *Germanium Nitride and Oxynitride Films for Surface Passivation of Ge Radiation Detectors.* Applied Surface Science, 2017. **393**: p. 119-126.

40. Hymes, D.J., *Growth and Materials Characterization of Native Germanium Oxynitride Thin Films on Germanium.* Journal of The Electrochemical Society, 1988. **135**(4): p. 961.

41. Paine, D.C., J.J. Rosenberg, S.C. Martin, D. Luo, and M. Kawasaki, *Evaluation of Device Quality Germanium-Germanium Oxynitride Interfaces by High-Resolution Transmission Electron Microscopy.* Applied Physics Letters, 1990. **57**(14): p. 1443-1445.

42. Kim, H., P.C. McIntyre, C.O. Chui, K.C. Saraswat, and M.-H. Cho, *Interfacial Characteristics of HfO2 Grown on Nitrided Ge (100) Substrates by Atomic-Layer Deposition.* Applied Physics Letters, 2004. **85**(14): p. 2902-2904.

43. Dimoulas, A., G. Mavrou, G. Vellianitis, E. Evangelou, N. Boukos, M. Houssa, and M. Caymax, *HfO2 High-κ Gate Dielectrics on Ge (100) by Atomic Oxygen Beam Deposition.* Applied Physics Letters, 2005. **86**(3): p. 032908.

44. Teplyakov, A.V., P. Lal, Y.A. Noah, and S.F. Bent, *Evidence for a Retro-Diels−Alder Reaction on a Single Crystalline Surface: Butadienes on Ge(100).* Journal of the American Chemical Society, 1998. **120**(29): p. 7377-7378.

45. Lal, P., A.V. Teplyakov, Y. Noah, M.J. Kong, G.T. Wang, and S.F. Bent, *Adsorption of Ethylene on the Ge(100)-2×1 Surface: Coverage and Time-Dependent Behavior.* The Journal of Chemical Physics, 1999. **110**(21): p. 10545-10553.

46. Lee, S.W., J.S. Hovis, S.K. Coulter, R.J. Hamers, and C.M. Greenlief, *Cycloaddition Chemistry on Germanium(001) Surfaces: the Adsorption and Reaction of Cyclopentene and Cyclohexene.* Surface Science, 2000. **462**(1): p. 6-18.

47. Hanrath, T. and B.A. Korgel, *Chemical Surface Passivation of Ge Nanowires.* Journal of the American Chemical Society, 2004. **126**(47): p. 15466-15472.

48. Kosuri, M.R., R. Cone, Q. Li, S.M. Han, B.C. Bunker, and T.M. Mayer, *Adsorption Kinetics of 1-Alkanethiols on Hydrogenated Ge(111).* Langmuir, 2004. **20**(3): p. 835-840.

49. Filler, M.A., J.A. Van Deventer, A.J. Keung, and S.F. Bent, *Carboxylic Acid Chemistry at the Ge(100)-2 × 1 Interface: Bidentate Bridging Structure Formation on a Semiconductor Surface.* Journal of the American Chemical Society, 2006. **128**(3): p. 770-779.

50. Ardalan, P., N. Davani, and C.B. Musgrave, *Attachment of Alanine and Arginine to the Ge(100)-2×1 Surface.* The Journal of Physical Chemistry C, 2007. **111**(9): p. 3692-3699.

51. Takenaka, M., K. Morii, M. Sugiyama, Y. Nakano, and S. Takagi, *Gas Phase Doping of Arsenic into (100), (110), and (111) Germanium Substrates Using a Metal–Organic Source.* Japanese Journal of Applied Physics, 2011. **50**: p. 010105.

52. Wang, G., M. Zhang, Y. Zhu, G. Ding, D. Jiang, Q. Guo, S. Liu, X. Xie, P.K. Chu, Z. Di, and X. Wang, *Direct Growth of Graphene Film on Germanium Substrate.* Scientific Reports, 2013. **3**(1): p. 2465.

53. Lee, J.-H., E.K. Lee, W.-J. Joo, Y. Jang, B.-S. Kim, J.Y. Lim, S.-H. Choi, S.J. Ahn, J.R. Ahn, M.-H. Park, C.-W. Yang, B.L. Choi, S.-W. Hwang, and D. Whang, *Wafer-Scale Growth of Single-Crystal Monolayer Graphene on Reusable Hydrogen-Terminated Germanium.* Science, 2014. **344**(6181): p. 286.

54. Kiraly, B., R.M. Jacobberger, A.J. Mannix, G.P. Campbell, M.J. Bedzyk, M.S. Arnold, M.C. Hersam, and N.P. Guisinger, *Electronic and Mechanical Properties of Graphene–Germanium Interfaces Grown by Chemical Vapor Deposition.* Nano Letters, 2015. **15**(11): p. 7414-7420.

55. Dai, J., D. Wang, M. Zhang, T. Niu, A. Li, M. Ye, S. Qiao, G. Ding, X. Xie, Y. Wang, P.K. Chu, Q. Yuan, Z. Di, X. Wang, F. Ding, and B.I. Yakobson, *How Graphene Islands Are Unidirectionally Aligned on the Ge(110) Surface.* Nano Letters, 2016. **16**(5): p. 3160-3165.

56. Lukosius, M., G. Lippert, J. Dabrowski, J. Kitzmann, M. Lisker, P. Kulse, A. Kruger, O. Fursenko, I. Costina, A. Trusch, Y. Yamamoto, A. Wolff, A. Mai, T. Schroeder, and G. Lupina, *(Invited) Graphene Synthesis and Processing on Ge Substrates.* ECS Transactions, 2016. **75**(8): p. 533-540.

57. Lukosius, M., J. Dabrowski, J. Kitzmann, O. Fursenko, F. Akhtar, M. Lisker, G. Lippert, S. Schulze, Y. Yamamoto, M.A. Schubert, H.M. Krause, A. Wolff, A. Mai, T. Schroeder, and G. Lupina, *Metal-Free CVD Graphene Synthesis on 200 mm Ge/Si(001) Substrates.* ACS Applied Materials & Interfaces, 2016. **8**(49): p. 33786-33793.

58. Rojas Delgado, R., R.M. Jacobberger, S.S. Roy, V.S. Mangu, M.S. Arnold, F. Cavallo, and M.G. Lagally, *Passivation of Germanium by Graphene.* ACS Applied Materials & Interfaces, 2017. **9**(20): p. 17629-17636.

59. Campbell, G.P., B. Kiraly, R.M. Jacobberger, A.J. Mannix, M.S. Arnold, M.C. Hersam, N.P. Guisinger, and M.J. Bedzyk, *Epitaxial Graphene-Encapsulated Surface Reconstruction of Ge(110).* Physical Review Materials, 2018. **2**(4): p. 044004.

60. Nan, W., Z. Qingchun, Z. Chunxiang, D.S.H. Chan, A. Du, N. Balasubramanian, M.F. Li, A. Chin, J.K.O. Sin, and D. Kwong, *A TaN-HfO2-Ge pMOSFET with Novel SiH4 Surface Passivation.* IEEE Electron Device Letters, 2004. **25**(9): p. 631-633.

61. Mitard, J., K. Martens, B. DeJaeger, J. Franco, C. Shea, C. Plourde, F.E. Leys, R. Loo, G. Hellings, G. Eneman, W. Wang, J.C. Lin, B. Kaczer, K. DeMeyer, T. Hoffmann, S. DeGendt, M. Caymax, M. Meuris, and M.M. Heyns. *Impact of Epi-Si Growth Temperature on Ge-pFET Performance*. in *2009 Proceedings of the European Solid State Device Research Conference*. 2009.

62. Chen, W.B. and A. Chin, *High Performance of Ge nMOSFETs Using SiO2 Interfacial Layer and TiLaO Gate Dielectric.* IEEE Electron Device Letters, 2010. **31**(1): p. 80-82.

63. Liu, Y., J. Yan, G. Han, H. Wang, M. Liu, C. Zhang, B. Cheng, and Y. Hao. *Strained Ge0.96Sn0.04 P-Channel MOSFETs with in Situ Low Temperature Si2H6 Surface Passivation*. in *2014 7th International Silicon-Germanium Technology and Device Meeting (ISTDM)*. 2014.

64. Xu, Y., G. Han, H. Liu, Y. Wang, Y. Liu, J. Ao, and Y. Hao, *Ge pMOSFETs with GeOx Passivation Formed by Ozone and Plasma Post Oxidation*. Nanoscale Research Letters, 2019. **14**(1): p. 126.

65. Konecny, R. and D.J. Doren, *Theoretical Prediction of a Facile Diels−Alder Reaction on the Si(100)-2×1 Surface*. Journal of the American Chemical Society, 1997. **119**(45): p. 11098-11099.

66. Teplyakov, A.V., M.J. Kong, and S.F. Bent, *Vibrational Spectroscopic Studies of Diels−Alder Reactions with the Si(100)-2×1 Surface as a Dienophile*. Journal of the American Chemical Society, 1997. **119**(45): p. 11100-11101.

67. Takenaka, M., K. Morii, M. Sugiyama, Y. Nakano, and S. Takagi, *Dark Current Reduction of Ge Photodetector by GeO2 Surface Passivation and Gas-Phase Doping*. Optics Express, 2012. **20**(8): p. 8718-8725.

68. Kennedy, N., S. Garvey, B. Maccioni, L. Eaton, M. Nolan, R. Duffy, F. Meaney, M. Kennedy, J.D. Holmes, and B. Long, *Monolayer Doping of Germanium with Arsenic: A New Chemical Route to Achieve Optimal Dopant Activation*. Langmuir, 2020. **36**(34): p. 9993-10002.

69. Kim, J., J. McVittie, K. Saraswat, Y. Nishi, S. Liu, and S. Tan, *Germanium Surface Cleaning with Hydrochloric Acid*. ECS Transactions, 2006. **3**(7): p. 1191-1196.

70.   Ponath, P., A.B. Posadas, and A.A. Demkov, *Ge(001) Surface Cleaning Methods for Device Integration.* Applied Physics Reviews, 2017. **4**(2): p. 021308.

71.   Deegan, T. and G. Hughes, *An X-Ray Photoelectron Spectroscopy Study of the HF Etching of Native Oxides on Ge(111) and Ge(100) Surfaces.* Applied Surface Science, 1998. **123-124**: p. 66-70.

72.   Park, K., Y. Lee, J. Lee, and S. Lim, *Oxidation Mechanism of Hydrogen-Terminated Ge(100) Surface.* Applied Surface Science, 2008. **254**(15): p. 4828-4832.

73.   Okumura, H., T. Akane, and S. Matsumoto, *Carbon Contamination Free Ge(100) Surface Cleaning for MBE.* Applied Surface Science, 1998. **125**(1): p. 125-128.

74.   He, J., Z.-H. Lu, S.A. Mitchell, and D.D.M. Wayner, *Self-Assembly of Alkyl Monolayers on Ge(111).* Journal of the American Chemical Society, 1998. **120**(11): p. 2660-2661.

75.   Choi, K. and J.M. Buriak, *Hydrogermylation of Alkenes and Alkynes on Hydride-Terminated Ge(100) Surfaces.* Langmuir, 2000. **16**(20): p. 7737-7741.

76.   Ulman, A., *Formation and Structure of Self-Assembled Monolayers.* Chemical Reviews, 1996. **96**(4): p. 1533-1554.

77.   Vericat, C., M.E. Vela, G. Corthey, E. Pensa, E. Cortés, M.H. Fonticelli, F. Ibañez, G.E. Benitez, P. Carro, and R.C. Salvarezza, *Self-Assembled Monolayers of Thiolates on Metals: a Review Article on Sulfur-Metal*

Chemistry and Surface Structures. RSC Advances, 2014. **4**(53): p. 27730-27754.

78. Cai, Q., B. Xu, L. Ye, Z. Di, S. Huang, X. Du, J. Zhang, Q. Jin, and J. Zhao, *1-Dodecanethiol Based Highly Stable Self-Assembled Monolayers for Germanium Passivation.* Applied Surface Science, 2015. **353**: p. 890-901.

79. Cao, X.a., X. Gan, Y. Peng, Y. Wang, X. Zeng, H. Lang, J. Deng, and K. Zou, *An Ultra-Low Frictional Interface Combining FDTS SAMs with Molybdenum Disulfide.* Nanoscale, 2018. **10**(1): p. 378-385.

80. Mandler, D. and S. Kraus-Ophir, *Self-Assembled Monolayers (SAMs) for Electrochemical Sensing.* Journal of Solid State Electrochemistry, 2011. **15**(7): p. 1535.

81. Singh, M., N. Kaur, and E. Comini, *The role of self-assembled monolayers in electronic devices.* Journal of Materials Chemistry C, 2020. **8**(12): p. 3938-3955.

82. Vericat, C., M.E. Vela, G. Benitez, P. Carro, and R.C. Salvarezza, *Self-Assembled Monolayers of Thiols and Dithiols on Gold: New Challenges for a Well-Known System.* Chemical Society Reviews, 2010. **39**(5): p. 1805-1834.

83. Folkers, J.P., P.E. Laibinis, and G.M. Whitesides, *Self-Assembled Monolayers of Alkanethiols on Gold: the Adsorption and Wetting Properties of Monolayers Derived from Two Components with Alkane Chains of Different Lengths.* Journal of Adhesion Science and Technology, 1992. **6**(12): p. 1397-1410.

84. Porter, M.D., T.B. Bright, D.L. Allara, and C.E.D. Chidsey, *Spontaneously Organized Molecular Assemblies. 4. Structural Characterization of n-Alkyl Thiol Monolayers on Gold by Optical Ellipsometry, Infrared Spectroscopy,*

and Electrochemistry. Journal of the American Chemical Society, 1987. **109**(12): p. 3559-3568.

85.   Kanukula, D.C.K., A. Boyapati, Y. Md, Iqbal, and S. Bojja, *Corrosion protection of copper by self assembled monolayers.* Indian Journal of Chemical Technology, 2009. **16**: p. 25-31.

86.   Tao, Y., P. Navaretti, R. Hauert, U. Grob, M. Poggio, and C.L. Degen, *Permanent Reduction of Dissipation in Nanomechanical Si Resonators by Chemical Surface Protection.* Nanotechnology, 2015. **26**(46): p. 465501.

87.   Maboudian, R., W.R. Ashurst, and C. Carraro, *Self-assembled monolayers as anti-stiction coatings for MEMS: characteristics and recent developments.* Sensors and Actuators A: Physical, 2000. **82**(1): p. 219-223.

88.   Yuan, F.W., H.J. Yang, and H.Y. Tuan, *Alkanethiol-Passivated Ge Nanowires as High-Performance Anode Materials for Lithium-Ion Batteries: The Role of Chemical Surface Functionalization.* ACS Nano, 2012. **6**(11): p. 9932-9942.

89.   Collins, G., P. Fleming, S. Barth, C. O'Dwyer, J.J. Boland, M.A. Morris, and J.D. Holmes, *Alkane and Alkanethiol Passivation of Halogenated Ge Nanowires.* Chemistry of Materials, 2010. **22**(23): p. 6370-6377.

Chapter 2
Characterisation Methods

2.1 X-Ray Photoelectron Spectroscopy

X-Ray photoelectron spectroscopy (XPS) is the main method of characterisation used in this study. The origins of XPS can be traced back to H. Hertz' investigations of the photoelectric effect, when he observed that a spark was produced when a negatively charged electrode was exposed to ultraviolet radiation.[1] However, it was A. Einstein in 1905 who formulated the photoelectric effect in terms of photons motivated by M. Planck's work on black body radiation.[2] In the decades following Einstein's paper, efforts were made to develop a spectroscopic technique that leveraged the photoelectric effect. Ultimately, X-ray photoelectron spectroscopy, a spectroscopic technique that can be described using the equation below, was develop.[3]

$$E_K = h\nu - (E_B + \Phi)$$

where E_K is the kinetic energy of the photoelectrons, $h\nu$ the incident photon energy, E_B the electron binding energy, and Φ is the work function of the sample and the analyser. Conceptually, the principle behind XPS is relatively simple; a photon of energy $h\nu$ penetrates the sample surface and is absorbed by an electron with a binding energy E_B below the vacuum level. This causes a photoemission process whereby the electron is emitted from the surface with kinetic energy E_K. Emitted electrons are detected and represented graphically whereby E_K (or more commonly E_B using the formula above) is plotted vs intensity (**Figure 1**). Since the energy of the

photoelectrons is quantised, the spectrum consists of a series of discrete peaks that reflect the 'shell' form of the electronic structure of the atoms at the surface of the sample. Ascertaining the binding energies of electrons emitted from the sample surface allows qualitative elemental analysis to be carried out. This seemingly simple process is complicated by the fact that photoelectrons may lose energy to collisions with atoms in the material itself or during detection in the spectrometer. This kind of energy loss is known as inelastic loss and is responsible for the 'steps' to low kinetic energy (high binding energy) that are observed in survey spectra.
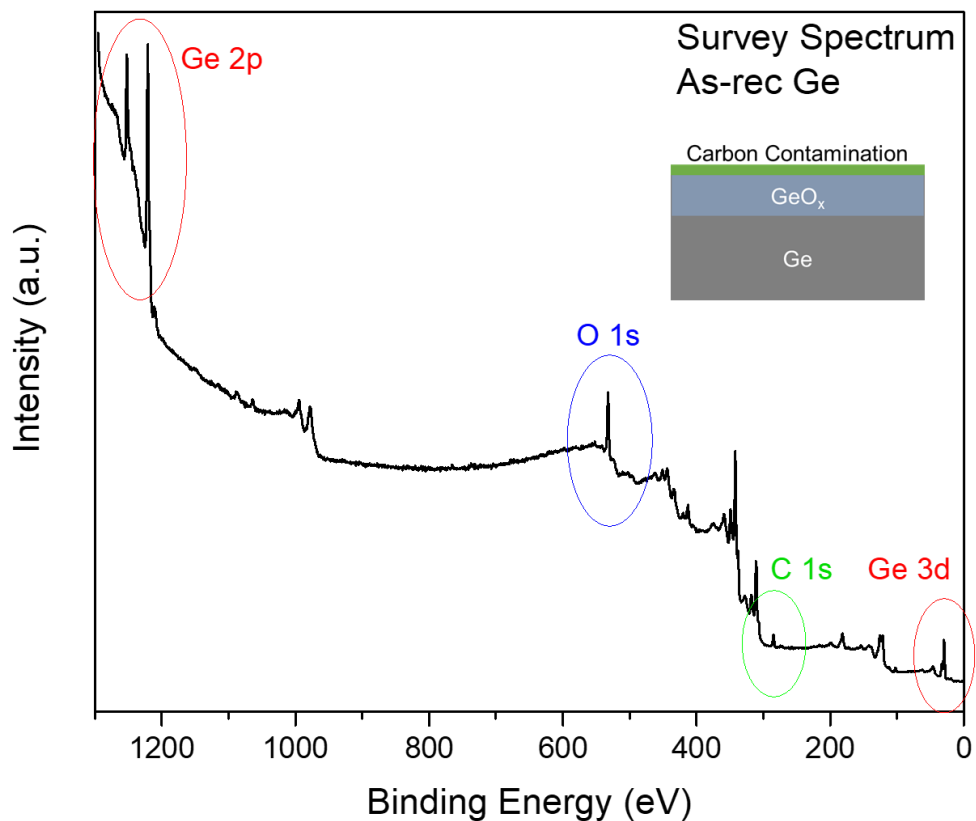
Figure 1. Survey spectrum of as-received Ge(100) highlighting the significant Ge, O and C peaks.

In **Figure 1** the survey spectrum for as as-received Ge(100) surface is displayed and the Ge, O and C peaks of interest are highlighted. The figure inset depicts a schematic of the Ge sample being characterised. As-received Ge is Ge that has undergone no processing other than cleaning by sonication in acetone followed by IPA and drying under a stream of N_2. Although the Ge surface has been cleaned, a thin layer of carbonaceous material (green) is present on the surface. This contamination is unavoidable when processing samples in air since adventitious carbon from the atmosphere deposits on all surfaces. In the survey spectrum, a C 1s peak is evident at 248.8 eV. Since adventitious carbon is always present, and it is known that C 1s electrons from a carbon atom bonded to another carbon atom have binding energies of 248.8 eV, this peak can be used to calibrate XPS spectra.

The X-ray induced photoemission process causes the sample surface to become positively charged. Ideally, the sample must be able to dissipate any positive charge that builds up during irriadiation. Surface charging can affect the kinetic energies (and thus the calculated binding energies) of electrons that are emitted from the surface since the electrons are attracted to the positively charged surface during the emission process. Modern XPS tools utilise electron guns and electrically grounded sample stubs to ensure surface charging does not hamper data interpretation. That said, slight shifts in peak position can and do occur and thus a calibration method is necessary. C 1s calibration is used throughout this study whereby the C 1s peak is fitted and set to 248.8 eV, the known binding energy for the peak. The same peak correction is applied to the survey spectrum and the core-level spectra also.

In **Figure 1**, there are two highlighted Ge features (red). At high binding energy, the Ge 2p peaks are found whereas the Ge 3d peaks are found at the lower end

of the binding energy scale. In both cases, a phenomenon known as spin-orbit coupling results in the presence of doublet peaks. This phenomenon is observed for all non s-level core levels (p, d & f) and occurs due to spin-orbit coupling between the electron spin and the angular momentum vector of the orbital from which the electron came. The difference in energy of the doublets arises from the parallel an anti-parallel nature of the spin and orbital angular momentum of the electron. The relative intensities of the doublet peaks are given by the ratio of their respective degeneracies (2j + 1) and thus the area ratios of the doublets is known (**Table 1**).

Sub-shell	j value	Area Ratio
s	1/2	-
p	1/2 , 3/2	1:2
d	3/2 , 5/2	2:3
f	5/2 , 7/2	3:4

Table 1. Spin-orbit coupling parameters

In this body of work, the Ge $2p_{3/2}$ peaks are used to study the Ge surface. The Ge $2p_{1/2}$ feature contains the same information at higher binding energy. The Ge 3d peaks are present at the lower end of the binding energy scale since the 3d electrons have high E_K upon photoemission. The Ge 2p peaks are more surface sensitive than 3d peaks. To understand why, one must first understand the inelastic mean-free path

(IMFP) of electrons. The IMFP is the average distance between collisions in which a photoelectron loses energy. If a photoelectron loses kinetic energy due to a collision, it will contribute to the spectrum background rather than to the characteristic 'no-loss' peak. The IMFP value for Ge 3d electrons is greater than that of Ge 2p electrons. Ge 3d electrons can therefore travel further through a film before losing energy to collisions and thus originate from deeper in the sample. Since the focus of this work is to probe organic SAMs on Ge and to measure oxide growth on a sub-2 nm scale, the surface sensitivity of the Ge 2p peaks makes them more useful for surface characterisation.

X-rays from an Al source (hv = 1486.6 eV) were used throughout this body of work. A range of other anode materials are available for XPS however the most commonly used among them are Mg X-ray sources (hv = 1253.6). Using a different X-ray source results in different X-ray energies and line widths in the acquired spectra.

Throughout, acquired XPS data is used to calculate oxide film thicknesses and in **Chapter 3**, XPS data is used to calculate the thickness of a 1-hexanethiol SAM on Ge. Oxide thicknesses were calculated using the method outlined previously by Murakami et al.[4]

$$d_{GeO_2} = \lambda_{GeO_2} sin\theta\ ln\left(\frac{I_{Ge}^{\infty}}{I_{GeO_2}^{\infty}}\frac{I_{GeO_2}}{I_{Ge}} + 1\right)$$

where λ_{GeO_2} is the inelastic mean free path for the Ge 2p transition, which is 0.9 nm; the photoemission angle θ is 90°; $I_{Ge}^{\infty}/I_{GeO_2}^{\infty}$ is the ratio of the Ge 2p signal from

infinitely thick Ge to infinitely thick GeO_2 and is 1.73; I_{GeO_2} is the intensity of the of native oxide (GeO_2) peak from curve fitting the Ge 2p feature; I_{Ge} is the intensity of the metallic Ge peak from curve fitting the Ge 2p peak. One might expect for the minimum non-zero oxide thickness to be ~ 2.8 Å since that is the GeO_2 unit cell length[2]; however, the calculated oxide thickness are representative of the average oxide thickness across the sample. Since islands of oxide are likely, reported oxide thicknesses may be less than the length of the GeO_2 unit cell.

Calculation of the thickness of the SAM overlayer was performed following the methodology originally defined by Cumpson et al. [5]

$$ln\left(\frac{I_o S_o}{I_s S_s}\right) - \left(\frac{\lambda_o}{\lambda_s}\right)\frac{1}{\lambda_o \cos\theta} - ln\,2 = ln\,sin\,h\left(\frac{t}{2\lambda_o \cos\theta}\right)$$

where I_o and I_s represent the respective measured peak intensities of the overlayer (HT-SAM) and the substrate peaks. S_o and S_s refer to the relative sensitivity factors for the overlayer and the substrate, respectively. λ_o and λ_s are the attenuation lengths of electrons in the overlayer and the substrate. θ is the emission angle with respect to the surface normal. The peak intensity of the overlayer peak, I_o, and the peak intensity of the substrate peak, I_s, were determined using CasaXPS software after a transmission correction. The relative sensitivity factors for the substrate peak S_s and the overlayer peak S_o were also obtained from the CasaXPS library. The practical electron attenuation length (EAL) in the overlayer, l_o, was estimated, using the NIST Electron Effective Attenuation Length (EAL) database, to be 2.58 ± 0.2 nm for the Ge 3d component.

2.2   Water Contact Analysis

Water contact analysis (WCA) is a powerful and relatively simple characterisation technique used to probe the wetting properties of thin films. The method uses the polar nature of water molecules to give insight into the kind of surface termination that is present on the sample being probed. Water molecules, having a dipole, will interact more favourably with surfaces where a dipole exists and thus will wet this kind of surface more than a surface without a separation of charge. For example, the non-polar head and carbon backbone of a thiol molecule repels water and so the wettability of a Ge surface passivated by thiol molecules is less than that of an as-received Ge surface – terminated by native oxide and thus electronegative O atoms. WCA is used throughout this thesis as a method of determining the hydrophobicity of surfaces that are terminated differently and when used in tandem with XPS, much about the surface of the Ge can be discerned.

2.3   Atomic Force Microscopy

Atomic force microscopy (AFM) is a high-resolution type of scanning probe microscopy (SPM) that is used by surface scientists to measure the surface topology of materials. AFM is utilised throughout this body of work to track any change in the roughness of Ge(100) surfaces. What may seem like a non-significant increase of roughness on planar Ge may translate to considerable roughness when transposed to Ge nanostructures. Roughness will be a critical factor in future devices that utilise GAA nanosheet or nanowire architectures since these structures have high surface to bulk ratios. As such, an effort to track and minimise Ge surface roughness is undertaken in this body of work. Unlike WCA and XPS, AFM (as it is used here) does

not give insight into Ge surface termination – simply an insight into surface roughness is ascertained.

An AFM consists of a cantilever with a sharp tip that is scanned across the sample surface at a desired scanning frequency. There are three AFM operating modes:

1. Contact mode: where the tip scans the sample in close contact with the surface and the cantilever traces the surface topology.

2. Non-contact mode: where the tip is hovered 10-150 Å above the sample surface. Weak, attractive van der Waals forces between the cantilever tip and the surface are detected and topographic images are constricted by scanning the tip above the sample surface.

3. Tapping mode: where the cantilever vertically oscillates at or near the resonant frequency of the cantilever such that it 'taps' the sample surface. When the cantilever is in contact with the surface, the oscillation is reduced due to energy loss caused by contacting the surface. The dampening of the oscillation amplitude is used to measure and identify surface features.

Tapping mode AFM is utilised throughout this study to measure Ge surface roughness. The value used to give insight into the roughness of a surface is known as the root-mean square (RMS) value. RMS is the root mean square average of the profile height deviations from the mean line. As-received Ge surfaces have a RMS value between 0.2 and 0.3 nm depending on the supplier.

2.4　First Principles Density Functional Theory Simulations

DFT is a computational quantum mechanical modelling method used across the sciences to investigate the electronic or nuclear structure of systems comprised of many bodies such as atoms or molecules.[6] First principle density functional theory simulations as implemented in the Vienna Ab Initio Software Package (VASP) [7, 8] are used to model thiol-passivated Ge(100) surfaces and specifically to model the effect humidity has on the stability of the SAM and the reoxidation of the passivated Ge surfaces in **Chapter 4** and the effect thiol chain length has on SAM stability in **Chapter 5**.

The simulations were performed by Dr. Barbara MacCioni and Dr. Michael Nolan in the Tyndall National Institute, Cork, Ireland. Since modelling of thiol SAMs on Ge was undertaken, the following valance electron configurations were used; for germanium; Ge $4s^2$ and $4p^2$, for chlorine; Cl $3s^2$ and $3p^5$, for sulfur; S $3s^2$ and $3p^4$, for carbon; C $2s^2$ and $2p^4$, for oxygen O $2s^2$ and $2p^4$, and for hydrogen; H $1s^1$. For the calculations, a plane wave basis set in a 3-dimentional periodic slab model of the Ge substrate with DFT-optimised lattice constants are used. Further information about the specific modelling methods are available in **Chapters 4 & 5** where DFT modelling is used.

2.5   References

1.   Hertz, H., *Untersuchungen uber die Ausbreitung der Elektrischen Kraft Einleitung*. Sandig Reprint Verlag, Veduz, 1993, 1894: p. 184-198.

2.   Einstein, A., *Über Einen die Erzeugung und Verwandlung des Lichtes Betreffenden Heuristischen Gesichtspunkt.* Annalen der Physik, 1905. **322**(6): p. 132-148.

3.   Rutherford, E., *XXXVII. The Connexion Between The β and γ Ray Spectra.* The London, Edinburgh, and Dublin Philosophical Magazine and Journal of Science, 1914. **28**(165): p. 305-319.

4.   Murakami, H., T. Fujioka, A. Ohta, T. Bando, S. Higashi, and S. Miyazaki, *Characterization of Interfaces between Chemically Cleaned or Thermally Oxidized Germanium and Metals*. 2010, ECS.

5.   Cumpson, P.J., *The Thickogram: a Method for Easy Film Thickness Measurement in XPS*. Surface and Interface Analysis, 2000. **29**(6): p. 403-406.

6.   Geerlings, P., F. De Proft, and W. Langenaeker, *Conceptual Density Functional Theory.* Chemical Reviews, 2003. **103**(5): p. 1793-1874.

7.   Kresse, G. and J. Furthmüller, *Efficiency of Ab-Initio Total Energy Calculations for Metals and Semiconductors using a Plane-Wave Basis Set.* Computational Materials Science, 1996. **6**(1): p. 15-50.

8.   Kresse, G. and J. Furthmüller, *Efficient Iterative Schemes for Ab-Initio Total-Energy Calculations using a Plane-Wave Basis Set.* Physical Review B, 1996. **54**(16): p. 11169-11186.

Chapter 3

Vapour-Phase Passivation of Chlorine-Terminated Ge(100) using Self-Assembled Monolayers of Hexanethiol

This chapter is adapted from the following *ACS Applied Materials & Interfaces* publication and EMRS presentation. Consequently, certain concepts within this chapter may be repeated in other chapters.

Publication:

S. Garvey, J.D. Holmes, Y.S. Kim, and B. Long, *Vapour-Phase Passivation of Chlorine-Terminated Ge(100) using Self-Assembled Monolayers of Hexanethiol.* ACS Applied Materials & Interfaces, **2020**.

Presentation:

S. Garvey, J.D. Holmes, B. Long, *Vapour-Phase Passivation of Germanium using Aliphatic Thiols for Integration into Silicon-Based Systems*, 2019 EMRS Spring Meeting, Nice, France, 27-31 May, **2019** (**Talk**).

3.1 Abstract

Continued scaling of electronic devices shows the need to incorporate high mobility alternatives to silicon, the cornerstone of the semiconductor industry, into modern field effect transistor (FET) devices. Germanium is well poised to serve as the channel material in FET devices as it boasts an electron and hole mobility more than twice and four times that of Si, respectively. However, its unstable native oxide makes its passivation a crucial step towards its potential integration into future FETs. The International Roadmap for Devices and Systems (IRDS™) predicts continued aggressive scaling not only of the device size but also of the pitch in nanowire arrays. The development of a vapour-phase chemical passivation technique will be required to prevent the collapse of these structures that can occur due to the surface tension and capillary forces that are experienced when tight pitched nanowire arrays are processed via liquid-phase chemistry. Reported here, is a vapour–phase process using hexanethiol for the passivation of planar Ge(100) substrates. Results benchmarking it against its well-established liquid-phase equivalent are also presented. X-ray photoelectron spectroscopy (XPS) was used to monitor the effectiveness of the developed vapour-phase protocol where the presence of oxide was monitored at 0 h, 24 h and 168 h. Water contact angle (WCA) measurements compliment these results by demonstrating an increase in hydrophobicity of the passivated substrates. Atomic force microscopy (AFM) monitored the surface topology before and after processing to ensure the process does not cause roughening of the surface, which is critical to demonstrate suitability for nanostructures. It is shown that a 200 minute vapour-phase passivation procedure generates stable, passivated surfaces with less roughness than the liquid-phase counterpart.

3.2   Introduction

Silicon (Si) is an essential part of modern technology since it forms the basis of the integrated circuits that are found in electronic devices. It also plays a critical role in infrared sensors [1], solar panels [2] and chemical sensors [3] and has been the semiconductor of choice for more than 60 years, owing to its relative abundance, mechanical strength and stable native oxide. However, as the need for faster, more efficient processors grows, other materials [4-7] and novel architectures [8] are being studied with the intention that they be incorporated in devices alongside Si.

As mentioned, germanium (Ge) is an attractive candidate as a channel material, however, the germanium's native oxide is a complex system with a range of oxidation states (+1, +2, +3, +4).[9] The bulk of this oxide, GeO_2, is problematic from a device perspective since it is unstable and the interface between it and the underlying Ge is characterised by defects which lead to charge trapping and poor overall device performance.[10] In FET devices, the interface between the dielectric and the underlying channel material is critical to the operation of the device. Ultimately, it is the nature of the native oxide that has hindered the practical use of Ge to date. GeO_2 can be removed by treating the Ge with a halide acid (most commonly HF or HCl) solution, however, the resulting H-terminated or Cl-terminated Ge surfaces have been shown to rapidly reoxidise upon exposure to the ambient.[11-13] It is for this reason that the oxide must be removed and replaced with a passivating layer which inhibits reoxidation such that a more reliable dielectric can be deposited on the passivated Ge surface.

There have been a number of reports on the passivation of Ge using liquid-phase chemistry. Cullen et al. first reported the liquid-phase chemical functionalisation of a Cl-terminated Ge surface using ethyl Grignard in 1962.[14] Choi and Buriak then

demonstrated the hydrogermylation of H-terminated Ge which mirrored the hydrosilylation reactions which had been carried out on Si.[15] Hanrath et al. have subsequently shown that the hydrogermylation reaction is applicable to H-terminated Ge nanowires also.[16] Both the Grignard chemistry and the hydrogermylation reaction result in a Ge-C bond. Alkanethiol liquid-phase chemistry has also been developed for Ge which results in the formation of a Ge-S bond.[17] The vapour-phase passivation of Group IVA semiconductors has also been explored and dates back to the early 1960's whereby Si and Ge were passivated by halides [14, 18-23], a range of organics [13, 24-29], nitrides and oxynitrides [30-33]. For example, Degen et al. have reported the vapour-phase passivation of Si(100) and Si(111) using short-chain alkynes for NEMS and MEMS devices.[34] Kosuri et al. have described the adsorption kinetics of 1-decyene on H-terminated Si(100)[35] and Si(111)[36] and also the adsorption kinetics of 1-alkanethiols on Ge(111)[37] surfaces. Takenaka et al. have reacted Ge surfaces with vaporised tertiarybutylarsine (TBA) which is an arsenic source for Ge doping.[38, 39] In this report, a facile approach for the vapour-phase passivation of oxide-free, chlorine-terminated Ge(100) using a short-chain alkanethiol (1-hexanethiol) at ambient pressure and low temperature (140°C) is demonstrated.

The International Roadmap for Devices and Systems (IRDS™) predicts that the fin/nanowire diameter, channel length and fin/nanowire pitch of these devices will all decrease in size from one technology node to another.[40] The greatest predicted decrease in size is in the fin/nanowire pitch. Vapour-phase passivation routes offer the ability to passivate structures with small dimensions and pitches without causing the damage that liquid-phase alternatives can cause. An example of the impact of liquid-phase chemical processing on the structure of suspended nanostructures can be seen in **Figure 1**, where released Si nanowires have stuck together due to capillary forces,

after etching in an aqueous solution of hydrofluoric acid (HF). An example of a novel liquid-phase approach that has been shown to be effective at passivating nanostructures is to conduct the passivation reactions in a critical-point drier as demonstrated by Tao et al. for the alkylation and amination of Si.[41] Otherwise, vapour-phase alternatives such as the one documented here, can be implemented.
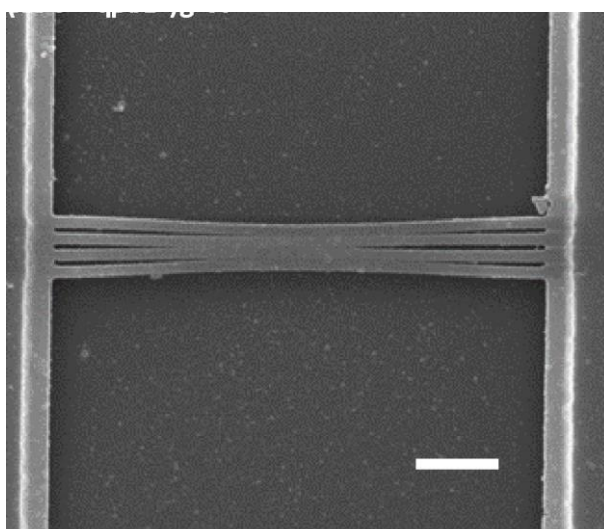
Figure 1. SEM image of 60 nm long Si nanowires with a 20 nm spacing after dipping in HF, highlighting the effect of the capillary forces experienced during liquid-phase processing.

To date, the bulk of the work carried out on self-assembled monolayers (SAMs) on Ge has focused on using 1-dodecanethiol, which has 12 carbon atoms, to form SAMs on the Ge surface.[37, 42, 43] The preference for this work was to choose a thiol molecule with the highest vapour pressure possible (to enable effective vapourisation) while still forming good quality monolayers. A range of aliphatic thiol molecules with carbon backbones ranging in length from 2 to 12 carbons were investigated for their ability to passivate Ge and inhibit oxidation of the underlying Ge in 24 hours (see **Figure 4**). 1-Hexanethiol (HT) was ultimately chosen as the aliphatic

thiol molecule to passivate Ge in this study due to its relatively high vapour pressure and effective passivation of Ge.
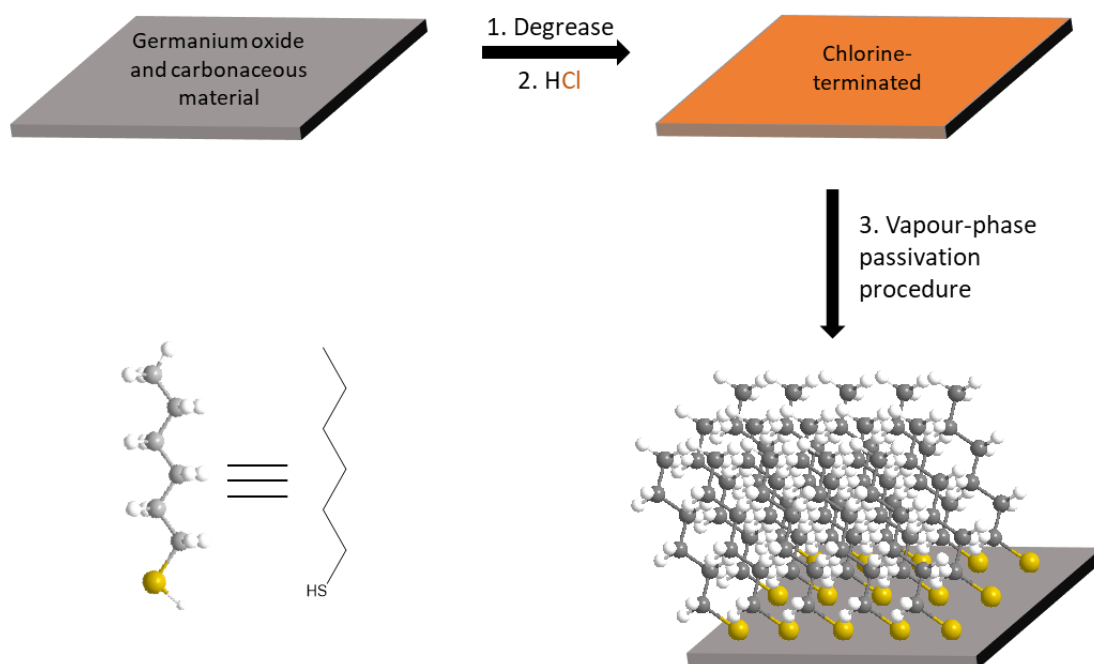
Figure 2. Schematic of oxide removal and passivation procedure for Ge using hexanethiol.

A SAM is formed when a single layer of molecules bonds to a surface in a self-limiting fashion to yield a surface that is chemically stable. Herein, HT molecules are reacted in the vapour-phase with a Cl-terminated Ge(100) surface. A mechanistic explanation for what occurs during the 1-alkanethiol passivation of Cl-terminated Ge(100) has been discussed by Bent et al.[13] They explore three possible routes for the passivation; namely a hydrohalogenic elimination pathway, an elimination and subsequent insertion pathway and a pathway which involves the cleavage of the dimer bond between Ge atoms at the surface. Their density functional theory calculations show that adsorption of 1-alkanethiols on halide-terminated Ge surface via hydrohalogenic acid elimination (**Figure 3**) is kinetically favourable at room

temperature. Thus, the reaction of HT with Cl-terminated Ge(100) is likely to occur via this pathway and the Ge dimer bond is likely to remain unbroken.[13]
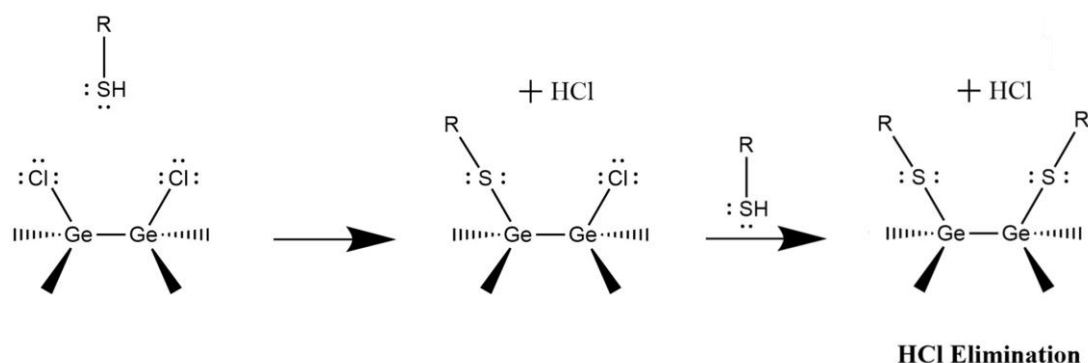
Figure 3. Proposed HCl elimination pathway for thiol reaction with Cl-terminated Ge.

The use of SAMs to augment the surface properties of a variety of materials such as gold,[44, 45] silicon[46] and copper[47] has been extensively documented in the literature. A common use for SAMs on Ge is to inhibit the growth of the unreliable oxide.[42, 43] In this study, the authors demonstrate a method to passivate oxide free, Cl-terminated Ge(100) using HT in the vapour-phase. This method is shown to be effective at preventing the regrowth of native Ge oxide for 24 hours.

3.3   Methods

All chemicals were purchased from Sigma-Aldrich unless otherwise stated. P-type germanium wafers were purchased from Umicore. Ge wafers were cut into 1 cm^2 coupons and degreased by sonication in acetone for 3 minutes then rinsed in IPA and dried under a stream of N$_2$. GeO$_2$ was removed by etching the coupons in 20% HCl for 10 minutes followed by drying under N$_2$. To achieve vapour-phase passivation, the coupons were loaded into a HiP MS series micro reactor (**Figure 4**) in a glovebox with

an atmosphere of < 0.5ppm O_2 and H_2O. The reactor was assembled in the glovebox to ensure no water vapour was present which could have oxidised the chlorine-terminated, oxide-free Ge prior to the vapour-phase thiol reaction. The assembled reactor was then connected to HiP three way/two stem connection valves on both the inlet and exhaust. The reactor was then loaded into a furnace.
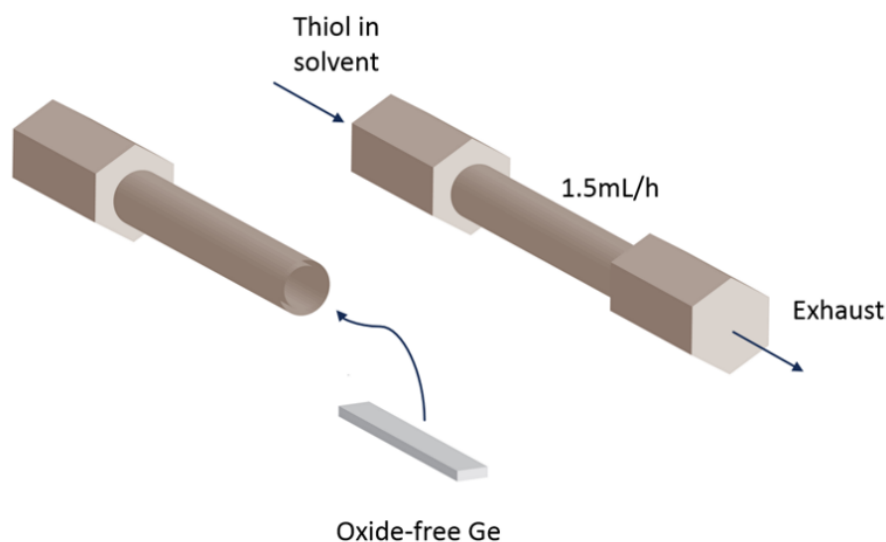
Figure 4. Schematic of HiP MS series micro reactor configuration.

A 0.1M solution of thiol in toluene was degassed using the freeze-pump-thaw (FPT) method. This method involves freezing the thiol solution under N_2 using liquid nitrogen and then allowing the solution thaw under vacuum (10^{-3} Torr) to remove undesirable gases present in the solvent. This method was repeated 3 times - until there was no more evolution of gas from the thiol solution. The degassed thiol solution was then syringed from the round-bottom flask using a 10 mL Luer-lock syringe which had been dried in a vacuum oven at 60°C overnight and then purged with N_2 prior to filling with the thiol solution. The Luer-lock syringe was used to pump the thiol solution at 1.5 mL/hr into the reactor at 140°C, carried by a constant flow of H_2 in Ar. After 200 minutes, the furnace was turned off and the injection of the thiol solution

into the reactor was stopped. At this point, 5 mL of the thiol solution had been pumped through the reactor. The reactor was then allowed to cool for 30 minutes before the samples were removed. The samples were then sonicated in acetone for 5 minutes, rinsed with propanol and dried under a stream of N_2. In the case of the Ge samples passivated using a liquid-phase chemical procedure, a 0.1M solution of the thiol molecule in toluene was degassed using the FPT method described previously. Oxide-free, Cl-terminated Ge samples were refluxed in the solution under an N_2 atmosphere using Schlenk line apparatus for 24 hours as is common in the literature to achieve thiol SAMs of high quality on Ge.[13, 29, 43] Samples were exposed to 40% relative humidity (RH) at 20°C in a Vötsch temperature test chamber to emulate ambient conditions for 24 hours to track what affect the ambient had on the samples. A 200 minute reaction time was shown to be a sufficient amount of time to create stable SAMs; however, the authors do not assert that this is the minimum amount of time required.

Atomic force microscopy was used to determine if the processing affected surface roughness. Water contact angle analysis was used to determine the hydrophobicity of the sample surface which gives an indication of the quality of the SAM and X-ray photoelectron spectroscopy was used to get elemental analysis of the Ge surface post reaction and after exposure to the ambient for 24 hours to determine if the passivated surface was resistant to oxidation. Passivated samples were transported under a positive pressure of N_2 in a SPI-DRY™ Sample Preserver to the characterisation tools.

3.3.1 Atomic Force Microscopy (AFM)

All AFM measurements in this study were taken using tapping mode Veeco Multimode V at room temperature over a 3 x 3 µm^2 scanning area. Tapping mode is preferred to contact mode when working with SAMs since the SAM can be affected by the probe being in constant contact with the surface. Tapping mode bypasses this problem since the probe is not dragged along the surface.

3.3.2 Water Contact Angle (WCA)

An image of a 50 µL drop of deionised water on the Ge surface was obtained and the angle formed between the water, Ge surface and air was measured. The greater the angle, the more hydrophobic the sample. Here, the wettability of a Ge surface gives an indication as to whether the thiol molecule has reacted with that surface. Considering the tail of the HT molecule is non-polar in nature, an increase in hydrophobicity indicates that a thiol SAM is present on the Ge surface.

3.3.3 X-Ray Photoelectron Spectroscopy (XPS)

XPS spectra were acquired on an Oxford Applied Research Escabase XPS System equipped with a CLASS VM 100 mm mean radius hemispherical electron energy analyser with multichannel detectors in an analysis chamber with a base pressure of 5.0×10^{-9} mbar. A pass energy of 50 eV, a step size of 0.7 eV and a dwell of 0.3 s was used for survey spectra which were swept twice. All core level scans other than the S 2p and 2s were acquired with a step size of 0.1 eV, a dwell time of 0.1 s and a pass energy of 20 eV averaged over 10 scans. The S 2p and 2s scans were acquired with a step size of 0.1 eV, a dwell time of 0.1 eV and a pass energy of 50 eV averaged over 20 scans. This was done to maximise the intensity of the S 2p peaks so accurate peak

fitting could be carried out. A non-monochromated Al-Kα X-ray source (1486.58 eV) at 100 W power (10 mA, 10kV) was used for all scans. All spectra were acquired at a take-off angle of 90° with respect to the analyser axis and were charge corrected with respect to the C 1s photoelectric line at 284.8 eV. A Shirley type background was used for construction and peak fitting of synthetic peaks. Synthetic peaks were a mix of Gaussian-Lorenzian, the Ge 2p spectra were fit using Gaussian-Lorentzian peak shape GL(90) for the elemental Ge peak and Lorentzian peak shape LA(1.53,243) for all other peaks. The relative sensitivity factors used are from a CasaXPS library containing Scofield cross-sections.

3.4   Results & Discussion

Alkanethiol passivation of Ge is a well-established process that has been used by many to augment the surface properties of Ge.[29, 48-50] However, the majority of the literature pertains to passivation using 1-dodecanethiol [42, 51, 52] since the heavily studied DT SAMs on Au system [45, 53] is the system from which best practices for Ge were adopted. Using the liquid-phase passivation method, a number of aliphatic thiol molecules with carbon backbones ranging in length from 2 to 12 carbons were used to passivate Ge in an effort to to select a thiol molecule suitable for vapour-phase passivation trials. The authors desired to select a thiol molecule which could easily be promoted into the vapour phase (relatively low Mw) while still able to form SAMs on Ge that inhibit Ge surface reoxidation. HT outperformed the other thiols tested in terms of Ge reoxidation upon exposure to ambient conditions for 24 hours (as evidenced by the Ge 2p spectra shown in **Figure 5)** and so was chosen for trials using the vapour-phase approach that is detailed in this work.
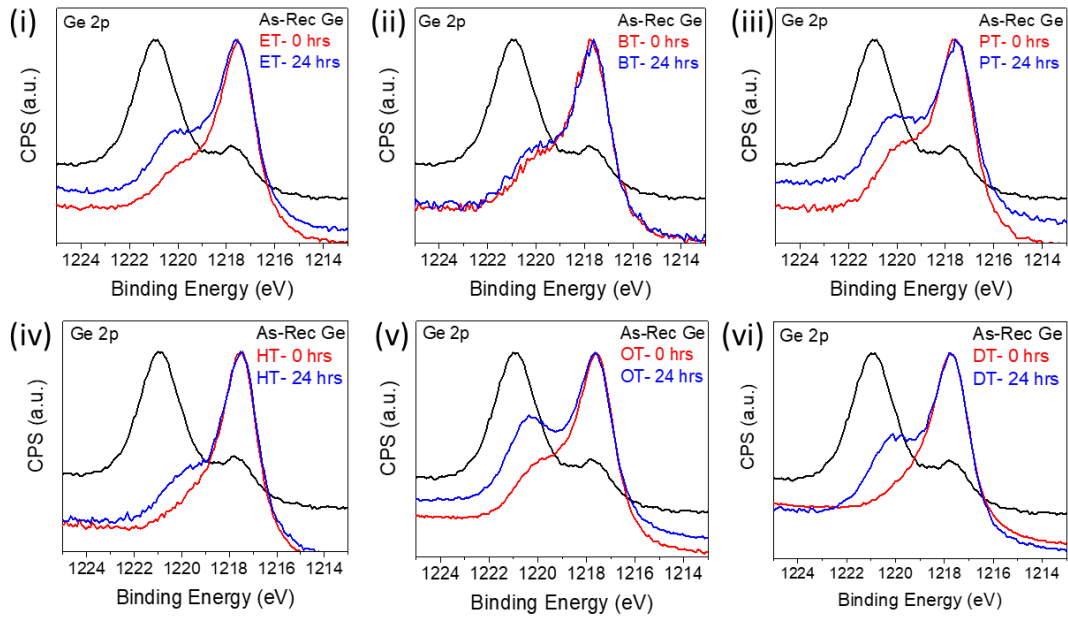
Figure 5. Ge 2p spectra of Ge passivated by **(i)** ethanethiol **(ii)** 1-butanethiol **(iii)** 1-pentanethiol **(iv)** 1-hexanethiol **(v)** 1-octanethiol and **(vi)** 1-dodecanethiol with 0 (red) and 24 (blue) hours exposure to ambient conditions.

3.4.3 Atomic Force Microscopy & Water Contact Analysis

An industry requirement for the passivation of Ge is that its surface remains oxide-free for a queue-time of 24 hours. This allows for maintenance or repair of instrumentation, which may result in the exposure of processed Ge to the ambient during device fabrication. Processed Ge wafers require a sufficiently robust passivation layer to avoid reoxidation of the substrates. Processes developed on planar Ge must be non-destructive such that they be transferrable to highly ordered, densely packed, high aspect-ratio Ge nanostructures. As a result, AFM was used to track the effect the processing had on the roughness of planar Ge surfaces. Since the surface to

bulk ratio for nanostructures is high, it is imperative that any processing has a negligible impact on surface roughness. Results for the liquid-phase passivation of Ge using HT are included for comparison.

Prior to the vapour-phase passivation of the Ge surface, the native oxide was removed using a 20% solution of HCl. This step relies on liquid-phase processing which would not be compatible with nanostructures, however in the context of an industrial setting a vapour phase alternative would be applied. The RMS value obtained for a clean Ge surface is 0.30 nm as seen in **Figure 6 (i)**. The inset in **Figure 6 (i)** highlights how the surface prior to any processing is hydrophilic, a shallow angle of less than 50° is obtained when a 50 uL drop of millipore deionised water is deposited onto the surface. This value is consistent for literature values of ultrasonic cleaned Ge surfaces.[54] The surface is hydrophilic since the water interacts favourably with the GeO_2 film present on the surface. After the HCl etch, a Cl-terminated Ge surface with an RMS value of 0.30 nm was obtained. Removing the oxide with HCl does not cause an increase in the surface roughness. The inset in **Figure 6 (ii)** illustrates how the chlorine-terminated Ge surface is also hydrophilic. A water contact angle of less than 50° is obtained since the water molecules interact favourably with the Cl-terminated Ge surface. This is consistent with the literature on Cl-terminated Ge whereby angles of 39-50° are observed.[54, 55] The AFM image in **Figure 6 (iii)**, illustrates how the vapour-phase HT passivation reaction does not cause an increase in Ge surface roughness and the degree of hydrophobicity of the Ge surface sharply increases to over 90° due to the presence of the thiol SAM. Increasing contact angle measurements for alkanethiol SAMs have been shown to correlate with the length of the alkanethiol molecule.[46] On Ge(100), alkanethiol SAMs consisting of 1-dodecanethiol molecules have been shown to display WCA of > 100°,[42] while SAMs consisting

of 1-octadecanethiol molecules (C18) have been shown to display WCA of > 115°.[52] In this study, HT, having a shorter C backbone, was found to form a SAM on Ge that yield a surface with a WCA of 90°. The sharp increase in the hydrophobicity of the Ge surface is a clear indication that the vapour-phase reaction occurred between the Cl-terminated Ge surface and the HT molecules. For comparison, the AFM and WCA data for a Ge surface which has been passivated using the liquid-phase chemistry approach have been included also. It is clear from the AFM image in **Figure 6 (iv)** that the surface roughness of the Ge is affected by the liquid-phase passivation procedure where an RMS value of 0.61 nm is observed along with a WCA of 85°. The increased WCA indicates that a HT-SAM is present on the surface however, the SAM is likely of lower quality than that obtained by the vapour-phase passivation since the WCA angle observed is lower.
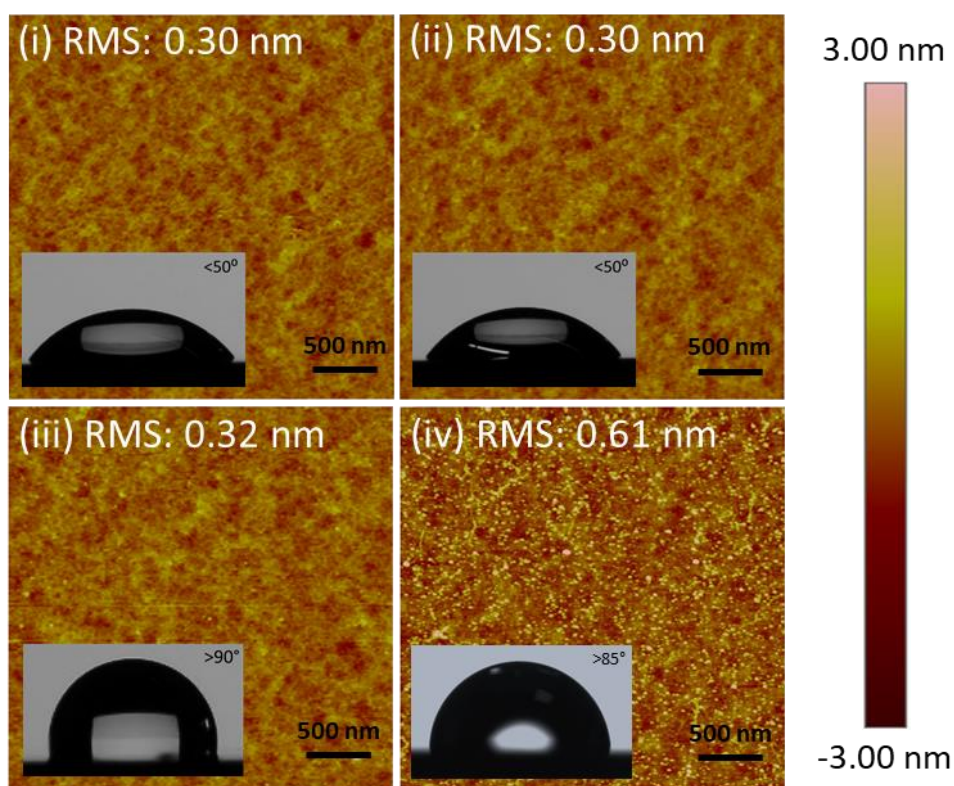
Figure 6. AFM images with water contact angle insets of **(i)** as-rec Ge **(ii)** HCl-treated Ge **(iii)** HT vapour-phase passivated Ge with 0 hours exposure to the ambient **(iv)** HT liquid-phase passivated Ge with 0 hours exposure to the ambient.

3.4.4 X-ray Photoelectron Spectroscopy Characterisation

In the literature, when discussing the oxidation of Ge, it is common to discuss the Ge 3d peak primarily; however, the 3d transition comes from electrons with high kinetic energy and therefore from a greater sampling depth when compared to the electrons from the 2p transition which have lower kinetic energy and so are more surface sensitive. Thus, in an attempt to highlight what is occurring at the surface of the Ge, the Ge 2p peak will be presented in this study. When fitting the oxide peaks, the suboxide peak position was fixed at 1.1 eV greater than the elemental Ge peak. GeO_2 peak position was not fixed since a trend was observed whereby the peak position shifted to higher binding energy upon oxidation. Oxide thickness was calculated using the method outlined by Murakami et al.[56]

$$d_{GeO_2} = \lambda_{GeO_2} sin\theta\, ln\left(\frac{I_{Ge}^{\infty}}{I_{GeO_2}^{\infty}}\frac{I_{GeO_2}}{I_{Ge}} + 1\right)$$

where λ_{GeO_2}, the inelastic mean free path for the Ge 2p transition is 0.9 nm; the photoemission angle θ is 90°; $I_{Ge}^{\infty}/I_{GeO_2}^{\infty}$ is the ratio of the Ge 2p signal from infinitely thick Ge to infinitely thick GeO_2 and is determined as 1.73; I_{GeO_2} is the intensity of

the of native oxide (GeO$_2$) peak from curve fitting the Ge 2p transition; I_{Ge} is the intensity of the metallic Ge peak from curve fitting the Ge 2p transition. This calculation was repeated to determine the thickness of the suboxide (GeO$_x$) component for each sample also. In this case, I_{GeO_x}, the fraction of suboxide (GeO$_x$) from curve fitting the Ge 2p was used in place of I_{GeO_2}.

Figure 7 (i) depicts the Ge 2p spectrum for an as-received Ge sample that has undergone no processing. As expected, there is a large peak at 1221.14 eV that corresponds to Ge^{+4} from GeO$_2$. There is also a peak evident at 1218.89 eV which is attributed to the suboxide, GeO. The thickness of the GeO$_2$ on as-rec Ge is 2.12 nm which is in agreement with literature values for as-rec Ge(100).[57] The thickness of the suboxide component was 0.56 nm. The suboxide component of Ge likely has contributions from Ge in +1, +2 and +3 states however these cannot be accurate resolved with the instrumentation available. Treatment of the as-received Ge with HCl removed both the native oxide and the suboxide component leaving a Cl-terminated surface which oxidised upon exposure to the ambient. This is evident in **Figure 7 (ii, iii)** where the Ge 2p peaks corresponding to the native oxide and suboxide are no longer present after the HCl etch but return after 24 hours of exposure to the ambient. A GeO$_2$ film, 0.34 nm thick grows in 24 hours of exposure to the ambient indicating that Cl-termination does not sufficiently prevent reoxidation of the Ge surface.
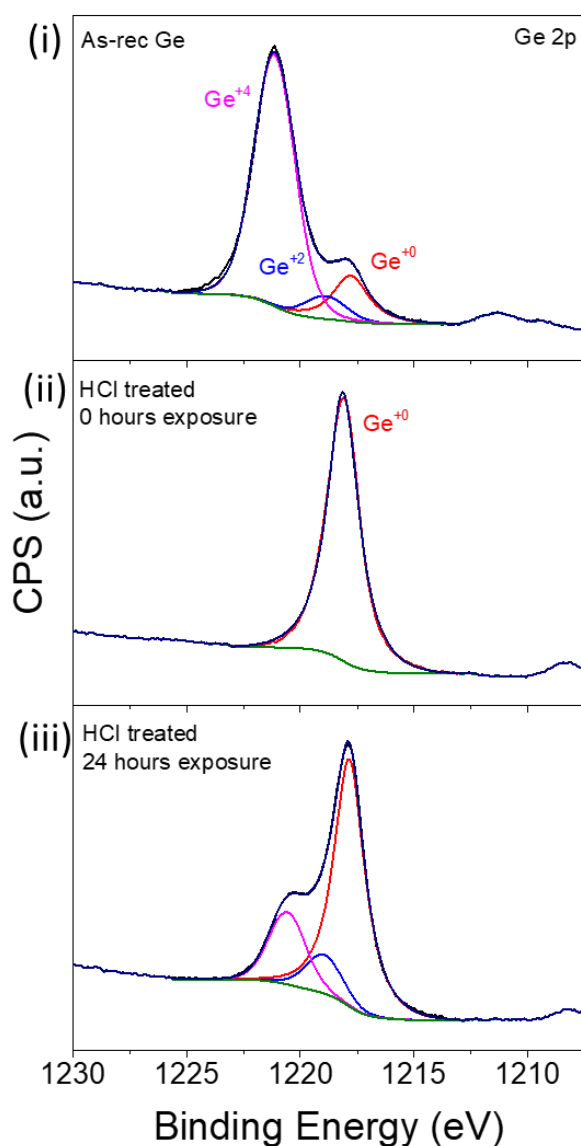
Figure 7. Ge 2p plots for **(i)** as-rec Ge **(ii)** and **(iii)** Cl-terminated Ge after 0 and 24 hours exposure to the ambient, respectively.

Figure 8 (i) depicts the Ge 2p spectra for a Ge sample that has had the native oxide removed by a HCl etch followed by passivation using HT in the vapour-phase. No GeO_2 is detected after the passivation reaction however, there is a component at 1219.2 eV which is likely attributable to Ge^{+2} from a mixture of Ge-O and Ge-S after the passivation reaction. An XPS tool with higher resolution would be needed to

attempt to resolve these components. The calculated thickness of these components is 0.16 nm. After 24 hours of exposure to the ambient, the GeO_2 film thickness was 0.08 nm. The growth of oxide is minimal and as such can be used as a proxy for quality of SAM on the Ge surface. The more stable and uniform the SAM, the slower the growth of oxide. In this case, the vapour-phase passivated Ge exhibits inhibition of oxide growth and thus one can infer that a stable SAM is present. The peak at 1219.2 eV is still present after the passivation reaction is unchanged with a calculated thickness of 0.16 nm. After 168 hours of exposure to the ambient, GeO_2 thickness was calculated to be 0.25 nm with the thickness of the component at 1219.2 eV calculated to be 0.20 nm indicating that continued oxidation does occur albeit slowly. The thickness of the oxide film on the HT vapour-phase passivated sample after 168 hours exposure to the ambient is less than that of the Cl-terminated sample after only 24 hours of exposure (0.25 nm vs. 0.34 nm).
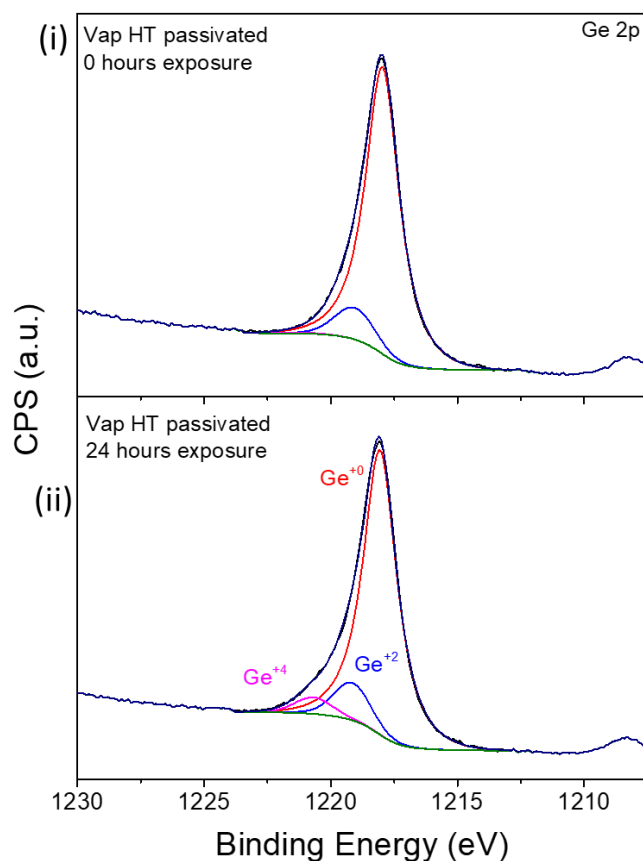
Figure 8. (i) and **(ii)** Ge 2p plots for HT vapour-phase passivated Ge with 0 and 24 hours exposure to the ambient, respectively.

An inspection of the O 1s peaks for the vapour-phase passivated Ge directly after the passivation reaction and after 24 and 168 hours of exposure to the ambient is illustrated in **Figure 9**. There is little growth in the intensity of the O 1s peak after 24 hours however after 168 hours some growth is observed indicating that the HT SAM passivation is effective at inhibiting oxidation of the Ge over 24 hours but that in the following 144 hours, a small amount of GeO_2 growth occurs (0.17 nm growth in the 144 hours proceeding the first 24 hours).
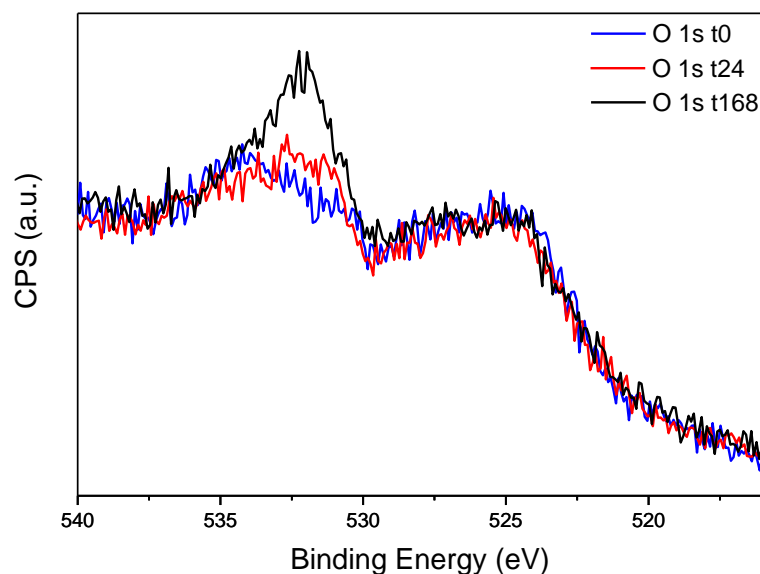
Figure 9. O 1s spectra of Ge passivated by HT in the vapour-phase after 0 (blue), 24 (red) and 168 (black) hours exposure to the ambient.

The S 2p peak occurs at 162.3 eV which overlaps with a Ge 3p satellite feature, however through peak fitting, the S 2p peak can be clearly differentiated from the Ge 3p sat. There is no S 2p peak present in the as-rec Ge sample (**Figure 10 (i)**), as expected. However, a clear S 2p peak is observed at 162.3 eV in **Figure 10 (ii)** for the HT passivated sample. That peak is still evident after 24 hours of exposure to the ambient (**Figure 10 (iii)**), albeit with slight lower intensity, which indicates that the thiol SAM is stable on the surface for 24 hours. A possible explanation as to why the intensity of the S 2p peak diminishes slightly in 24 hours is that the growth of a small amount of oxide on the surface in 24 hours displaces the thiol molecules, resulting in a slightly less intense S 2p peak. The XPS measurements showing the presence of sulfur on the vapour-phase HT-treated surface is clear indication that the vaporised HT reacted with the Cl-terminated Ge surface. The presence of the S 2p peak after 24 hours and the minimal growth of oxide observed in **Figure 8** indicates that the HT-

SAM on the Ge surface is stable and more effective than chlorine at preventing oxidation from exposure to the ambient for 24 hours.
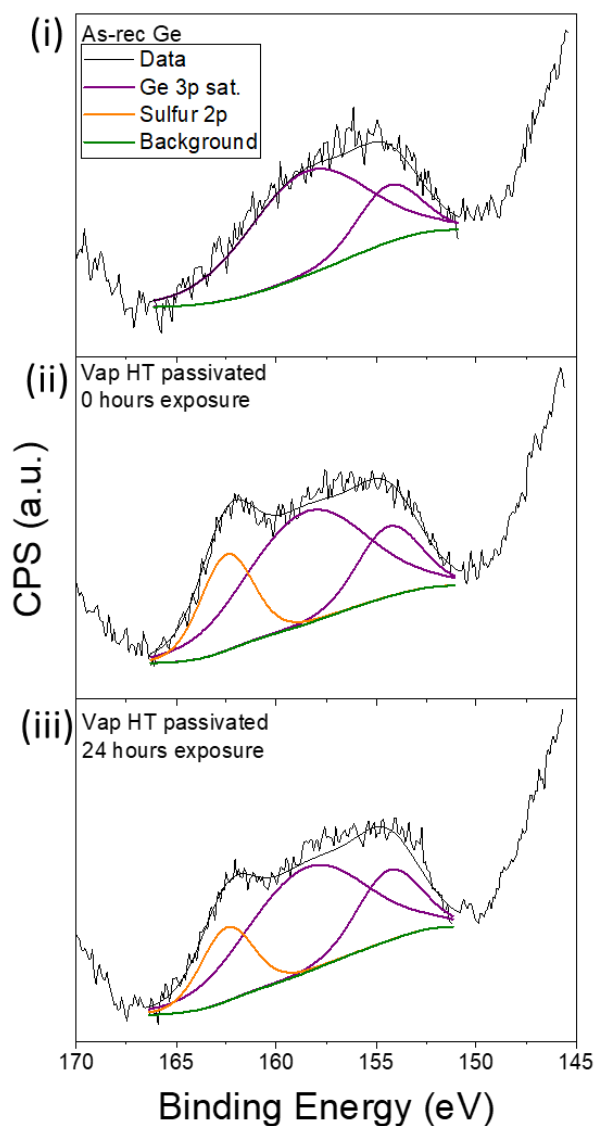
Figure 10. (i) as-rec Ge showing no S peak **(ii)** HT vapour-phase passivated Ge with 0 hours exposure to the ambient **(iii)** HT vapour-phase passivated Ge with 24 hours exposure to the ambient.

For comparison with the vapour-phase passivation approach, **Figure 11** elucidates the liquid-phase passivation of Ge, where some native oxide is present

directly after the passivation reaction and the oxide thickness is 0.21 nm. The presence of this oxide indicates that the during the 24-hour processing, a small amount of Ge oxidation occurs. This is not the case with the shorter (~200 minute) vapour-phase reaction where there is no detectable GeO_2 directly after the passivation reaction. Shorter processing times are desirable since they decrease the likelihood that oxidation can occur. The thickness of the oxide for the liquid-phase passivated sample increases to 0.34 nm after 24 hours of exposure to ambient conditions (a growth of 0.13 nm).
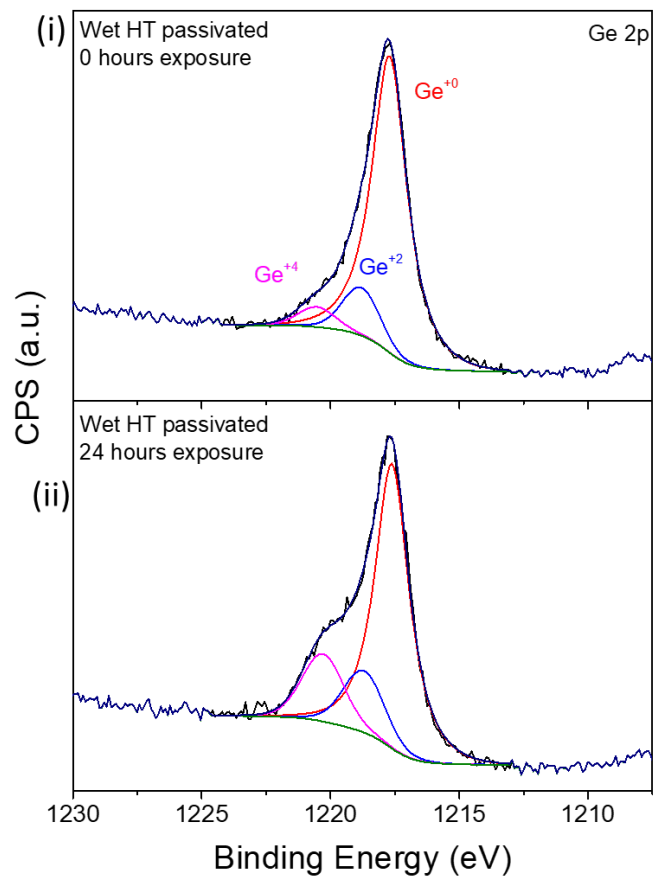
Figure 11. (i) and **(ii)** Ge 2p spectra for the liquid-phase passivation of Ge illustrating the presence of native oxide after 0 and 24 hours exposure to the ambient, respectively.

This XPS data, coupled with the WCA data from **Figure 6** indicate that the liquid-phase passivation reaction yields a SAM of which does not inhibit oxidation of the Ge as effectively as the vapour-phase passivated sample. The vapour-phase passivation method results eclipse those of the liquid-phase chemical passivation in relation to oxidation inhibition over 24 hours of exposure to the ambient. A summary of the oxide thicknesses is tabulated in **Table 1.**

	GeO_2 thickness (nm)	
Sample (Ge)	0 hrs exposure	24 hrs exposure
As-Rec.	2.12	2.12
HCl-treated	0	0.38
Vap. HT-passivated	0	0.08
Liq. HT-passivated	0.21	0.34

Table 2. Oxide thicknesses for as-rec, HCl-treated, vapour-phase passivated and liquid-phase passivated Ge(100) samples.

3.4.5 Estimation of Overlayer Thickness

XPS thickness measurement of the SAM overlayer for the vapour-phase passivated Ge was performed following the methodology originally defined by Cumpson et al. *[58]*

$$ln\left(\frac{I_o S_o}{I_s S_s}\right) - \left(\frac{o}{s}\right) \frac{1}{_o\, cos\, cos} - ln\, ln\, 2 = ln\, ln\, \square\square\square\, sin\, h\left(\frac{t}{2\,\, _o\, cos\, cos}\right)$$

where I_o and I_s represent the respective measured peak intensities of the overlayer (HT molecules) and the substrate peaks, S_o and S_s refer to the relative sensitivity factors for the overlayer and the substrate, respectively. L_o and L_s are the attenuation lengths of electrons in the overlayer and the substrate. l is the emission angle with respect to the surface normal. The peak intensity of the overlayer peak, I_o, and the peak intensity of the substrate peak, I_s, were determined using CasaXPS software after a transmission correction. The relative sensitivity factors for the substrate peak S_s and the overlayer peak S_o were also obtained from the CasaXPS library and manually inputted into the data processing software to remove instrumental factors which may affect quantification. The practical electron attenuation length (EAL) in the overlayer, l_o, was estimated, using the NIST Electron Effective Attenuation Length database, to be 2.58 $\pm$ 0.2 nm for the Ge 3d component. Using this method, the thickness of the SAM overlayer was estimated to be approximately 1 nm which is in accordance with the length of one HT molecule – the expected thickness of the monolayer.

3.5 Conclusions

In this study, a method to achieve the vapour-phase passivation of Ge(100) surfaces is outlined. The developed method is used to create HT-SAMs that inhibit reoxidation of the underlying Ge(100) surface for 24 hours and shows improved resistance to reoxidation up to 168 hours when compared to Cl-terminated Ge(100) surfaces. It was found that a 200 minute reaction time is sufficient to create SAMs that inhibit the

growth of oxide which improves on state-of-the-art liquid-phase processes that require up to 24 hours. To gain industry-acceptance, reduced reaction times are necessary. The procedure does not cause an increase in surface roughness of planar Ge and therefore demonstrates suitability for trials on Ge nanostructures that would otherwise be damaged by liquid-phase chemical processing.

3.6   References

1.   Singh, V., P.T. Lin, N. Patel, H. Lin, L. Li, Y. Zou, F. Deng, C. Ni, J. Hu, J. Giammarco, A.P. Soliani, B. Zdyrko, I. Luzinov, S. Novak, J. Novak, P. Wachtel, S. Danto, J.D. Musgraves, K. Richardson, L.C. Kimerling, and A.M. Agarwal, *Mid-Infrared Materials and Devices on a Si Platform for Optical Sensing.* Science and Technology of Advanced Materials, 2014. **15**(1): p. 014603.

2.   Pillai, S., K.R. Catchpole, T. Trupke, and M.A. Green, *Surface Plasmon Enhanced Silicon Solar Cells.* Journal of Applied Physics, 2007. **101**(9): p. 093105.

3.   Cui, Y., Q. Wei, H. Park, and C.M. Lieber, *Nanowire Nanosensors for Highly Sensitive and Selective Detection of Biological and Chemical Species.* Science, 2001. **293**(5533): p. 1289.

4.   Gupta, A., T. Sakthivel, and S. Seal, *Recent Development in 2D Materials Beyond Graphene.* Progress in Materials Science, 2015. **73**: p. 44-126.

5.   Manzeli, S., D. Ovchinnikov, D. Pasquier, O.V. Yazyev, and A. Kis, *2D Transition Metal Dichalcogenides.* Nature Reviews Materials, 2017. **2**: p. 17033.

6.   Mirabelli, G., C. McGeough, M. Schmidt, E.K. McCarthy, S. Monaghan, I.M. Povey, M. McCarthy, F. Gity, R. Nagle, G. Hughes, A. Cafolla, P.K. Hurley, and R. Duffy, *Air Sensitivity of MoS2, MoSe2, MoTe2, HfS2, and HfSe2.* Journal of Applied Physics, 2016. **120**(12): p. 125102.

7.   Tomioka, K., M. Yoshimura, and T. Fukui, *A III–V Nanowire Channel on Silicon for High-Performance Vertical Transistors.* Nature, 2012. **488**(7410): p. 189-192.

8.   Su, C., T. Tsai, Y. Liou, Z. Lin, H. Lin, and T. Chao, *Gate-All-Around Junctionless Transistors With Heavily Doped Polysilicon Nanowire Channels.* IEEE Electron Device Letters, 2011. **32**(4): p. 521-523.

9.   Schmeisser, D., R.D. Schnell, A. Bogen, F.J. Himpsel, D. Rieger, G. Landgren, and J.F. Morar, *Surface Oxidation States of Germanium.* Surface Science, 1986. **172**(2): p. 455-465.

10.   Binder, J.F., P. Broqvist, and A. Pasquarello, *Charge Trapping in Substoichiometric Germanium Oxide.* Microelectronic Engineering, 2011. **88**(7): p. 1428-1431.

11.   Bodlaki, D., H. Yamamoto, D.H. Waldeck, and E. Borguet, *Ambient Stability of Chemically Passivated Germanium Interfaces.* Surface Science, 2003. **543**(1): p. 63-74.

12.   Loscutoff, P.W. and S.F. Bent, *Reactivity of the Germanium Surface: Chemical Passivation and Functionalization.* Annual Review of Physical Chemistry, 2006. **57**: p. 467-495.

13.   Ardalan, P., Y. Sun, P. Pianetta, C.B. Musgrave, and S.F. Bent, *Reaction Mechanism, Bonding, and Thermal Stability of 1-Alkanethiols Self-Assembled on Halogenated Ge Surfaces.* Langmuir, 2010. **26**(11): p. 8419-8429.

14.   Cullen, G.W., J.A. Amick, and D. Gerlich, *The Stabilization of Germanium Surfaces by Ethylation.* Journal of The Electrochemical Society, 1962. **109**(2): p. 124-127.

15. Choi, K. and J.M. Buriak, *Hydrogermylation of Alkenes and Alkynes on Hydride-Terminated Ge(100) Surfaces.* Langmuir, 2000. **16**(20): p. 7737-7741.

16. Hanrath, T. and B.A. Korgel, *Chemical Surface Passivation of Ge Nanowires.* Journal of the American Chemical Society, 2004. **126**(47): p. 15466-15472.

17. Han, S.M., W.R. Ashurst, C. Carraro, and R. Maboudian, *Formation of Alkanethiol Monolayer on Ge(111).* Journal of the American Chemical Society, 2001. **123**(10): p. 2422-2425.

18. Bachelet, G.B. and M. Schlüter, *Structural Determination of Cl Chemisorption on Si[1] and Ge{111} by Total-Energy Minimization.* Physical Review B, 1983. **28**(4): p. 2302-2304.

19. Citrin, P.H., J.E. Rowe, and P. Eisenberger, *Direct Structural Study of Cl on Si {111} and Ge {111} Surfaces: New Conclusions.* Physical Review B, 1983. **28**(4): p. 2299-2301.

20. Fouchier, M., M.T. McEllistrem, and J.J. Boland, *Novel Adatom-Terminated Step Structure on the Ge(111)-(1×1):Br Surface.* Surface Science, 1997. **385**(1): p. l905-l910.

21. Göthelid, M., G. LeLay, C. Wigren, M. Björkqvist, and U.O. Karlsson, *Iodine Reaction and Passivation of the Ge(111) Surface.* Surface Science, 1997. **371**(2): p. 264-276.

22. Dharma-wardana, M.W.C., M.Z. Zgierski, D. Ritchie, J.G. Ping, and H. Ruda, *Comparison of Cluster and Slab Models of the Surface Structure of Cl-Terminated Ge(111) and GaAs(111) Surfaces.* Physical Review B, 1999. **59**(24): p. 15766-15771.

23. Cao, S., J.C. Tang, and S.L. Shen, *Multiple-Scattering and DV-Xa Analyses of a Cl-Passivated Ge(111) Surface.* Journal of Physics: Condensed Matter, 2003. **15**(30): p. 5261-5268.

24. Lal, P., A.V. Teplyakov, Y. Noah, M.J. Kong, G.T. Wang, and S.F. Bent, *Adsorption of Ethylene on the Ge(100)-2×1 Surface: Coverage and Time-Dependent Behavior.* The Journal of Chemical Physics, 1999. **110**(21): p. 10545-10553.

25. Teplyakov, A.V., P. Lal, Y.A. Noah, and S.F. Bent, *Evidence for a Retro-Diels−Alder Reaction on a Single Crystalline Surface: Butadienes on Ge(100).* Journal of the American Chemical Society, 1998. **120**(29): p. 7377-7378.

26. Lee, S.W., J.S. Hovis, S.K. Coulter, R.J. Hamers, and C.M. Greenlief, *Cycloaddition Chemistry on Germanium(001) Surfaces: the Adsorption and Reaction of Cyclopentene and Cyclohexene.* Surface Science, 2000. **462**(1): p. 6-18.

27. Filler, M.A., J.A. Van Deventer, A.J. Keung, and S.F. Bent, *Carboxylic Acid Chemistry at the Ge(100)-2 × 1 Interface: Bidentate Bridging Structure Formation on a Semiconductor Surface.* Journal of the American Chemical Society, 2006. **128**(3): p. 770-779.

28. Ardalan, P., N. Davani, and C.B. Musgrave, *Attachment of Alanine and Arginine to the Ge(100)-2×1 Surface.* The Journal of Physical Chemistry C, 2007. **111**(9): p. 3692-3699.

29.   Ardalan, P., C.B. Musgrave, and S.F. Bent, *Formation of Alkanethiolate Self-Assembled Monolayers at Halide-Terminated Ge Surfaces.* Langmuir, 2009. **25**(4): p. 2013-2025.

30.   Paine, D.C., J.J. Rosenberg, S.C. Martin, D. Luo, and M. Kawasaki, *Evaluation of Device Quality Germanium-Germanium Oxynitride Interfaces by High-Resolution Transmission Electron Microscopy.* Applied Physics Letters, 1990. **57**(14): p. 1443-1445.

31.   Tindall, C. and J.C. Hemminger, *HREELS Studies of the Chemistry of Nitrogen Hydrides on Ge(100): Formation of a Surface Nitride at Low Temperatures.* Surface Science, 1995. **330**(1): p. 67-74.

32.   Kim, H., P.C. McIntyre, C.O. Chui, K.C. Saraswat, and M.-H. Cho, *Interfacial Characteristics of HfO2 Grown on Nitrided Ge (100) Substrates by Atomic-Layer Deposition.* Applied Physics Letters, 2004. **85**(14): p. 2902-2904.

33.   Maggioni, G., S. Carturan, L. Fiorese, N. Pinto, F. Caproli, D.R. Napoli, M. Giarola, and G. Mariotto, *Germanium Nitride and Oxynitride Films for Surface Passivation of Ge Radiation Detectors.* Applied Surface Science, 2017. **393**: p. 119-126.

34.   Tao, Y., R. Hauert, and C.L. Degen, *Exclusively Gas-Phase Passivation of Native Oxide-Free Silicon(100) and Silicon(111) Surfaces.* ACS Applied Materials & Interfaces, 2016. **8**(20): p. 13157-13165.

35.   Kosuri, M.R., H. Gerung, Q.M. Li, S.M. Han, B.C. Bunker, and T.M. Mayer, *Vapor-Phase Adsorption Kinetics of 1-Decene on H-Terminated Si(100).* Langmuir, 2003. **19**(22): p. 9315-9320.

36.   Kosuri, M., H. Gerung, Q. li, S. Han, P. Herrera-Morales, and J. Weaver, *Vapor-Phase Adsorption Kinetics of 1-Decene on Hydrogenated Si(111).* Surface Science, 2005. **596**: p. 21-38.

37.   Kosuri, M.R., R. Cone, Q. Li, S.M. Han, B.C. Bunker, and T.M. Mayer, *Adsorption Kinetics of 1-Alkanethiols on Hydrogenated Ge(111).* Langmuir, 2004. **20**(3): p. 835-840.

38.   Takenaka, M., K. Morii, M. Sugiyama, Y. Nakano, and S. Takagi, *Gas Phase Doping of Arsenic into (100), (110), and (111) Germanium Substrates Using a Metal–Organic Source.* Japanese Journal of Applied Physics, 2011. **50**: p. 010105.

39.   Takenaka, M., K. Morii, M. Sugiyama, Y. Nakano, and S. Takagi, *Dark Current Reduction of Ge Photodetector by GeO2 Surface Passivation and Gas-Phase Doping.* Optics Express, 2012. **20**(8): p. 8718-8725.

40.   *International Roadmap for Devices and Systems*, in *More Moore*. 2018.

41.   Tao, Y., P. Navaretti, R. Hauert, U. Grob, M. Poggio, and C.L. Degen, *Permanent Reduction of Dissipation in Nanomechanical Si Resonators by Chemical Surface Protection.* Nanotechnology, 2015. **26**(46): p. 465501.

42.   Cai, Q., B. Xu, L. Ye, Z. Di, S. Huang, X. Du, J. Zhang, Q. Jin, and J. Zhao, *1-Dodecanethiol Based Highly Stable Self-Assembled Monolayers for Germanium Passivation.* Applied Surface Science, 2015. **353**: p. 890-901.

43.   Collins, G., D. Aureau, J.D. Holmes, A. Etcheberry, and C. O'Dwyer, *Germanium Oxide Removal by Citric Acid and Thiol Passivation from Citric Acid-Terminated Ge(100).* Langmuir, 2014. **30**(47): p. 14123-14127.

44.	Graupe, M., T. Koini, H.I. Kim, N. Garg, Y.F. Miura, M. Takenaga, S.S. Perry, and T.R. Lee, *Self-Assembled Monolayers of CF3-Terminated Alkanethiols on Gold.* Colloids and Surfaces A: Physicochemical and Engineering Aspects, 1999. **154**(1): p. 239-244.

45.	Vericat, C., M.E. Vela, G. Benitez, P. Carro, and R.C. Salvarezza, *Self-Assembled Monolayers of Thiols and Dithiols on Gold: New Challenges for a Well-Known System.* Chemical Society Reviews, 2010. **39**(5): p. 1805-1834.

46.	Bhartia, B., S.R. Puniredd, S. Jayaraman, C. Gandhimathi, M. Sharma, Y.-C. Kuo, C.-H. Chen, V.J. Reddy, C. Troadec, and M.P. Srinivasan, *Highly Stable Bonding of Thiol Monolayers to Hydrogen-Terminated Si via Supercritical Carbon Dioxide: Toward a Super Hydrophobic and Bioresistant Surface.* ACS Applied Materials & Interfaces, 2016. **8**(37): p. 24933-24945.

47.	Laibinis, P.E. and G.M. Whitesides, *Self-Assembled Monolayers of n-Alkanethiolates on Copper are Barrier Films that Protect the Metal Against Oxidation by Air.* Journal of the American Chemical Society, 1992. **114**(23): p. 9022-9028.

48.	Collins, G., P. Fleming, S. Barth, C. O'Dwyer, J.J. Boland, M.A. Morris, and J.D. Holmes, *Alkane and Alkanethiol Passivation of Halogenated Ge Nanowires.* Chemistry of Materials, 2010. **22**(23): p. 6370-6377.

49.	Wang, D., Y.L. Chang, Z. Liu, and H. Dai, *Oxidation Resistant Germanium Nanowires: Bulk Synthesis, Long Chain Alkanethiol Functionalization, and Langmuir-Blodgett Assembly.* Journal of the American Chemical Society, 2005. **127**(33): p. 11871-11875.

50.   Yuan, F.W., H.J. Yang, and H.Y. Tuan, *Alkanethiol-Passivated Ge Nanowires as High-Performance Anode Materials for Lithium-Ion Batteries: The Role of Chemical Surface Functionalization.* ACS Nano, 2012. **6**(11): p. 9932-9942.

51.   Bergsman, D.S., T.-L. Liu, R.G. Closser, K.L. Nardi, N. Draeger, D.M. Hausmann, and S.F. Bent, *Formation and Ripening of Self-Assembled Multilayers from the Vapor-Phase Deposition of Dodecanethiol on Copper Oxide.* Chemistry of Materials, 2018. **30**(16): p. 5694-5703.

52.   Hohman, J.N., M. Kim, H.R. Bednar, J.A. Lawrence, P.D. McClanahan, and P.S. Weiss, *Simple, Robust Molecular Self-Assembly on Germanium.* Chemical Science, 2011. **2**(7): p. 1334-1343.

53.   Inkpen, M.S., Z.F. Liu, H. Li, L.M. Campos, J.B. Neaton, and L. Venkataraman, *Non-chemisorbed gold–sulfur binding prevails in self-assembled monolayers.* Nature Chemistry, 2019. **11**(4): p. 351-358.

54.   Bal, J., S. Kundu, and S. Hazra, *Hydrophilic-Like Wettability of Cl-Passivated Ge(001) Surface.* Chemical Physics, 2012. **406**: p. 72.

55.   van Dorp, D.H., D. Weinberger, S. Van Wonterghem, S. Arnauts, K. Strubbe, F. Holsteyns, and S. De Gendt, *Nanoscale Etching: Dissolution of III-As and Ge in HCl/H2O2 Solutions.* ECS Transactions, 2015. **69**(8): p. 235-242.

56.   Murakami, H., T. Fujioka, A. Ohta, T. Bando, S. Higashi, and S. Miyazaki, *Characterization of Interfaces between Chemically Cleaned or Thermally Oxidized Germanium and Metals*. 2010, ECS.

57.   Deegan, T. and G. Hughes, *An X-Ray Photoelectron Spectroscopy Study of the HF Etching of Native Oxides on Ge(111) and Ge(100) Surfaces.* Applied Surface Science, 1998. **123-124**: p. 66-70.

58.   Cumpson, P.J., *The Thickogram: a Method for Easy Film Thickness Measurement in XPS.* Surface and Interface Analysis, 2000. **29**(6): p. 403-406.

Chapter 4

Humidity-Mediated Oxidation of Thiol-SAM-Passivated Ge(100)

This chapter has been prepared as a manuscript for submission to the *ACS Applied Materials & Interfaces* journal. Consequently, certain concepts within this chapter may be repeated in other chapters.

Manuscript:

S. Garvey, A. Serino, B. Maccioni, J.D. Holmes, M. Nolan, N. Draeger, E. Gurer, B. Long, *Humidity-Mediated Oxidation of Thiol-SAM Passivated Ge(100)*. ACS Applied Materials & Interfaces, **(in review).**

4.1 Abstract

Germanium's (Ge) native oxide is a complex system, comprising GeO_2 and sub-stoichiometric oxides where Ge can exist with a range of oxidation states (+1, +2 and +3). Not only is the oxide more complex than that of Si, but the native Ge oxide is problematic from a CMOS device perspective since it is water-soluble. Many of the processing steps used in traditional device fabrication are water based which would cause oxide etching, ultimately rendering the devices useless. Consequently, for CMOS devices, it may be advantageous to replace the Ge oxide with a stable passivating layer during fabrication. Self-assembled monolayers (SAMs) of thiols on Ge have been shown previously to inhibit oxidation however, reoxidation does eventually occur when exposed to ambient conditions. It had been speculated that humidity may play a role in the degradation of the SAM, ultimately resulting in reoxidation. To test this hypothesis, thiol-passivated Ge(100) surfaces are exposed to controlled humidity environments with different levels of relative humidity. The rate of reoxidation of the Ge surfaces are tracked using X-ray photoelectron spectroscopy (XPS) and water contact angle (WCA) analysis to discern what role relative humidity plays in the reoxidation of the Ge and the degradation of the SAM passivation. Atomic force microscopy (AFM) data is presented to show that humidity-mediated reoxidation of the Ge has little or no impact on the route mean square (RMS) roughness of those surfaces. Atomistic modelling of thiol-SAM passivated Ge in the presence of water molecules has been studied using first principles density functional theory (DFT) in order to simulate experimental conditions and to understand the atomic level processes that determine stability in hydrophilic and hydrophobic configurations.

4.2 Introduction

Traditionally, Si was chosen as the semiconductor material of choice due to its relative abundance [1] and mechanical strength [2], but most importantly because of its stable native oxide and high quality oxide/Si interface.[3] However, as aggressive device scaling has continued, traditional dielectrics such as SiO_2 have shown to be ineffective at insulating the channel from the gate.[4] At such small dimensions, electrons can tunnel through the gate oxide resulting in high leakage current and poor device performance.[5, 6] As a result, there has been a shift from traditional dielectrics to high-κ dielectrics such as HfO_2 and ZrO_2 in an effort to circumvent the aforementioned tunnelling issue.[7] Regardless, continued transistor scaling has been driving efforts to find higher mobility semiconductor materials with properties suited to the modern demands of CMOS device fabrication and performance. Other high mobility materials such as III-V semiconductors [8, 9] and two-dimensional transition metal dichalcogenides (TMDs) [10, 11] are being scrutinised for their potential use in future devices also. Germanium, however, is a very attractive alternative for a number of reasons. Critically, it boasts an electron and hole mobility more than twice and four times that of silicon, respectively, and its similarity to Si, as another Group IVA element, would allow it to be seamlessly incorporated using similar fabrication processes. The global reserves of Ge are estimated to be approximately 2-3 thousand tonnes.[12] By comparison, Si as the second most abundant element in the earth's crust, has an annual production of approximately 7 million tonnes. Given these relative abundances it is unlikely that Ge will replace Si entirely. However, it is plausible that Ge will be integrated into the Si platform as the channel material and efforts to do such are well underway.[13-15] Current transistor manufacturing includes channels

consisting of SiGe alloys to gain the partial benefits of Ge. In 2020, Intel published results for a gate-all-around nanosheet PMOS transistor using $Si_{0.4}Ge_{0.6}$.[16]

A contributing factor as to why pure Ge has not yet been integrated into current devices is that Fermi level pinning of the Ge surface occurs when contacting a metal due to unpassivated acceptor-like gap states present at the interface.[17, 18] Dimoulas et al. have hypothesised that since the Fermi level in Ge lies higher than the charge neutrality level (CNL), the gap states at the interface fill easily, building up a fixed negative charge preventing the efficient inversion in the inversion layer of the CMOS device resulting in sub-optimal device performance.[19] Many of the other issues with Ge are specifically related to the nature of the oxide. For example, the Ge/GeO_2 interface is characterised by interfacial dangling bonds and vacancies which trap charge, hindering device performance.[20, 21] Also, significant GeO desorption occurs at the high temperatures necessary to grow high quality GeO_2 films on Ge whereas this is not the case with the Si system.[22] The desorption of GeO during thermal oxidation affects the qualities of both the Ge/GeO_2 interface and the bulk GeO_2 itself. With that said, Toriumi et al. have performed Ge oxidation under high-pressure O_2 (HPO) conditions at high temperatures to supress the GeO desorption and avoid deteriorating the GeO_2 bulk film quality or Ge/GeO_2 interface.[23] Finally, GeO_2 is water soluble, making it extremely problematic for aqueous wafer-processing steps which are currently common in device manufacturing.[24] In fact, native oxide etching of GeO_2 using water, results in the formation of the suboxide, GeO, which can then be removed by annealing at temperatures above 450°C leaving a pristine Ge surface.[25] However, upon exposure to ambient conditions, the native oxide readily regrows. For the reasons outlined, when working with Ge, it may be advantageous to

remove the native oxide and to store the oxide-free Ge under an inert atmosphere, UHV conditions or to passivate the surface to ensure no oxide regrowth occurs.

Many methods to passivate Ge have been explored and are discussed in the scientific literature – these include both wet and dry methods of passivation using halides [26, 27], carboxylic acids [28], sulfur [29], nitride [30], oxynitride [31], passivation by graphene [20, 32, 33], and self-assembled monolayers (SAMs).[34, 35] SAMs have been the subject of extensive research throughout the latter half of the 20th century and well into the 21st, as it is understood that organic functionalisation of surfaces can dramatically affect the properties of those surfaces. The early literature on SAMs focused on their assembly onto planar gold [36]; however, since then the study of SAMs has expanded to many other materials such as copper [37, 38], bismuth [39], graphene [40], III-Vs [41, 42] and semiconductors such as Si, SiGe and Ge.[34, 42] A SAM is formed through the adsorption of molecules onto a surface, followed by a slower period of organisation whereby the molecules rearrange themselves on the surface to form a system that is energetically favourable. This results in a self-limiting process that minimally impacts the substrate but enables the alteration of surface properties such as the wettability and oxidation resistance.[34, 35] There are myriad reasons to form organic monolayers on the surfaces of semiconductor materials [43]; however, some examples include; for mono-layer doping [44-47], to enhance the stability and efficiency of solar cells [48, 49] and for electrochemical sensors.[50]

Several studies have explored the use of alkanethiol SAMs for inhibiting oxide growth on germanium. However, reported stabilities are widely variable.[51-53] Herein, we investigate the role the environment, specifically humidity, plays in thiol desorption and subsequent Ge oxidation. In this study, thiol SAMs are used to

passivate Ge(100) surfaces which are then placed in a controlled humidity environment with different levels of relative humidity (RH). CMOS compatible devices incorporating Ge are on the technological horizon. Understanding the mechanism for surface instability is crucial for SAMs to gain industry adoption for Ge oxide control.
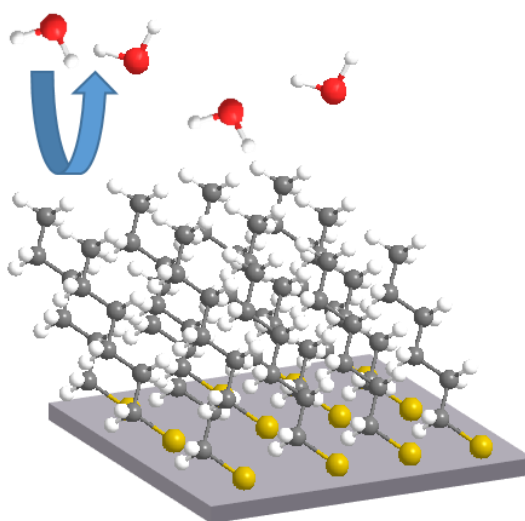
Figure 1. Schematic of thiol-SAM on Ge.

4.3   Methods & Materials

4.3.1 Preparation of SAMs on Ge surfaces

Samples were prepared by three different methods, (i) vapour-phase passivation of 1-hexanethiols, (ii) vapour-phase passivation of 1-octanethiols, and (iii) liquid-phase passivation of 1-dodecanethiols. The first method was conducted in an academic setting and used for identifying a humidity trend, the latter two were conducted in an industrial setting. No direct comparisons were made between the two settings.

4.3.1.1   Vapour-Phase Passivation using Hexanethiol

Passivation of the Ge(100) surface was achieved using vaporised 1-hexanethiol (HT) using a method previously outlined by the authors.[54] The passivated Ge coupons were exposed to air in low (5%), ambient (40%) and high (90%) RH environments for 168 hours to determine what effect the water vapour in air had on the Ge surfaces. For the purposes of this study, the humidity-controlled environment with 40% RH is referred to as 'ambient humidity'. In an attempt to isolate the water vapour from the low humidity environment without also isolating O_2, compressed air (which has a low water content) was used. In this case, Ge coupons were held in a glass vessel filled with desiccant through which compressed air was flowed continuously. A humidity sensor was used to track the humidity in the glass vessel. For both the ambient and high humidity tests, a Vötsch humidity-controlled chamber was used. In all cases, the samples were exposed to a constant temperature of 20°C. After 24 and 168 hours in their respective environments, samples were characterised using AFM, WCA and XPS.

4.3.1.2   Vapour-Phase Passivation using Octanethiol

Coupons of Ge(100) were etched with an HCl based proprietary etch designed to remove surface oxides and contaminants and provide a temporary Cl termination, and dried under a nitrogen gas stream. Samples were transferred to a custom low-pressure vacuum deposition chamber, with a transfer time up to 5 minutes. *1*-octanethiol (OT) was deposited using vapour draw at 80° C and 800 mTorr for 3 cycles of 10 minute doses. Samples were removed and rinsed with anhydrous ethanol, dried under a nitrogen stream, and immediately placed in target environments. The passivated Ge coupons were exposed to low (5%) and ambient (~40%) RH environments for 24

hours at room temperature and analysed by XPS. For the low humidity case, Ge coupons were held in a vessel filled with desiccant. A humidity and oxygen sensor were used to monitor the humidity and oxygen levels to ensure consistency.

4.3.1.3   Liquid-Phase Passivation using Dodecanethiol

Coupons of Ge(100) and $Si_{0.25}Ge_{0.75}$(100) (SiGe75) were etched with the same HCl based proprietary etch as vapour-phase passivation of OT. Samples were immediately transferred to a solution of 25 mM *1*-dodecanethiol (DDT) in anhydrous ethanol at room temperature. After 24 hours, samples were removed and rinsed with anhydrous ethanol, dried under a nitrogen stream, and immediately placed in target environments. The passivated Ge coupons were exposed to low (5%) and ambient (~40%) RH environments at room temperature for 24 hours and analysed by XPS. For the low humidity case, Ge coupons were held in a vessel filled with desiccant. A humidity and oxygen sensor was used to monitor the humidity and oxygen levels to ensure consistency.

4.3.2 Characterisation Methods

All AFM measurements were taken using tapping mode Veeco Multimode V at room temperature over a 3 x 3 μm^2 scanning area.

For water contact analysis (WCA), an image of a 50 μL drop of deionised water on the Ge surface was obtained and the angle formed between the water, Ge surface, and air was measured.

X-ray photoelectron spectroscopy measurements were carried out on two instruments. Vapour-phase deposited hexanethiol samples were analysed using an

Oxford Applied Research Escabase XPS System with a CLASS VM 100 mm mean radius hemispherical electron energy analyser with multichannel detectors in an analysis chamber with a base pressure of 5.0×10^{-9} mbar. Survey scans were swept twice and were acquired using a pass energy of 50 eV, a step size of 0.7 eV and a dwell of 0.3 s. All core level scans, were averaged over 10 scans and were acquired with a step size of 0.1 eV, a dwell time of 0.1 s and a pass energy of 20 eV except for the S 2s, which was acquired with a pass energy of 50 eV averaged over 20 scans. This was done to maximise the intensity of the sulfur peaks to allow for accurate peak fitting. A non-monochromated Al-Kα X-ray source (1486.58 eV) at 100W power (10 mA, 10 kV) was used for all scans.

Vapour-phase passivated OT and liquid-phase passivated DDT samples were analysed using a ThermoFisher Scientific Theta 300 at 1×10^{-9} Torr with a monochromatic Al-Kα source at 100 W (6.67 mA and 15 kV) with a 400 μm spot size. A pass energy of 50 eV was used to collect high energy resolution spectra with a step size of 0.1 eV, a dwell time of 50 ms, and 15, 15, and 20 sweeps for C 1, Ge 2p, and S 2s, respectively.

All spectra were acquired at a take-off angle of 90° with respect to the analyser axis and were charge corrected with respect to the C 1s photoelectric line at 284.8 eV. A Shirley type background was used for construction and peak fitting of synthetic peaks. Synthetic peaks were a mix of Gaussian-Lorenzian; the Ge 2p spectra were fit using Gaussian-Lorentzian peak shape GL(90) for the elemental Ge peak and Lorentzian peak shape LA(1.53,243) for all other peaks. The relative sensitivity factors used are from a CasaXPS library containing Scofield cross-sections.

4.3.3 First Principles Density Functional Theory Simulations

First principles density functional theory (DFT) calculations as implemented in the Vienna Ab Initio Software Package (VASP) [55, 56] have been used to model alkanethiol SAMs on the Ge(100) surface and to explore how humidity could influence Ge surface passivation. The calculations utilise a plane wave basis set in a 3-dimensional periodic slab model of the substrate with DFT-optimised lattice constants. The core electrons are described by projector augmented wave (PAW) [57] potentials and the exchange and correlation energies are modelled according to the generalised gradient approximation (GGA) with the Perdew-Burke-Ernzerhof (PBE) [58] gradient corrected functional. In order to take into account the van der Waals interactions between alkanethiols and water, we used the DFT-D3 dispersion correction method [59] that incorporates the long-range dispersion contribution to the exchange-correlation PBE functional. We use the following valance electron configurations; for germanium; Ge $4s^2$ and $4p^2$, for chlorine; Cl $3s^2$ and $3p^5$, for sulfur; S $3s^2$ and $3p^4$, for carbon; C$2s^2$ and $2p^4$, for oxygen; O $2s^2$ and $2p^4$, and for hydrogen; H $1s^1$. All the calculations were executed using an energy cut-off for the valence electron plane wave basis set at 420 eV and the convergence criteria for electronic relaxations and ionic relaxations at 10^{-4} eV and 0.02 eV/Å, respectively. The Brillouin zone was sampled with ($2 \times 2 \times 1$) Monkhorst-Pack k-point grids.[60]

4.4 Results & Discussion

4.4.1 Impact of Humidity on Thiol-SAM Stability

The primary characterisation method for the study of SAM degradation and Ge oxidation is XPS since it gives accurate determination of elemental composition and oxidation states of those elements at the surface (~10 nm sampling depth) of the samples being characterised. As such, the growth of GeO_2 was tracked as a function of exposure time to different levels of RH. For the purposes of this study, Ge 2p spectra from XPS were used to track oxidation of the Ge(100) surfaces since the Ge 2p transition is more surface sensitive than Ge 3d. In addition, to track the presence of sulfur, the S 2s spectra were acquired. Oxide thickness was calculated using the method outlined previously by Murakami et al.[61]

$$d_{GeO_2} = \lambda_{GeO_2} sin\theta \; ln\left(\frac{I_{Ge}^{\infty}}{I_{GeO_2}^{\infty}}\frac{I_{GeO_2}}{I_{Ge}} + 1\right)$$

where λ_{GeO_2} is the inelastic mean free path for the Ge 2p transition, which is 0.9 nm; the photoemission angle θ is 90°; $I_{Ge}^{\infty}/I_{GeO_2}^{\infty}$ is the ratio of the Ge 2p signal from infinitely thick Ge to infinitely thick GeO_2 and is 1.73 and 3.25 for the Oxford Applied Research and ThermoFisher instruments, respectively; I_{GeO_2} is the intensity of the of native oxide (GeO_2) peak from curve fitting the Ge 2p feature; I_{Ge} is the intensity of the metallic Ge peak from curve fitting the Ge 2p transition. This calculation was repeated to determine the thickness of the suboxide (GeO_x) component for each

sample. In this case, I_{GeO_x}, the fraction of suboxide (GeO$_x$) from curve fitting the Ge 2p was used in place of I_{GeO_2}.

Figure 2. (i) Ge 2p and **(ii)** S 2s spectra for HT-passivated Ge showing increasing in intensity of GeO$_2$ peak and decrease in intensity of sulfur peak for the high RH sample over 168 hours.

In **Figure 2 (i)**, the Ge 2p XPS spectra for HT-passivated Ge with 0, 24 and 168 hours of exposure to the high RH environment is shown. Directly after the passivation reaction, after 0 hours of exposure, only the peaks corresponding to Ge^{+0} at 1218.2 eV (red) and Ge^{+2} at 1219.3 eV (blue) are present. There is no peak corresponding to Ge^{+4} since the initial HCl etch has effectively removed the native

oxide entirely and the subsequent passivation procedure has prevented re-growth of native oxide. As stated, there is a contribution from Ge in a +2 oxidation state (blue). This contribution is likely present due to a combination of the suboxide (GeO) and Ge bonded to S (1219.1 eV) [62] after the passivation reaction. A peak separation of 1.1 eV between the Ge^{+0} and Ge^{+2} components was observed for the sample with 0 hours exposure to high humidity. In **Figure 2 (ii)**, the S 2s peak at 226.9 eV after 0 hours of exposure is also displayed. Here, a clear S signal is observed which confirms that the thiol molecules have bonded to the Ge surface. Upon exposure to the high humidity environment for 24 hours, an increase in the intensity of the GeO_2 peak at 1220.9 eV (pink) is observed in the Ge 2p spectrum and after 168 hours, a greater increase in peak intensity is observed with the peak shifting slightly (0.05 eV) to higher binding energy as the GeO_2 film thickness increases from 0.07 nm after 24 hours to 0.38 nm after 168 hours. Also, the S 2s signal decreases in intensity from 0 to 24 hours of exposure indicating that some of the thiol molecules have been displaced from the Ge surface. After 168 hours, S is no longer detectable by XPS suggesting that the majority of the SAM has been displaced by oxide. The changes observed in the XPS over 168 hours of exposure to the high RH environment can be contextualised and the role water vapour has on the thiol-passivated Ge can be understood when the same measurements are taken for samples exposed to lower levels of humidity over the same period of time.
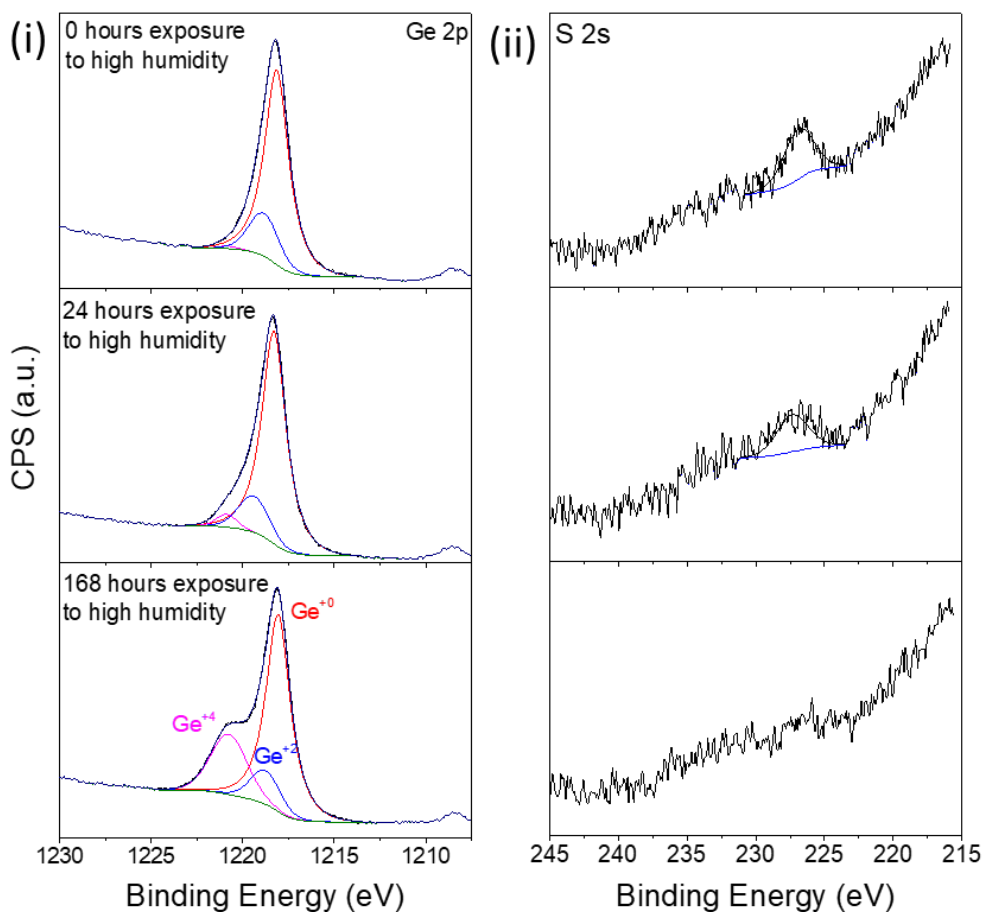
Figure 3. (i) Ge 2p and **(ii)** S 2s spectra for HT-passivated Ge showing increasing in intensity of GeO_2 peak and decrease in intensity of S peak for ambient humidity sample over 168 hours.

In **Figure 3**, the Ge 2p **(i)** and S 2s **(ii)** XPS data for the HT-passivated Ge which was exposed to ambient humidity for 168 hours, is shown. As was observed with the high humidity samples, there is no GeO_2 present directly after the passivation reaction and after 24 hours of exposure to the ambient - the GeO_2 thickness is calculated to be 0.06 nm. After 168 hours of exposure to the ambient, the GeO_2 peak at 1220.8 eV increases in intensity and the oxide thickness is calculated to be 0.25 nm. While there is a growth of GeO_2 in 168 hrs, there is also a loss of S as can be seen in

Figure 3 (ii), whereby the S 2s peak diminishes within the first 24 hours and over the following 144 hours. With that said, there is still detectable S after the 168 hour period. These results differ from the high humidity samples. For one, there is less GeO_2 growth over the 168 hour exposure period, 0.25 nm relative to 0.38 nm at high humidity, and S is still detectable on the surface over that same period – an indication that the SAM is still present and lending partial oxidation resistance to the Ge surface.
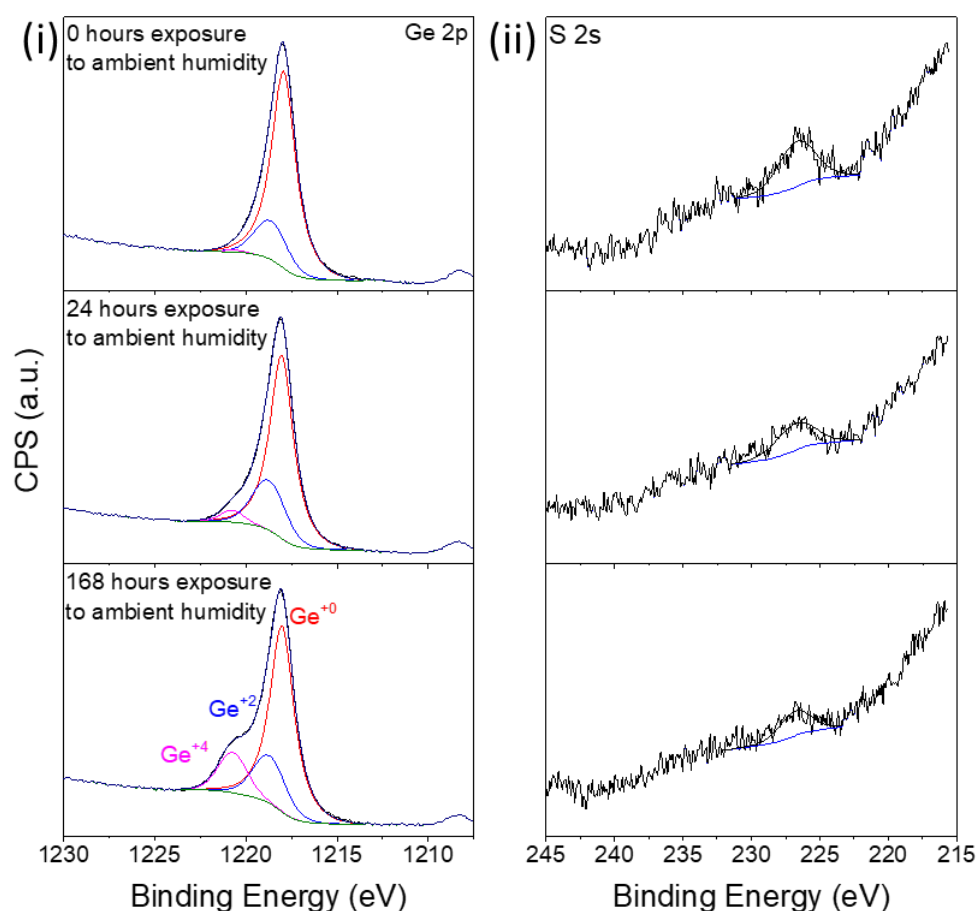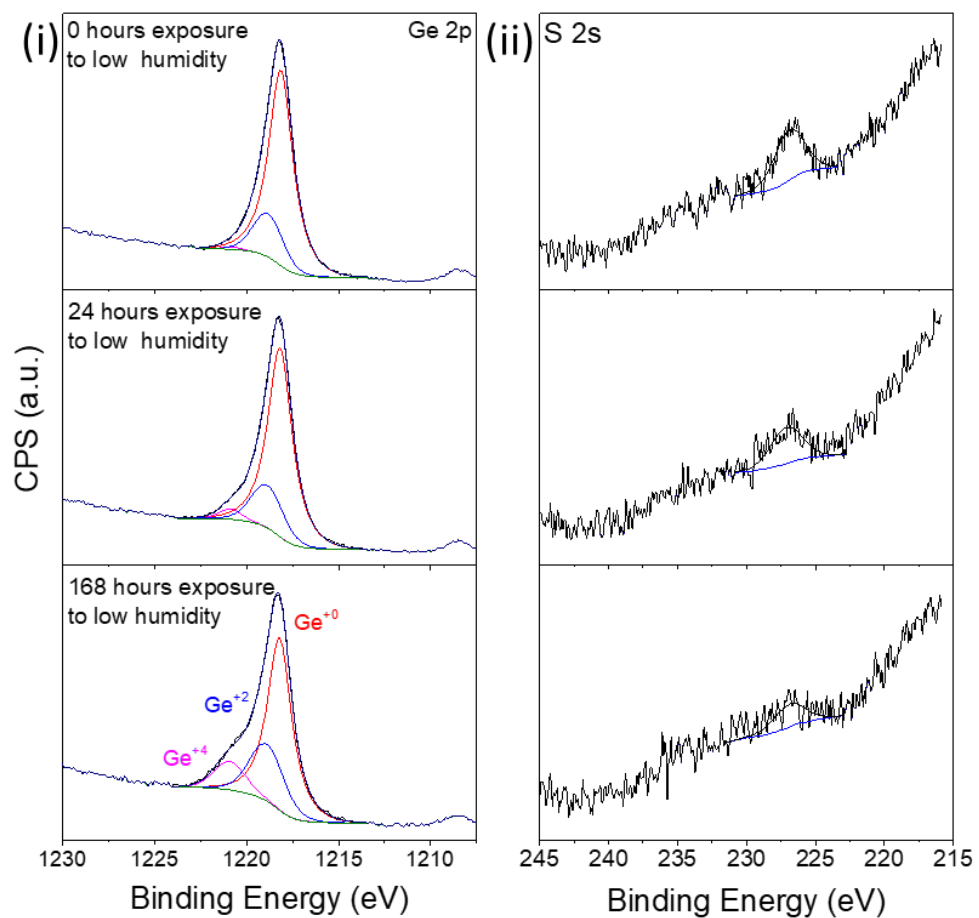

Figure 4. (i) Ge 2p and **(ii)** S 2s spectra for HT-passivated Ge showing increasing in intensity of GeO2 peak and decrease in intensity of sulfur peak for low humidity sample over 168 hours.

To complete the picture, passivated Ge surfaces were exposed to a low humidity environment and again, characterised by XPS. In **Figure 4**, the Ge 2p **(i)** and S 2s **(ii)** XPS plots for the sample exposed to the low humidity environment are displayed. After 24 hours of exposure to the low RH environment, there is 0.04 nm of GeO_2 growth and a slightly reduced intensity S 2s peak when compared with that after 0 hours of exposure. After 168 hours, 0.18 nm of the native oxide has grown and S is still detectable by XPS on the surface. The XPS data from **Figures 2**, **3** and **4** combine to reveal what effect humidity has on the surface of the Ge. It is apparent that in the presence of water vapour, the passivated Ge begins to oxidise over time and the amount of S on the surface decreases as the thiol molecules desorb from the surface. The progressive growth in GeO_2 for each sample set is displayed in **Figure 5**.

Figure 5. GeO_2 thicknesses of HT-passivated Ge exposed to low, ambient and high relative humidity for 0, 24 and 168 hours.

It is clear from **Figure 5** that oxidation of the Ge surface trends with humidity. It was not possible to achieve a 0% RH environment in air at 20°C and therefore the growth of oxide observed for the low RH case can be attributed to the small but non-negligible amount of water vapour in the air.
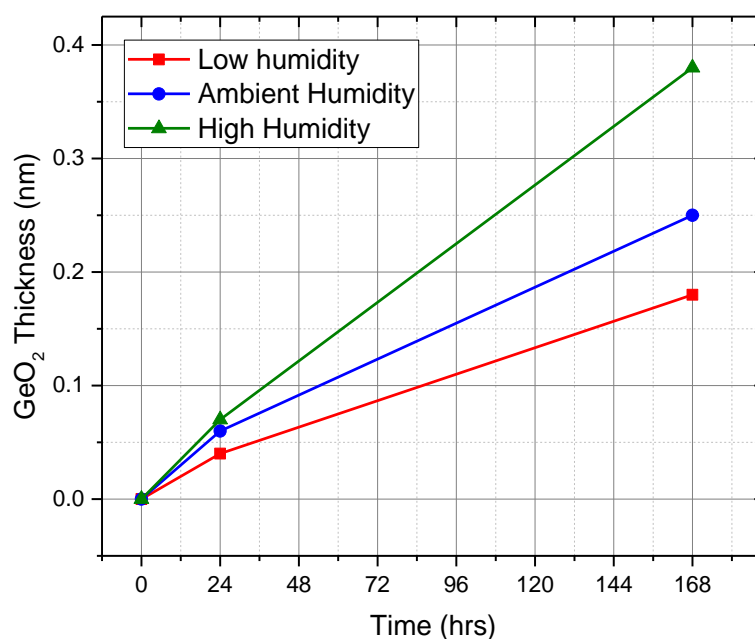
Water contact angle (WCA) analysis was carried out on each sample directly after the passivation procedure and after 24 and 168 hours in their respective environments. This is a quantitative measurement technique that gives an indication of the wettability of a surface. The wettability of the Ge surface is affected by how the surface is terminated. For example, the as-received Ge surface with its native oxide interacts favourably with water, resulting in a hydrophilic surface and a shallow contact angle between the water droplet, Ge and air. When the oxide is replaced with the methyl-terminated monolayer, a more hydrophobic termination, the polar water molecules in the droplet interact less favourably and thus do not wet the surface, resulting in a steep contact angle between water, Ge and air. In **Figure 6 (ii)**, a contact angle of 95° is measured for the HT-passivated Ge. By tracking the changes in the angle of the water droplet with the substrate and air, we gain insights into how exposure to the environment with different levels of RH affects the presence of the SAM. The WCA for the sample exposed to the low humidity environment decreases by 5° in 24 hours but does not decrease further in the following 144 hours (**Figure 6 (iii)** and **(iv)**). A similar result is observed for the sample exposed to the ambient humidity – a decrease of 5° in the WCA is observed in the first 24 hours of exposure to the ambient and over the next 144 hours of exposure, the contact angle only decreases by a further 2°.

The largest change in contact angle is observed for the sample exposed to the high humidity environment for 168 hours. In this case, the WCA drops by 8° over the first 24 hours and by a further 13° in the following 144 hours (**Figure 6 (vii)** and **(viii)**). Over the 168 hour period of exposure to the high humidity environment, the WCA decreased by a total of 22°. This indicates that the longer-term stability of the SAM is influenced greatly by the exposure to the high humidity environment.

Taking this data together with the XPS results in **Figure 2** elucidates how the water vapour damages the SAM allowing surface oxidation, evidenced by an increase in the intensity of the peaks corresponding to GeO_2. A summary of the WCA results are displayed in **Figure 7**. The AFM images in **Figure 6** show what effect, if any, exposure to the respective environments had on the surface roughness of the Ge. A pristine surface with roughness RMS value of 0.26 nm is observed for degreased Ge (**Figure 6 (i)**). For all other samples, an increase in surface roughness is observed and for the samples exposed to the high relative humidity, some spots are observed that may be oxide formations on the Ge surface at point defects.
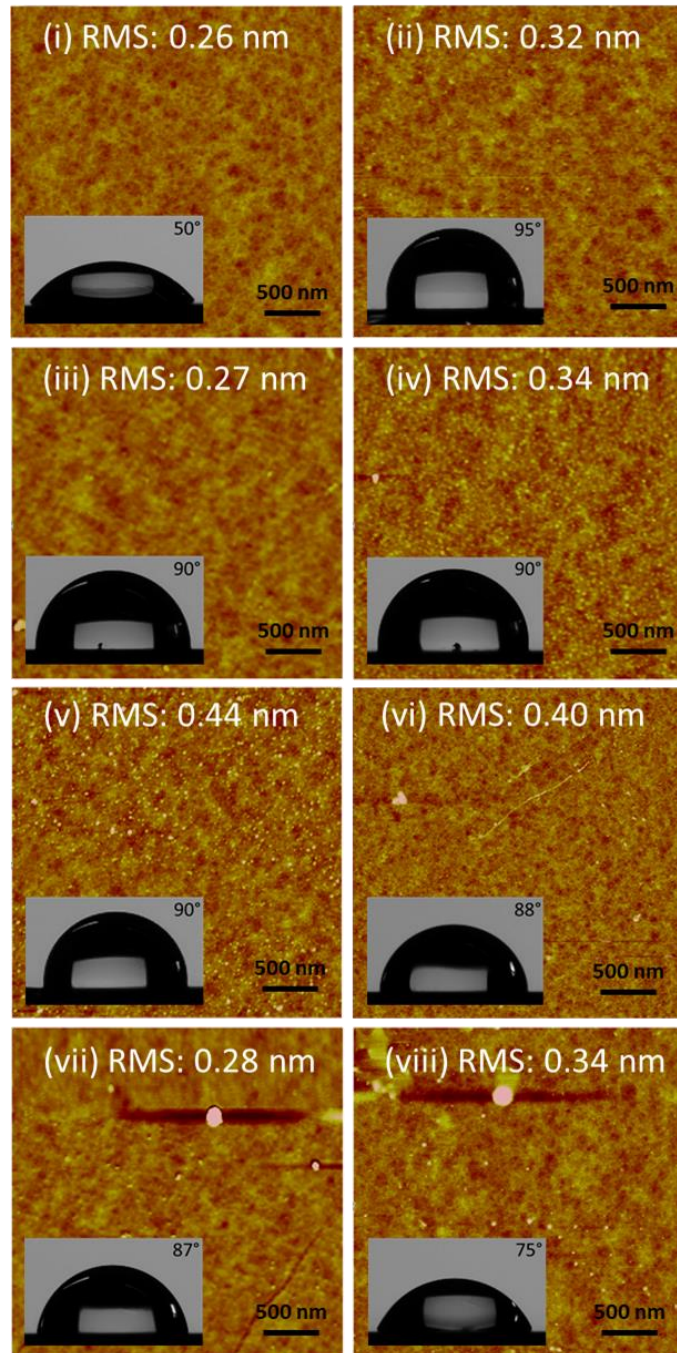
Figure 6. WCA and AFM data for **(i)** as-rec Ge **(ii)** HT-passivated Ge **(iii)** and **(iv)** HT-passivated Ge with 24 and 168 hours exposure to the low humidity environment, respectively. **(v)** and **(vi)** HT-passivated Ge with 24 and 168 hours exposure to the ambient humidity environment, respectively. **(vii)** and **(viii)** HT-passivated Ge with 24 and 168 hours exposure to high humidity environment, respectively.
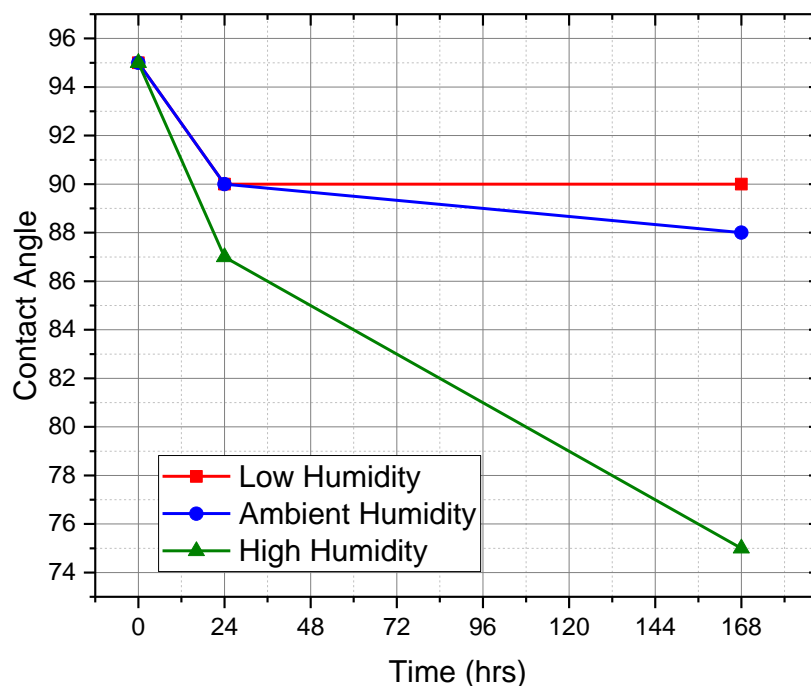
Figure 7. WCA data for HT-passivated Ge plotted against time spent in respective RH environments. WCA for as-received Ge is 50°.[63]

Previous reports explored the stability of DT-SAMs that were formed on Ge(100) through liquid-phase passivation. To demonstrate further the role of humidity in this work, the growth of GeO_2 over time in low and ambient humidity environments for alkanethiol SAMs formed by vapour-phase passivation is compared to that of liquid-phase passivation in **Figure 8**. Due to the difficulty of achieving the vapour-phase passivation of Ge using DT, which is a result of the molecule's high vapour pressure, OT is used, which is a similar long-chain alkyl-thiol but has a lower vapour pressure. The vapour-phase passivation shows a similar trend to what has been reported previously in this work, where GeO_2 growth is 0.01 and 0.13 nm for low and ambient humidity environment samples, respectively. This trend continues for liquid-phase passivation where the GeO_2 growth is 0.25 and 0.64 nm for low and ambient

humidity environment samples, respectively. This data also suggests that passivation method, and thus SAM quality, plays a role in stability as well-ordered, hydrophobic alkyl-backbones contribute to preventing water molecules from reaching the SAM-Ge interface.

While the goal is to eventually replace Si with pure Ge in devices, $Si_{1-x}Ge_x$ is the current alternative. As the percentage of Ge increases in SiGe alloys, the native oxide challenges associated with Ge become more pronounced. Today, mainstream logic devices in high volume manufacturing are limited to $\leq$60% Ge. In **Figure 8**, liquid-phase passivation of DT on SiGe75 is shown. The GeO_2 growth is -0.05 and 0.35 nm for low and ambient humidity, respectively. While the data suggests a decrease in GeO_2 for the low humidity sample, it is likely a result of sample variation. The growth of GeO for SiGe75 in ambient humidity and the lack of growth for low humidity indicates that the role humidity plays follows the same trends for SiGe alloys as for pure Ge. By controlling for humidity, SAM stability on SiGe can be increased, thus reducing the amount of germanium oxide growth.
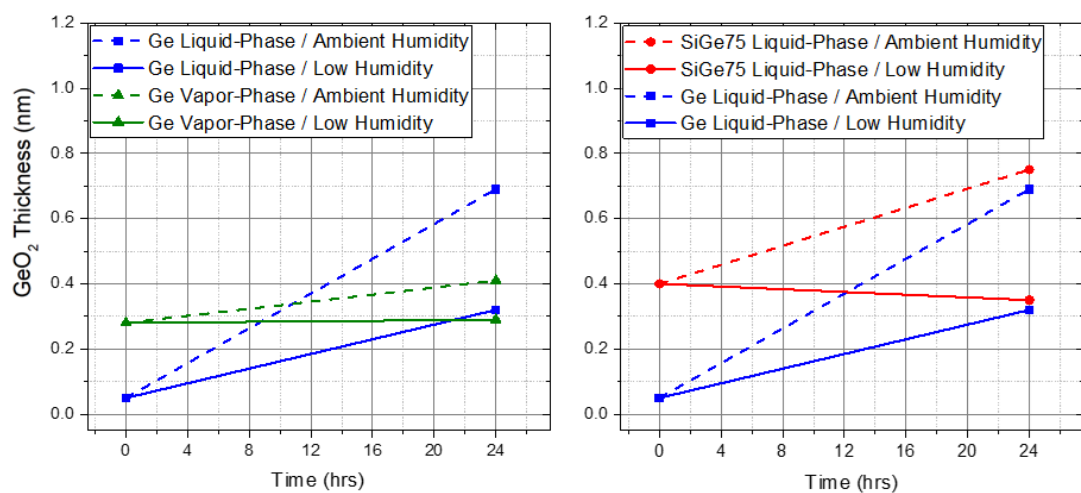
Figure 8. GeO_2 thicknesses of (left) Ge samples passivated by vapour-phase deposited OT and liquid-phase deposited DT and (right) DT-passivated SiGe75 exposed to low

and ambient relative humidity for 0 and 24 hours. Values extracted from Ge 2p spectra from **Appendix Figure S4.1**.

4.4.2 Modelling SAM-Passivated Ge and the Impact of Humidity

Density Functional Theory (DFT) calculations were performed to understand the atomic level detail of the SAM stability and the interaction between SAMs and water molecules. We use extensive static relaxations to explore how water interacts with SAMs and behaves at the Ge-SAM interface. While ab initio molecular dynamics (MD) would be useful to explore this in more detail, such analysis requires significant calculations beyond the scope of this work.

The Ge(100) surface is modelled with a (2x2) surface supercell expansion with 128 atoms while the 40 Å of vacuum separating the slabs along the periodic direction perpendicular to the surface allows for a range of alkanethiol chain lengths from two to twelve carbon atoms to be explored while removing periodic interactions perpendicular to the surface. To simulate the conditions of the bulk, Ge atoms in the bottom layer of the slab are fixed. The top surface, composed by 8 Ge atoms, was initially fully passivated with Cl atoms.

We first determine the stable structures of alkanethiols on Ge and then we explore the influence of humidity for the SAMs with 4 and 6 carbon-atom-backbones as these are computationally tractable. The search for the most stable interface structure of the SAM on Ge was carried out by calculating the adsorption energies of

these alkanethiols on Ge surfaces at various coverages. With 8 Ge atoms in the outermost (terminal) surface layer, coverages from 12.5% to 100% can be constructed.

The adsorption energy of the thiols at the Ge(100) surface is computed with adsorption in the thiolated form, in which the S–H bond breaks during adsorption onto the Ge surface, and leads to HCl formation. We calculated the adsorption energies (E_{ads}) with the following expression:

$$E_{ad} = E(tot) + E(n\ HCl) - [\ E\ (Cl:Ge) + E(\ n\ HS\text{-}C_xH_{2x+1})\ ]$$

where $E(tot)$ is the total energy of the thiol-functionalised Ge surface, with n adsorbed thiol molecules; $E(n\ HCl)$ is the energy of the isolated HCl molecule multiplied by the number, n, of HCl molecules; $E\ (Cl:Ge)$ is the energy of the Cl passivated Ge(100) surface and $E\ (nHS\text{-}C_xH_{2x+1})$ is the energy of n alkanethiol molecules. All the energies have been computed using the same parameters including the van der Waals corrections.[59]

We have examined different coverages and arrangements of the thiol molecules on Ge(100) for the examples of C4 and C6 alkanethiolates. The relaxed structures of the most stable butane- and hexanethiol-passivated Ge(100) surfaces at different coverages and the respective adsorption energies are reported in **Figure 9**. These stable thiolate coverages are used as models for humidity explorations.
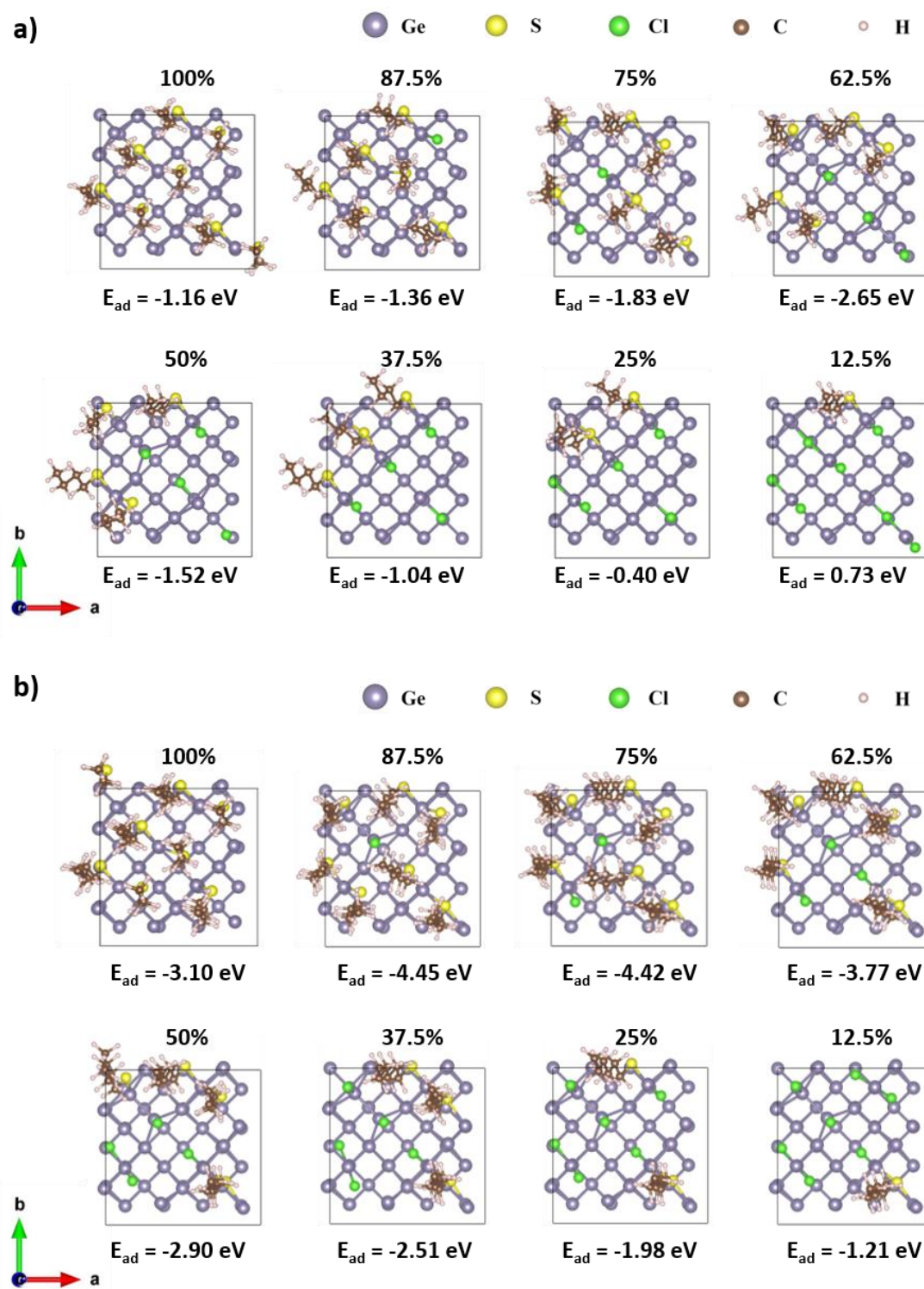
Figure 9. Atomic structures of **a)** butanethiol and **b)** hexanethiol on Ge(100) at different coverages, with respective computed adsorption energies.

For C4 and C6 alkanethiols, the most favourable coverages on the Ge(100) surface are 62.5% and 87.5%, respectively, with computed adsorption energies of -2.65 eV and -4.45 eV, respectively. We see that the C6 thiolate chain shows a stronger interaction with the Ge(100) surface, which can be attributed to the alkyl chain-chain interactions that are stronger for longer thiol chains. A detailed discussion of the stability and structure of a wide range of thiolate SAMs on Ge(100) is presented in **Chapter 5**.

In **Table 1**, we present computed interaction energies of water at butane- and hexanethiol-passivated Ge surfaces at full SAM coverage. For each SAM, two energies are presented – E_{int} is the interaction energy relative to n water molecules ($n = 1 - 8$), while E_{int} / n is the interaction energy per water molecule.

n H$_2$O	Butanethiol on Ge(100) at 100%		Hexanethiol on Ge(100) at 100%	
	E_{int} (eV)	E_{int} /n (eV)	E_{int} (eV)	E_{int} /n (eV)
1	-0.09	-0.09	-0.09	-0.09
2	-0.39	-0.19	-0.48	-0.24
3	-0.82	-0.27	-0.84	-0.28
4	-1.38	-0.35	-1.36	-0.34
5	-1.73	-0.35	-2.24	-0.45
6	-2.08	-0.35	-2.18	-0.36
7	-3.26	-0.47	-2.67	-0.38
8	-3.66	-0.46	-3.63	-0.45

Table 1. Calculated interaction energies of Ge(100) surfaces with full coverage of alkanethiolates at different concentration of water molecules. The two energies presented for each thiolate are the total interaction energy for n water molecules (E_{int}) and the interaction energy per water molecule (E_{int}/n).

From **Table 1**, the magnitude of the interaction energy increases with the number of water molecules. However, the computed interaction energy per molecule is -0.25 ± 0.05 eV for low concentration (n = 2 - 4) and -0.40 ± 0.05 eV for high concentration (n = 5 - 8) in both SAM-Ge systems and therefore the influence of the chain length on the interaction with water is constant for these thiolate chains. This is most likely due to the presence of the terminating methyl group in the thiolates, which repels the water molecules and is independent of the length of the thiolate chain.

The hydrophobic property of Ge(100) passivated by butanethiol- and hexanethiol-SAMs can be seen from the structures presented in **Figure 10**. Water molecules are initially positioned to interact with the thiolates at the chain-vacuum interface and are repelled from the SAM after relaxation in both low and high water concentration scenarios.

a)

b)
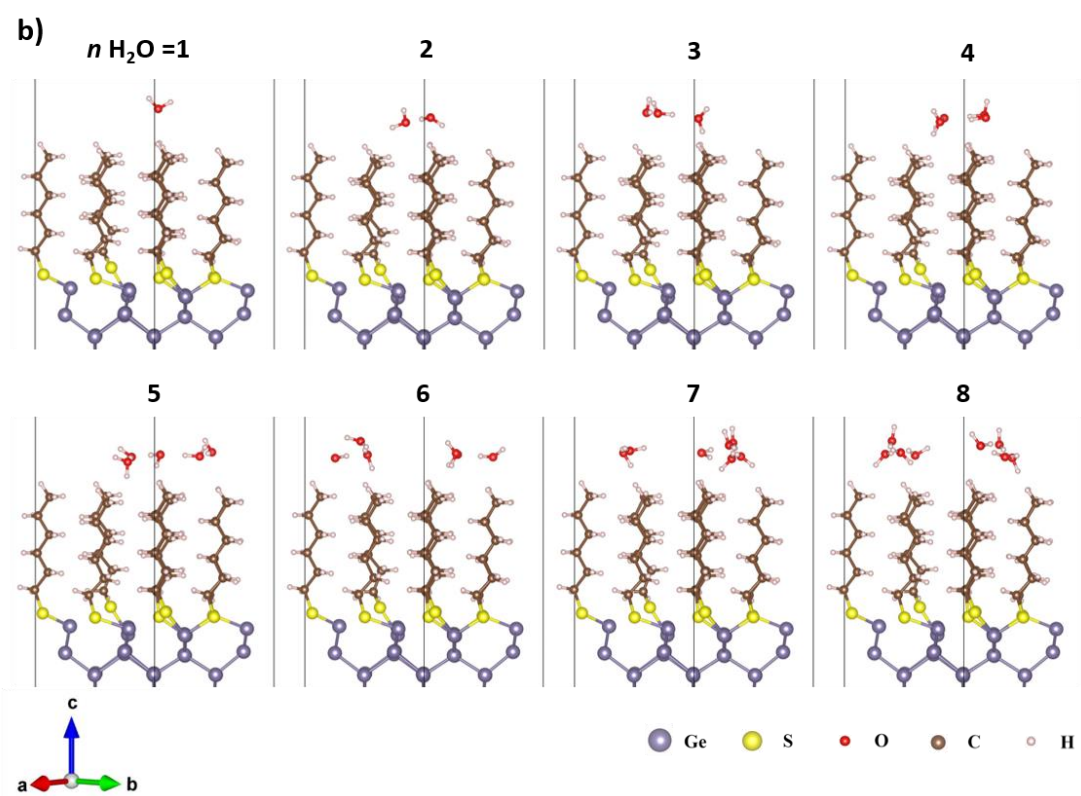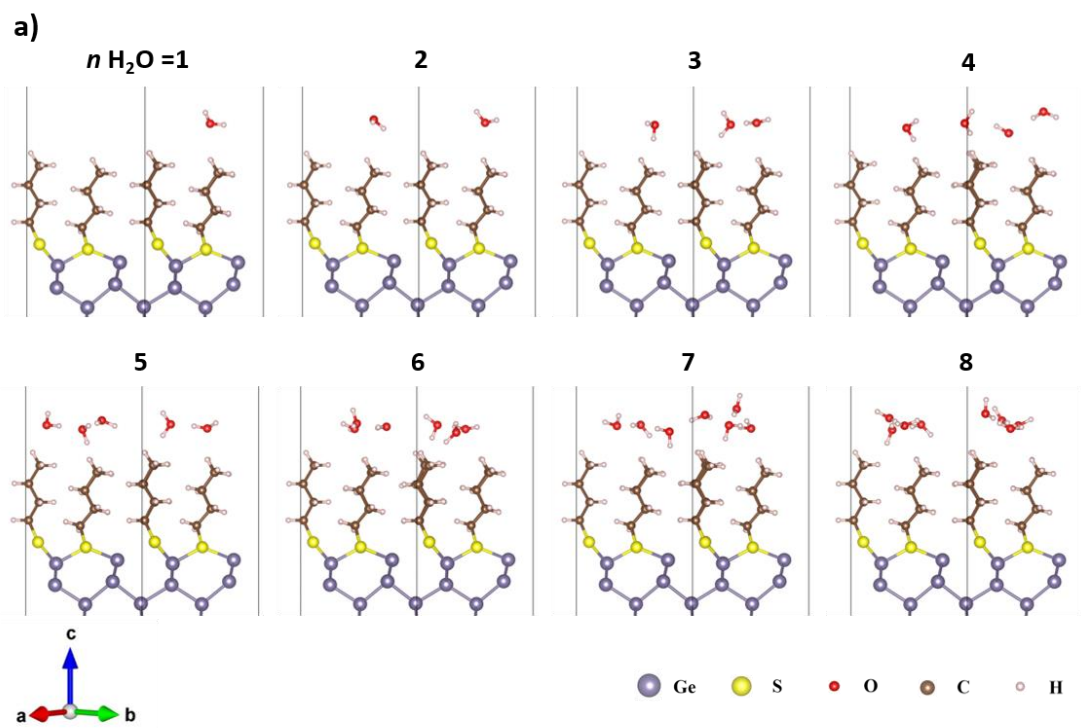
Figure 10. Atomic structures of Ge(100) entirely covered by **a)** butanethiol and **b)** hexanethiol with n (1, …, 8) water molecules positioned at the chain-vacuum interface before relaxation.

In the case of a partially covered Ge surface, water molecules may migrate through any gaps between the chains but are still not easily able to reach the Ge surface because the SAM acts as a barrier, as demonstrated in the experimental work where Ge reoxidation requires > 24 hours. In **Figure 11**, we show two initial configurations of a water molecule positioned in the space between thiol chains and near the Ge surface for hexanethiol-SAMs at a surface coverage of 75%. After relaxation, both arrangements assume the same configuration with an interaction energy between water and the SAM-Ge system (E_{int}) of - 0.40 eV. Even if the water molecule is positioned near the thiolate-Ge interaction, it appears to relax away from the surface, trapped between two thiolate chains.
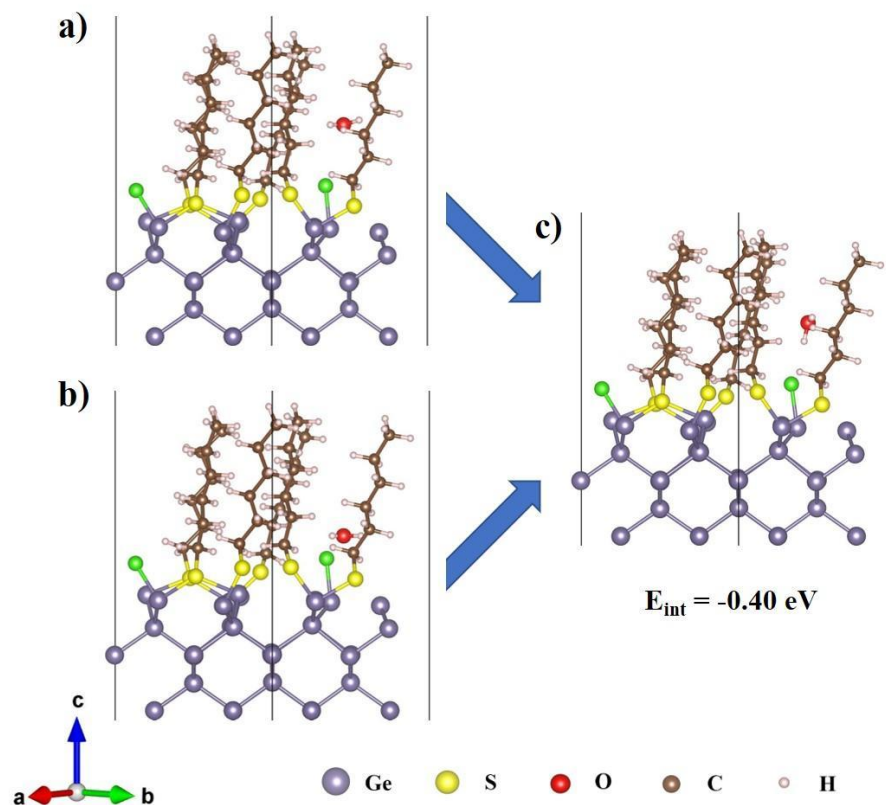
Figure 11. Atomistic structure of Ge(100) with 75% hexanethiol coverage with a water molecule placed **a)** in the middle of the chains and **b)** near the Ge surface before the relaxation and **c)** after relaxation.

Interactions between water and a butanethiol-passivated Ge surface at 62.5% coverage as a function of water concentration are shown in **Figure 12**. The SAM acts as a barrier at low water concentration and water molecules begin to be repelled by the chains as the number of water molecules increases. At the highest water concentration, the water molecules are repelled by the terminating methyl group, as confirmed by Howell et al.'s work on water–SAM interactions.[64] Calculated interaction energies of these structures are also reported in **Figure 12**, as the number of water molecules increases, the interaction energy is always increasingly negative but interestingly, the interaction energy per molecule is higher at low concentration (n

= 1, ..., 4) than at high concentration (n = 5, ..., 8), in which it appears to be constant around -0.50 ± 0.05 eV.

nH$_2$O = 1	2	3	4
E_{int} = - 0.75 eV	E_{int} = - 1.31 eV E_{int}/n = -0.66 eV	E_{int} = -1.64 eV E_{int}/n = -0.55 eV	E_{int} = -2.40 eV E_{int}/n = - 0.60 eV

5	6	7	8
E_{int} = -2.45 eV E_{int}/n = -0.49 eV	E_{int} = -3.18 eV E_{int}/n = -0.53 eV	E_{int} = -3.25 eV E_{int}/n = -0.46 eV	E_{int} = -3.94 eV E_{int}/n = -0.49 eV
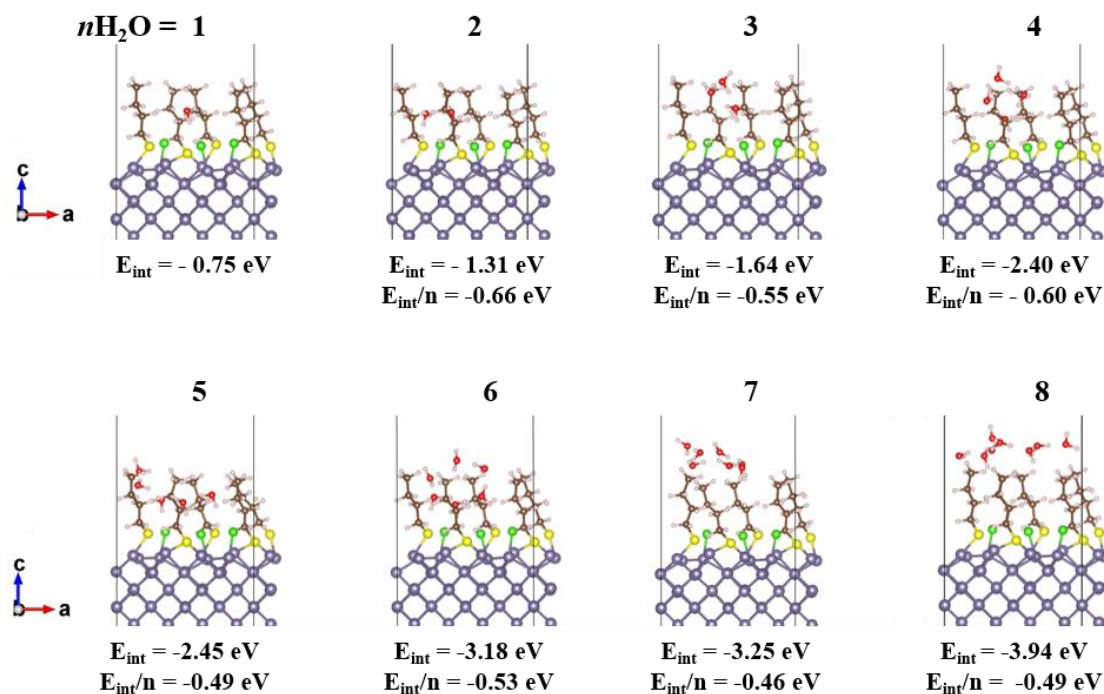
Figure 12. Calculated adsorption energies and optimised structures of Ge(100) with 62.5% butanethiol coverage, with n (1, ..., 8) water molecules.

For this SAM-Ge structure, we also investigated a range of initial configurations in which a water molecule that is present at the Ge-SAM interface can dissociate into one of two species. The first is the formation of a thiol molecule, with an S-H bond which migrates away from the surface and a surface Ge-OH bond. The second is formation of a HCl molecule which migrates from the surface and a surface Ge-OH bond; this can also promote Ge oxidation by removing the surface passivating Cl species, as illustrated in **Figure 13**.
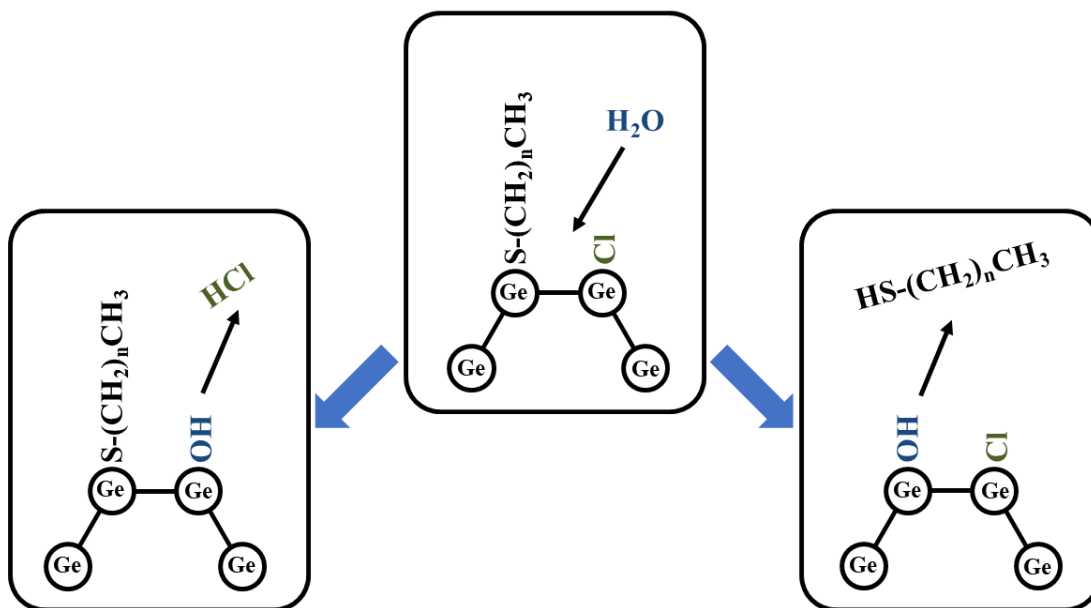
Figure 13. Schematic indicating possible reaction pathways for water attacking Ge surface, both cases involving the displacement of a passivant by an OH group.

In the case of butanethiol-passivated Ge at 62.5% coverage, a water molecule can dissociate into hydrogen and hydroxide ions and relax to form a protonated HS-thiol molecule and a new Ge-OH bond with an interaction energy of -0.85 eV. This is comparable to the configuration in which H_2O does not dissociate but instead interacts at the interface between the SAM and Ge, as shown in **Figure 14**.
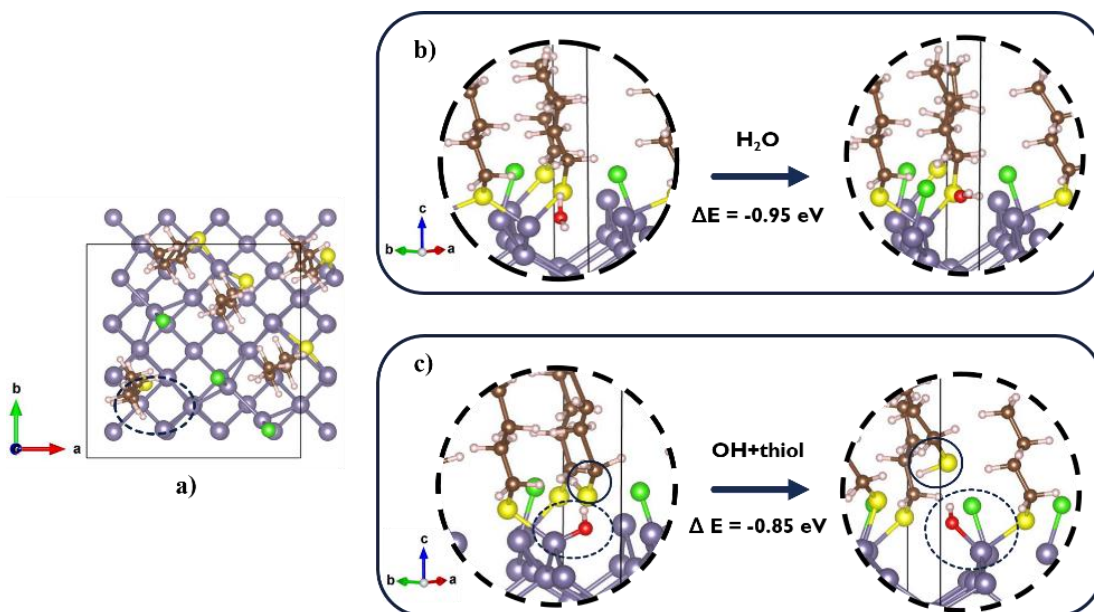
Figure 14. a) Model used to explore possible water dissociation in Ge(100) with butanethiol coverage of 62.5%, **b)** a solution in which molecular water remains confined around the initial position, **c)** water dissociation, in which water dissociates into hydrogen and hydroxide ions forming a Ge-OH bond and HS-thiol.

In **Figure 15**, we show an example of the hexanethiol-Ge system at 62.5% SAM coverage, where upon water dissociation, a HCl molecule is released and a Ge-OH species is formed. While this shows an apparently less favourable interaction energy of -0.19 eV compared to butanethiol, it is nonetheless competitive with the stability of a water molecule interacting at the SAM-Ge interface. This process removes the Cl species that passivates Ge in the absence of thiolates and also forms a new Ge-OH bond, which was proposed as the first step in reoxidation of halide-passivated Ge in a previous work.[65]
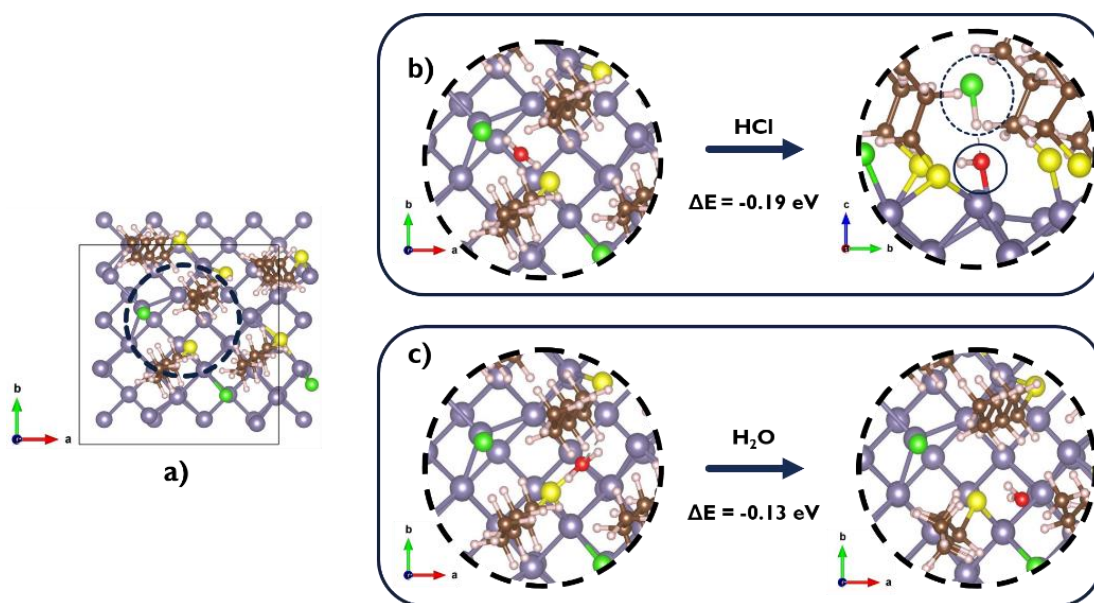
Figure 15. a) Model used to explore possible water dissociation in Ge(100) with hexanethiol coverage of 62.5%, **b)** water dissociation, water breaks into hydrogen and hydroxide ions forming a Ge-OH bond and HCl molecule, **c)** water remains confined around the initial position.

We propose that reoxidation can occur through two pathways, both involving water dissociation. One is the removal of Cl from the Ge surface as HCl and the other involves the removal of the SAM is as sketched in **Figure 13**, while both result in Ge-OH at the surface.

4.5　Conclusions

By tracking the growth of native GeO_2 in time using XPS, the role that water vapour plays in SAM degradation and Ge surface oxidation is elucidated. The XPS results obtained indicate that higher humidity environments result in increased rates of oxidation of the thiol-passivated Ge surface. The WCA analysis complements these results wherein a greater decrease in contact angle is observed for the Ge samples exposed to the high humidity environment in contrast to those subjected to lower humidity environments. There are two potential avenues for SAM removal and Ge oxidation, (i) H_2O attacking the Cl-Ge bond, which remain after the HCl etch, to form HCl and Ge-OH, and (ii) H_2O attacking the R-S-Ge bond to form R-SH and Ge-OH. This reaction paves the way for oxygen in the air to attack Ge-Ge bonds.[65] The methyl termination in the tail group plays a crucial role in acting as a barrier to water in the air, preventing water from migrating to the Ge-SAM interface. Oxidation that does occur is likely due to the presence of defect sites in the SAM, which allow water to easily migrate to the surface. The Ge surfaces discussed in this work are assumed atomically flat. In reality, surface features such as ledges and steps are present which cause the structure of the SAM to be interrupted and offer sites for water molecules to diffuse through the SAM to the Ge surface. Thus, DFT simulations which incorporate such surface features are warranted and would complement this work. The experimental and modelling results highlight that by controlling the humidity of the environment the thiol-passivated Ge coupons are exposed to, the longevity of the SAM can be improved and thus the resistance to oxidation of the underlying Ge. Alternatively, improving the SAM can also have an impact on stability, for example by increasing the hydrophobicity of the tail group termination by using a fluorinated group, by increasing the chain alignment and packing density, or by decreasing the

defect density. Lastly, water induced thiol desorption could be a promising method for non-destructively removing the SAM during the fabrication process, as AFM showed little to no impact on surface roughness. This desorption process warrants further investigation.

4.6   References

1.   Taylor, S.R., *Abundance of Chemical Elements in the Continental Crust: A New Table.* Geochimica et Cosmochimica Acta, 1964. **28**(8): p. 1273-1285.

2.   Petersen, K.E., *Silicon as a Mechanical Material.* Proceedings of the IEEE, 1982. **70**(5): p. 420-457.

3.   Pacchioni, G., L. Skuja, and D. Griscom, *Defects in SiO2 and Related Dielectrics: Science and Technology.* 2000.

4.   Wilk, G.D., R.M. Wallace, and J.M. Anthony, *High-κ Gate Dielectrics: Current Status and Materials Properties Considerations.* Journal of Applied Physics, 2001. **89**(10): p. 5243-5275.

5.   Hirose, M., *Electron Tunneling Through Ultrathin SiO2.* Materials Science and Engineering: B, 1996. **41**(1): p. 35-38.

6.   Maserjian, J. and N. Zamani, *Behavior of the Si/SiO2 interface observed by Fowler-Nordheim tunneling.* Journal of Applied Physics, 1982. **53**(1): p. 559-567.

7.   Gusev, E.P., D.A. Buchanan, E. Cartier, A. Kumar, D. DiMaria, S. Guha, A. Callegari, S. Zafar, P.C. Jamison, D.A. Neumayer, M. Copel, M.A. Gribelyuk, H. Okorn-Schmidt, C.D. Emic, P. Kozlowski, K. Chan, N. Bojarczuk, L.

Ragnarsson, P. Ronsheim, K. Rim, R.J. Fleming, A. Mocuta, and A. Ajmera. *Ultrathin High-K Gate Stacks for Advanced CMOS Devices.* in *International Electron Devices Meeting. Technical Digest (Cat. No.01CH37224).* 2001.

8.   Gupta, A., T. Sakthivel, and S. Seal, *Recent Development in 2D Materials Beyond Graphene.* Progress in Materials Science, 2015. **73**: p. 44-126.

9.   Tomioka, K., M. Yoshimura, and T. Fukui, *A III–V Nanowire Channel on Silicon for High-Performance Vertical Transistors.* Nature, 2012. **488**(7410): p. 189-192.

10.   Mirabelli, G., C. McGeough, M. Schmidt, E.K. McCarthy, S. Monaghan, I.M. Povey, M. McCarthy, F. Gity, R. Nagle, G. Hughes, A. Cafolla, P.K. Hurley, and R. Duffy, *Air Sensitivity of MoS2, MoSe2, MoTe2, HfS2, and HfSe2.* Journal of Applied Physics, 2016. **120**(12): p. 125102.

11.   Manzeli, S., D. Ovchinnikov, D. Pasquier, O.V. Yazyev, and A. Kis, *2D Transition Metal Dichalcogenides.* Nature Reviews Materials, 2017. **2**: p. 17033.

12.   Crowson, P., *Germanium*, in *Minerals Handbook*. 1996, Palgrave Macmillan: London.

13.   Dal, M.J.H.v., G. Vellianitis, G. Doornbos, B. Duriez, M.C. Holland, T. Vasen, A. Afzalian, E. Chen, S.K. Su, T.K. Chen, T.M. Shen, Z.Q. Wu, and C.H. Diaz. *Ge CMOS Gate Stack and Contact Development for Vertically Stacked Lateral Nanowire FETs.* in *2018 IEEE International Electron Devices Meeting (IEDM).* 2018.

14. Shang, H., H. Okorn-Schimdt, J. Ott, P. Kozlowski, S. Steen, E.C. Jones, H.P. Wong, and W. Hanesch, *Electrical Characterization of Germanium p-Channel MOSFETs.* IEEE Electron Device Letters, 2003. **24**(4): p. 242-244.

15. Huiling, S., L. Kam-Leung, P. Kozlowski, C.D. Emic, I. Babich, E. Sikorski, I. Meikei, H.P. Wong, K. Guarini, and W. Haensch, *Self-Aligned n-Channel Germanium MOSFETs with a Thin Ge Oxynitride Gate Dielectric and Tungsten Gate.* IEEE Electron Device Letters, 2004. **25**(3): p. 135-137.

16. A. Agrawal, S.C., W. Rachmady, S. Vishwanath, S. Ghose, M. Mehta, J. Torres, A.A. Oni, X. Weng, H. Li, D. Merrill, M. Metz, A. Murthy, J. Kavalieros, *Gate-All-Around Strained Si0.4Ge0.6 Nanosheet PMOS on Strain Relaxed Buffer for High Performance Low Power Logic Application*. 2020: Intel Newsroom.

17. Luo, X., T. Nishimura, T. Yajima, and A. Toriumi, *Understanding of Fermi level pinning at metal/germanium interface based on semiconductor structure.* Applied Physics Express, 2020. **13**(3): p. 031003.

18. Nishimura, T., K. Kita, and A. Toriumi, *Evidence for strong Fermi-level pinning due to metal-induced gap states at metal/germanium interface.* Applied Physics Letters, 2007. **91**(12): p. 123123.

19. Dimoulas, A., P. Tsipas, A. Sotiropoulos, and E.K. Evangelou, *Fermi-Level Pinning and Charge Neutrality Level in Germanium.* Applied Physics Letters, 2006. **89**(25): p. 252110.

20. Rojas Delgado, R., R.M. Jacobberger, S.S. Roy, V.S. Mangu, M.S. Arnold, F. Cavallo, and M.G. Lagally, *Passivation of Germanium by Graphene.* ACS Applied Materials & Interfaces, 2017. **9**(20): p. 17629-17636.

21. Weber, J.R., A. Janotti, and C.G. Van de Walle, *Dangling Bonds and Vacancies in Germanium.* Physical Review B, 2013. **87**(3): p. 035203.

22. Toriumi, A., *High Electron Mobility Germanium (Ge) Metal Oxide Semiconductor Field Effect Transistors (MOSFETs)*, in *Silicon–Germanium (SiGe) Nanostructures*, Y. Shiraki and N. Usami, Editors. 2011, Woodhead Publishing. p. 528-550.

23. Wang, S.K., K. Kita, C.H. Lee, T. Tabata, T. Nishimura, K. Nagashio, and A. Toriumi, *Desorption Kinetics of GeO From GeO2/Ge Structure.* Journal of Applied Physics, 2010. **108**(5): p. 054104.

24. Bodlaki, D., H. Yamamoto, D.H. Waldeck, and E. Borguet, *Ambient Stability of Chemically Passivated Germanium Interfaces.* Surface Science, 2003. **543**(1): p. 63-74.

25. Zhang, X.J., G. Xue, A. Agarwal, R. Tsu, M.A. Hasan, J.E. Greene, and A. Rockett, *Thermal Desorption of Ultraviolet–Ozone Oxidized Ge(001) for Substrate Cleaning.* Journal of Vacuum Science & Technology A, 1993. **11**(5): p. 2553-2561.

26. Dharma-wardana, M.W.C., M.Z. Zgierski, D. Ritchie, J.G. Ping, and H. Ruda, *Comparison of Cluster and Slab Models of the Surface Structure of Cl-Terminated Ge(111) and GaAs(111) Surfaces.* Physical Review B, 1999. **59**(24): p. 15766-15771.

27. Molina, A., J.R. Shallenberger, and S.E. Mohney, *Vapor Phase Passivation of (100) Germanium Surfaces with HBr.* Journal of Vacuum Science & Technology A, 2020. **38**(2): p. 023208.

28. Filler, M.A., J.A. Van Deventer, A.J. Keung, and S.F. Bent, *Carboxylic Acid Chemistry at the Ge(100)-2 × 1 Interface: Bidentate Bridging Structure Formation on a Semiconductor Surface.* Journal of the American Chemical Society, 2006. **128**(3): p. 770-779.

29. Roche, J., P. Ryan, and G.J. Hughes, *Core Level Photoemission Studies of the Sulphur Terminated Ge(100) Surface.* Applied Surface Science, 2001. **174**(3): p. 271-274.

30. Maggioni, G., S. Carturan, L. Fiorese, N. Pinto, F. Caproli, D.R. Napoli, M. Giarola, and G. Mariotto, *Germanium Nitride and Oxynitride Films for Surface Passivation of Ge Radiation Detectors.* Applied Surface Science, 2017. **393**: p. 119-126.

31. Kim, H., P.C. McIntyre, C.O. Chui, K.C. Saraswat, and M.-H. Cho, *Interfacial Characteristics of HfO2 Grown on Nitrided Ge (100) Substrates by Atomic-Layer Deposition.* Applied Physics Letters, 2004. **85**(14): p. 2902-2904.

32. Campbell, G.P., B. Kiraly, R.M. Jacobberger, A.J. Mannix, M.S. Arnold, M.C. Hersam, N.P. Guisinger, and M.J. Bedzyk, *Epitaxial Graphene-Encapsulated Surface Reconstruction of Ge(110).* Physical Review Materials, 2018. **2**(4): p. 044004.

33. Kiraly, B., R.M. Jacobberger, A.J. Mannix, G.P. Campbell, M.J. Bedzyk, M.S. Arnold, M.C. Hersam, and N.P. Guisinger, *Electronic and Mechanical Properties of Graphene–Germanium Interfaces Grown by Chemical Vapor Deposition.* Nano Letters, 2015. **15**(11): p. 7414-7420.

34. Collins, G., D. Aureau, J.D. Holmes, A. Etcheberry, and C. O'Dwyer, *Germanium Oxide Removal by Citric Acid and Thiol Passivation from Citric Acid-Terminated Ge(100).* Langmuir, 2014. **30**(47): p. 14123-14127.

35. Garvey, S., J.D. Holmes, Y.S. Kim, and B. Long, *Vapor-Phase Passivation of Chlorine-Terminated Ge(100) using Self-Assembled Monolayers of Hexanethiol.* ACS Applied Materials & Interfaces, 2020.

36. Bain, C.D., H.A. Biebuyck, and G.M. Whitesides, *Comparison of Self-Assembled Monolayers on Gold: Coadsorption of Thiols and Disulfides.* Langmuir, 1989. **5**(3): p. 723-727.

37. Bergsman, D.S., T.-L. Liu, R.G. Closser, K.L. Nardi, N. Draeger, D.M. Hausmann, and S.F. Bent, *Formation and Ripening of Self-Assembled Multilayers from the Vapor-Phase Deposition of Dodecanethiol on Copper Oxide.* Chemistry of Materials, 2018. **30**(16): p. 5694-5703.

38. Kanukula, D.C.K., A. Boyapati, Y. Md, Iqbal, and S. Bojja, *Corrosion protection of copper by self assembled monolayers.* Indian Journal of Chemical Technology, 2009. **16**: p. 25-31.

39. Alessio Verni, G., B. Long, F. Gity, M. Lanius, P. Schüffelgen, G. Mussler, D. Grützmacher, J. Greer, and J.D. Holmes, *Oxide Removal and Stabilization of Bismuth Thin Films Through Chemically Bound Thiol Layers.* RSC Advances, 2018. **8**(58): p. 33368-33373.

40. Long, B., M. Manning, M. Burke, B.N. Szafranek, G. Visimberga, D. Thompson, J.C. Greer, I.M. Povey, J. MacHale, G. Lejosne, D. Neumaier, and A.J. Quinn, *Non-Covalent Functionalization of Graphene Using Self-*

Assembly of Alkane-Amines. Advanced Functional Materials, 2012. **22**(4): p. 717-725.

41.   Zerulla, D. and T. Chassé, *Structure and Self-Assembly of Alkanethiols on III– V Semiconductor (110) Surfaces.* Journal of Electron Spectroscopy and Related Phenomena, 2009. **172**(1): p. 78-87.

42.   Muscat, A.J., *Self-Assembly of Functionalized Organic Molecules on Flat Solid Surfaces*, in *Encyclopedia of Interfacial Chemistry: Surface Science and Electrochemistry*. 2018. p. 810-816.

43.   Singh, M., N. Kaur, and E. Comini, *The role of self-assembled monolayers in electronic devices.* Journal of Materials Chemistry C, 2020. **8**(12): p. 3938-3955.

44.   Takenaka, M., K. Morii, M. Sugiyama, Y. Nakano, and S. Takagi, *Gas Phase Doping of Arsenic into (100), (110), and (111) Germanium Substrates Using a Metal–Organic Source.* Japanese Journal of Applied Physics, 2011. **50**: p. 010105.

45.   Kennedy, N., S. Garvey, B. Maccioni, L. Eaton, M. Nolan, R. Duffy, F. Meaney, M. Kennedy, J.D. Holmes, and B. Long, *Monolayer Doping of Germanium with Arsenic: A New Chemical Route to Achieve Optimal Dopant Activation.* Langmuir, 2020. **36**(34): p. 9993-10002.

46.   Sgarbossa, F., S.M. Carturan, D.D. Salvador, G.A. Rizzi, E. Napolitani, G. Maggioni, W. Raniero, D.R. Napoli, G. Granozzi, and A. Carnera, *Monolayer Doping of Germanium by Phosphorus-Containing Molecules.* Nanotechnology, 2018. **29**(46): p. 465702.

47.   Sgarbossa, F., G. Maggioni, G.A. Rizzi, S.M. Carturan, E. Napolitani, W. Raniero, C. Carraro, F. Bondino, I. Píš, and D. De Salvador, *Self-Limiting Sb Monolayer as a Diffusion Source for Ge Doping.* Applied Surface Science, 2019. **496**: p. 143713.

48.   Wolff, C.M., L. Canil, C. Rehermann, N. Ngoc Linh, F. Zu, M. Ralaiarisoa, P. Caprioglio, L. Fiedler, M. Stolterfoht, S. Kogikoski, I. Bald, N. Koch, E.L. Unger, T. Dittrich, A. Abate, and D. Neher, *Perfluorinated Self-Assembled Monolayers Enhance the Stability and Efficiency of Inverted Perovskite Solar Cells.* ACS Nano, 2020. **14**(2): p. 1445-1456.

49.   Yalcin, E., M. Can, C. Rodriguez-Seco, E. Aktas, R. Pudi, W. Cambarau, S. Demic, and E. Palomares, *Semiconductor Self-Assembled Monolayers as Selective Contacts for Efficient PiN Perovskite Solar Cells.* Energy & Environmental Science, 2019. **12**(1): p. 230-237.

50.   Mandler, D. and S. Kraus-Ophir, *Self-Assembled Monolayers (SAMs) for Electrochemical Sensing.* Journal of Solid State Electrochemistry, 2011. **15**(7): p. 1535.

51.   Cai, Q., B. Xu, L. Ye, Z. Di, S. Huang, X. Du, J. Zhang, Q. Jin, and J. Zhao, *1-Dodecanethiol Based Highly Stable Self-Assembled Monolayers for Germanium Passivation.* Applied Surface Science, 2015. **353**: p. 890-901.

52.   Hohman, J.N., M. Kim, H.R. Bednar, J.A. Lawrence, P.D. McClanahan, and P.S. Weiss, *Simple, Robust Molecular Self-Assembly on Germanium.* Chemical Science, 2011. **2**(7): p. 1334-1343.

53.   Wang, D., Y.L. Chang, Z. Liu, and H. Dai, *Oxidation Resistant Germanium Nanowires: Bulk Synthesis, Long Chain Alkanethiol Functionalization, and*

Langmuir-Blodgett Assembly. Journal of the American Chemical Society, 2005. **127**(33): p. 11871-11875.

54.   Silva-Quinones, D., C. He, R.E. Butera, G.T. Wang, and A.V. Teplyakov, *Reaction of BCl3 with H- and Cl-Terminated Si(100) as a Pathway for Selective, Monolayer Doping through Wet Chemistry.* Applied Surface Science, 2020: p. 146907.

55.   Kresse, G. and J. Furthmüller, *Efficiency of Ab-Initio Total Energy Calculations for Metals and Semiconductors using a Plane-Wave Basis Set.* Computational Materials Science, 1996. **6**(1): p. 15-50.

56.   Kresse, G. and J. Furthmüller, *Efficient Iterative Schemes for Ab-Initio Total-Energy Calculations using a Plane-Wave Basis Set.* Physical Review B, 1996. **54**(16): p. 11169-11186.

57.   Blöchl, P.E., *Projector augmented-wave method.* Physical Review B, 1994. **50**(24): p. 17953-17979.

58.   Perdew, J.P., K. Burke, and M. Ernzerhof, *Generalized Gradient Approximation Made Simple.* Physical Review Letters, 1996. **77**(18): p. 3865-3868.

59.   Grimme, S., J. Antony, S. Ehrlich, and H. Krieg, *A Consistent and Accurate Ab-Initio Parametrization of Density Functional Dispersion Correction (DFT-D) for the 94 Elements H-Pu.* The Journal of Chemical Physics, 2010. **132**(15): p. 154104.

60.   Monkhorst, H.J. and J.D. Pack, *Special Points for Brillouin-Zone Integrations.* Physical Review B, 1976. **13**(12): p. 5188-5192.

61. Murakami, H., T. Fujioka, A. Ohta, T. Bando, S. Higashi, and S. Miyazaki, *Characterization of Interfaces between Chemically Cleaned or Thermally Oxidized Germanium and Metals*. 2010, ECS.

62. Morgan, W.E. and J.R. Van Wazer, *Binding energy shifts in the x-ray photoelectron spectra of a series of related Group IVa compounds*. The Journal of Physical Chemistry, 1973. **77**(7): p. 964-969.

63. Bal, J., S. Kundu, and S. Hazra, *Hydrophilic-Like Wettability of Cl-Passivated Ge(001) Surface*. Chemical Physics, 2012. **406**: p. 72.

64. Howell, C., R. Maul, W. Wenzel, and P. Koelsch, *Interactions of Hydrophobic and Hydrophilic Self-Assembled Monolayers with Water as Probed by Sum-Frequency-Generation Spectroscopy*. Chemical Physics Letters, 2010. **494**(4): p. 193-197.

65. Sun, S., Y. Sun, Z. Liu, D.-I. Lee, and P. Pianetta, *Roles of Oxygen and Water Vapor in the Oxidation of Halogen Terminated Ge(111) Surfaces*. Applied Physics Letters, 2006. **89**(23): p. 231925.

Chapter 5

Effect of Thiol Chain Length on Oxidation Resistance of Thiol-SAM-Passivated Ge(100) Surfaces

This chapter is adapted from the following *ACS Applied Materials & Interfaces* manuscript. Consequently, certain concepts within this chapter may be repeated in other chapters.

Manuscript:

5.1 Abstract

Germanium (Ge) has long been a considered a primary candidate to serve as the channel material in CMOS devices. The International Roadmap for Devices and Systems (IRDS™) predicts that from 2024, Ge, 2D materials or III-Vs will be the channel materials of choice for logic devices. However, since Ge is currently more easily integrable into VLSI (Very Large Scale Integration) lines than the other candidates, it has received more interest. Unfortunately, the complexity and water solubility of the native oxide of Ge has complicated its use as a channel material. Methods to remove the native oxide and replace it with a stable, passivating layer are being scrutinised in the hope that issues with the oxide can be circumvented. It is hoped that this will promote widespread use of Ge as the channel material. One such passivation method is the use of self-assembled monolayers (SAMs) of organic molecules. In the present work, a series of 1-alkanethiols, with varying carbon chain lengths are used to create SAMs on Ge(100) and a study of the reoxidation of the passivated Ge upon exposure to ambient conditions is undertaken. The longer thiol molecules outperform their shorte-chain counterparts in inhibiting reoxidation over 168 hours of exposure to ambient. At the same time, we find that Ge surfaces passivated by the short-chain thiols (down to C_4H_9SH) still display acceptable resistance to reoxidation and therefore offer a passivation method that also reduces the C content on the Ge surface. These results also highlight the significance of the van der Waals interactions between the backbones of the thiols in relation to SAM stability and prevention of oxide growth.

5.2   Introduction

In 1946, when Zisman published a paper on the self-assembly of a surfactant molecule onto a metal surface, interest in the scientific community was muted since the potential of self-assembly had not yet been recognised.[1] Self-assembly is a process by which a disordered system of components forms an organised structure or pattern due to local interactions among the components themselves.[2] This phenomenon occurs naturally in biological cells to form supramolecular organisations of complex systems [3]; however, it was Zisman who introduced the concept to technologists for the purposes of surface property modification and engineering of materials. Since then, self-assembled monolayers (SAMs) have been used to augment the surface properties of many different materials [4] as they can have considerable effect on surface properties while being relatively easy to prepare. The system that has been studied most is thiol-SAMs on gold.[5-8] In 2005, Whitesides et al. published an in-depth review on the topic [9]; however, this system is still being scrutinised and recently it has been discovered that non-chemisorbed gold-sulfur binding prevails in self-assembled monolayers.[10] The list of uses for SAMs is a lengthy one; however, some uses include corrosion prevention,[11] friction reduction,[12, 13] and as anti-stiction coatings in MEMs fabrication.[14]

Specifically, in relation to forming SAMs on Ge, a review of the literature shows that there are three main methods. Namely, using the Grignard reaction, [15, 16] alkanethiol passivation [17, 18] and through hydrogermylation.[19] Both the Grignard reaction and hydrogermylation approach result in the creation of Ge-C bonds whereas the alkanethiol passivation route involves the formation of Ge-S bonds.[20] The vast majority of the literature on alkanethiol ($CH_3(CH_2)_{n-1}SH$) passivation of Ge

pertains to 1-dodecanethiol ($C_{12}H_{26}S$).[21-25] That said, Han et al. have demonstrated that SAMs of both 1-octadecanethiolates ($C_{18}H_{37}S$) and 1-octanethiolates ($CH_3(CH_2)_7S$) can be formed when an oxide-free, H-terminated Ge(111) surface is reacted with a solution of the thiol molecules.[26] In both cases, they found the surface coverage of the SAM to be good with a high degree of orientational ordering and thermal stability of the passivation layers up to 450 K indicating that the Ge-S bond is a covalent bond. In this study, alkanethiol passivation of oxide-free Ge is conducted using a range of aliphatic thiol molecules with a range of carbon chain lengths in an effort to discern what effect the length of the thiol chain has on the effectiveness of the SAM at inhibiting Ge oxidation over the course of 168 hours. The main motivation to use short-chain thiols for Ge passivation relates to processing temperatures. Thiols with lower molecular weights have higher vapour pressures and thus require less heat to form the thiol vapour necessary to achieve a vapour-phase passivation. Reducing the processing temperatures required to achieve passivation is advantageous since a low thermal budget allows the passivation process to be carried out further down the device fabrication line and previous processing steps are less likely to be affected.

Ge is a very promising channel material candidate for CMOS devices since it has both higher electron and hole mobilities than Si [27] (over 2 and 4 times, respectively) while being easier to integrate into current CMOS processing lines than the other high-mobility channel material candidates (TMDs, III-Vs). The native Ge oxide (the bulk of which is GeO_2) is not a suitable dielectric with characteristics that make it undesirable from a device perspective. For example, unlike SiO_2, GeO_2 is water-soluble and thus the aqueous processing steps that are currently used in device manufacturing would cause oxide etching and regrowth upon exposure to air – multiple cycles of which would cause loss of Ge, an issue which is critical when

working with Ge nanostructures such as nanoribbons or pillars.[20] Also, the interface between Ge and its native oxide is not ideal with vacancies that trap charge carriers and hinder device performance.[28] Consequently, methods to replace the Ge oxide are of interest to those who wish to circumvent the aforementioned issues to work towards enabling the use of Ge as a channel material in future CMOS devices. Alkanethiol SAMs have been shown to be effective at inhibiting oxide growth on Ge upon exposure to the ambient.[23, 29] The alkanethiol passivation of Ge is a two-step process. The native oxide must first be replaced with a surface termination layer that is reactive toward thiols. The native oxide can be removed using acid halides (HX, X = F, Cl, Br).[30-34] Removing the oxide using HF yields a H-terminated surface which can be further functionalised by thiol molecules. However, the H-terminated surface itself does not offer prolonged oxidation resistance, in fact, the surface begins to reoxidise within minutes.[35] As such, achieving passivation without also causing oxidation of the H-terminated Ge surface can be challenging. Therefore, terminating the Ge with a layer, which is more robust than the H-termination yet still reactive toward further functionalisation, is advantageous. Other acid halides can be used for this purpose since unlike with HF, upon oxide removal, the surface is terminated by the halide atoms (Cl, Br) rather than H atoms.[30, 34] The Cl-terminated surface specifically, while still being reactive toward thiols, oxidises at a slower rate when compared to H-terminated Ge surfaces.[30] The Cl-terminated Ge surface therefore allows for alkanethiol passivation with less risk of concurrent oxide growth.

The stability of thiol-passivated Ge surfaces is dependent on a number of factors. Alkanethiol chain length is hypothesised to be a critical factor in the stability of the SAM since longer alkane chains maximise the van der Waals (vdW) interactions between adjacent alkanethiol molecules in the SAM. VdW interactions are weak

interactions that occur between atoms that are in close proximity to each other. In the case of an alkanethiol-SAM, the $-CH_2$ units in the backbones of adjacent molecules interact with one another. Although this local interaction is weak in nature, the global effect can be considerable. The significance of this phenomenon is made evident by the fact that thiol SAMs on gold are stable even though non-chemisorbed gold-sulfur binding prevails, as previously mentioned.[10]

Another contributing factor to the stability of the SAM is the parity of the molecule used to achieve the SAM - whether there is an odd or even number of C atoms in the backbone of the passivating thiol molecule. Odd-even effects are a widely observed phenomenon across the sciences but in biology, physical chemistry and material science in particular.[36] Generally, the effect can be described as an alteration in the structure and/or properties of a system based on whether there are an odd or even number of units in a molecule.[36] In thiol SAMs, the unit is a $-CH_2$ moiety. These kinds of effects have been observed on Ag [37-39]; however, due to the chemical inertness of Au under ambient conditions and the excellent reproducibility in preparing high-quality SAMs as a consequence, the majority of the literature on the odd-even effect of SAMs is on Au.[40-44] When forming a SAM, thiol molecules with an odd number of $-CH_2$ units in the C backbone pack differently to those with an even number of $-CH_2$ units. In **Figure 1**, thiol molecules of opposite parity are displayed. The orientation of the terminal group is different in each case. This has been shown to have implications on the properties of the SAM itself. Baghbanzadeh et al. observed an odd-even effect on the tunnelling current density through Au junctions passivated by SAMs of n-alkanethiolates with odd and even numbers of $-CH_2$ units.[45] Also, Amara et al. have elucidated how properties such as capacitance,

dielectric constant and surface hydrophobicity of Au passivated by thiol-SAMs depend on both the length and parity of the thiol molecules used.[43]

CH$_3$(CH$_2$)$_n$SGe SAM

= S
= H
= Ge
= C

n$_{even}$ **n$_{odd}$**
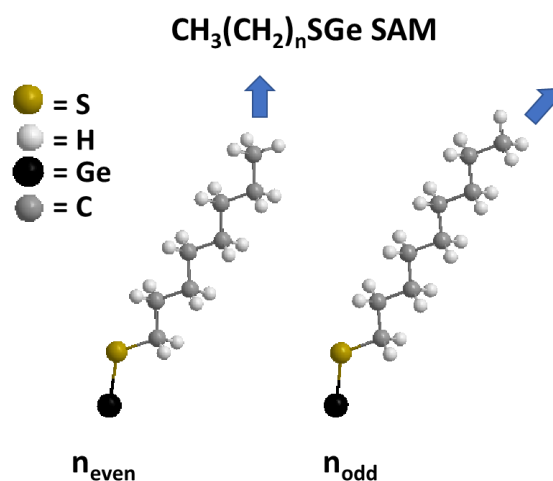
Figure 1. Thiol molecules with even and odd numbers of –CH$_2$ units in the backbone are displayed. The difference in the orientation of the terminal group is apparent.

In an effort to elucidate the impact of the thiol chain length on the stability of a SAM on Ge and its oxidation resistance we present a detailed investigation of the preparation and properties of thiol SAM functionalised Ge and a set of first principles density functional theory (DFT) calculations of model SAM-Ge systems. We chose to simplify the analysis and neglect odd-even effects in the thiols and therefore only thiol molecules with an even number of –CH$_2$ units in the thiol backbone are used in this study.

5.3 Methods

5.3.1 Preparation of SAMs on Ge surfaces

Passivation of the Ge was achieved using a range of aliphatic thiol molecules purchased from Sigma-Aldrich using a vapour-phase method previously outlined.[29] Specifically, 97% ethanethiol (C2), 99% 1-butanethiol (C4), 99% 1-hexanethiol (C6), 98.5% 1-octanethiol (C8) and 98% 1-dodecanethiol (C12) were used. For comparison, a Cl-terminated Ge surface was prepared also simply by etching in 20% HCl for 10 minutes to remove the native oxide followed by drying under a stream of N_2. Between measurements, the samples were stored in a temperature and humidity controlled environment (Vötsch temperature test chamber). To emulate ambient conditions, the relative humidity (RH) and temperature were set to 40% and 20°C, respectively. XPS measurements were taken directly after the passivation reaction and after 24 and 168 hours of exposure to the controlled ambient environment.

5.3.2 Characterisation Methods

5.3.2.1 X-ray Photoelectron Spectroscopy (XPS)

Spectra were acquired on an Oxford Applied Research Escabase XPS System equipped with a CLASS VM 100 mm mean radius hemispherical electron energy analyser with multichannel detectors in an analysis chamber with a base pressure of 5.0×10^{-9} mbar. A step size of 0.7 eV, pass energy of 50 eV and a dwell of 0.3 s was used for survey spectra which were swept twice. All core level scans other than the S 2p were acquired with a step size of 0.1 eV, a dwell time of 0.1 s and a pass energy of 20 eV averaged over 10 scans. The S 2p scans were acquired with a step size of 0.1 eV, a dwell time of 0.1 eV and a pass energy of 50 eV averaged over 20 scans in an

effort to maximise the intensity of the S 2p peaks. A non-monochromated Al-Kα X-ray source (1486.58 eV) at 100 W power (10 mA, 10kV) was used for all scans. All spectra were acquired at a take-off angle of 90° with respect to the analyser axis and were charge corrected with respect to the C 1s photoelectric line at 284.8 eV. A Shirley type background was used for construction and peak fitting of synthetic peaks. Synthetic peaks were a mix of Gaussian-Lorenzian, the Ge 2p spectra were fit using Gaussian-Lorentzian peak shape GL(90) for the elemental Ge peak and Lorentzian peak shape LA(1.53,243) for all other peaks. The relative sensitivity factors used are from a CasaXPS library containing Scofield cross-sections. The fitted Ge 2p peaks used to determine oxide thicknesses are displayed in the **Appendix** section (**Figure S5.1** & **S5.2**). Oxide thickness was calculated using the method outlined previously by Murakami et al.[46]

$$d_{GeO_2} = \lambda_{GeO_2} sin\theta \; ln\left(\frac{I_{Ge}^{\infty}}{I_{GeO_2}^{\infty}} \frac{I_{GeO_2}}{I_{Ge}} + 1 \right)$$

where λ_{GeO_2} is the inelastic mean free path for the Ge 2p transition, which is 0.9 nm; the photoemission angle θ is 90°; $I_{Ge}^{\infty}/I_{GeO_2}^{\infty}$ is the ratio of the Ge 2p signal from infinitely thick Ge to infinitely thick GeO_2 and is 1.73; I_{GeO_2} is the intensity of the of native oxide (GeO_2) peak from curve fitting the Ge 2p feature; I_{Ge} is the intensity of the metallic Ge peak from curve fitting the Ge 2p transition.

5.3.2.2   Water Contact Analysis (WCA)

An image of a 50 µL drop of deionised water that was deposited on to the Ge surface was taken such that the angle between the water, Ge surface and air could be measured. Increased hydrophobicity of the passivated Ge surfaces is used as an indirect indication that the passivation layer is present.

5.3.3 First Principles Simulation Methodology

We studied alkanethiolate SAMs on the Ge(100) surface from first principles density functional theory (DFT) using a basis set of periodic plane wave as implemented in the Vienna Ab Initio Software Package (VASP5.4).[47, 48] The core electrons are described by projector augmented wave (PAW) [49] potentials and the exchange and correlation energies are approximated by the generalised gradient approximation (GGA) with the Perdew-Burke-Ernzerhof (PBE) [50] gradient corrected functional. In order to take into account the van der Waals interactions between alkanethiols, we used the DFT-D3 dispersion correction method [51] that incorporates the long-range dispersion contribution to the exchange-correlation PBE functional. We use the following valance electron configurations; for germanium; Ge $4s^2$ and $4p^2$, for chlorine; Cl $3s^2$ and $3p^5$, for sulfur; S $3s^2$ and $3p^4$ and for carbon; C$2s^2$ and $2p^4$. All the calculations use an energy cut-off for the valence electron plane wave basis set of 420 eV and the convergence criteria for electronic relaxations and ionic relaxations are 10^{-4} eV and 0.02 eV/Å, respectively. In addition, the conjugate-gradient algorithm was used for the relaxation of the ions during the calculations, and a 2×2×1 Monkhorst–Pack k-points grid [52] was used for the integrals in the Brillouin zone for a correct energy convergence.

5.4 Results & Discussion

XPS is an extremely useful method for probing SAMs and thin films in general since it allows for the elemental composition, chemical state and electronic structure of the surface of a material to be ascertained. XPS is used in this study to track the reoxidation of the passivated Ge(100) surfaces upon exposure to ambient conditions to elucidate what effect thiol chain length has on the effectiveness of the SAMs at inhibiting Ge oxidation. Thiol SAMs have previously been shown to be effective at inhibiting oxidation of Ge.[23] It is hypothesised that long-chain thiols rather than short-chain thiols are better at preventing Ge oxidation since the SAM is stabilised by vdW forces between the C backbones of the adjacent thiol molecules. The global vdW interaction increases with carbon chain length. However, to the knowledge of the authors, this has not yet been experimentally determined for thiol-SAMs on Ge. Five thiol molecules were chosen for this study, each containing an even number of $-CH_2$ units in the thiol backbone. They are as follows: ethanethiol (C2), 1-butanethiol (C4), 1-hexanethiol (C6), 1-octanethiol (C8) and 1-dodecanethiol (C12). These molecules were used to passivate Ge and a study of the reoxidation of Ge upon exposure to ambient conditions was carried out.

The calculated GeO_2 thicknesses after 0, 24 and 168 hours are graphically represented in **Figure 2** and tabulated in **Table 1**. Fitted Ge 2p spectra are included in the **Appendix** section – **Figures S5.1** & **S5.2**. For reference, a Cl-terminated Ge surface is included in the study as a baseline for Ge reoxidation upon exposure to ambient conditions. In the case of BT, HT, OT and DT no GeO_2 was detectable by XPS directly after passivation. This was not the case with ET-passivated Ge. The authors could not passivate Ge with ET without also causing a non-negligible amount

of Ge oxidation (0.06 nm). It is hypothesised that the alkanethiol chain is too short in the case of ET for any meaningful stabilisation effect from vdW forces to occur. Consequently, the sample begins to oxidise in the short space of time (5 minutes) that is required to clean the sample after passivation and to load into the XPS chamber.

From **Figure 2**, a clear pattern is observed whereby Ge oxidation trends with thiol chain length. That is, SAMs of thiol molecules consisting of longer chains inhibit the oxidation of Ge more effectively than SAMs comprised of shorter chains upon exposure to ambient conditions for 168 hours. Over the course of the 168 hour period, 0.08 nm of GeO_2 grows on the DT-passivated Ge whereas 0.12 nm, 0.14 nm and 0.16 nm grows on OT-, HT- and BT-passivated Ge, respectively. These results are tabulated in **Table 1**. Included in this table are the calculated oxide thicknesses for as-received Ge and Cl-terminated Ge after 0, 24 and 168 hours of exposure to ambient conditions.
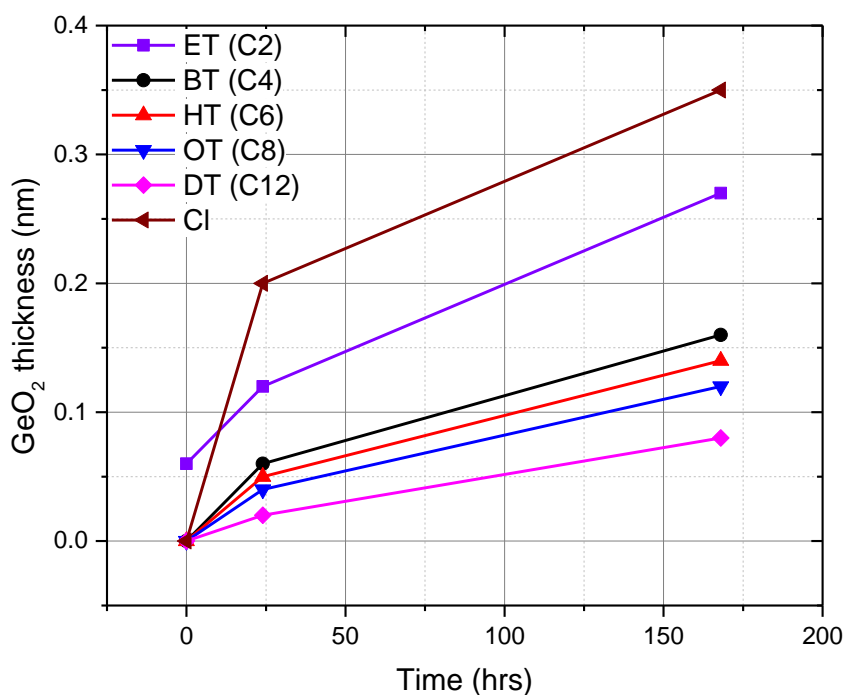
Figure 2. GeO$_2$ growth over 24 and 168 hours for Ge passivated by ET (purple), BT (black), HT (red), OT (blue), DT (pink), Cl (brown).

The rate of oxidation for each sample is greatest in the first 24 hours of exposure to ambient conditions indicating that the sites in the SAM that are susceptible to in-diffusion of water molecules facilitate oxidation at that spot on the Ge and the growth of the seed oxide is a slower process. In addition, oxidation rates strongly trend with thiol chain length over the first 24 hours of exposure; however, the rate of oxidation over the proceeding 144 hours is less dependent on thiol chain length evidenced by similar but not equal rates of oxidation.

Surface termination	As-Rec	Cl-Ge	ET (C2)	BT (C4)	HT (C6)	OT (C8)	DT (C12)
Exposure time (hrs)	Oxide Thickness (nm)						
0	2.12	0	0.06	0	0	0	0
24	2.12	0.2	0.12	0.06	0.05	0.04	0.02
168	2.12	0.35	0.27	0.16	0.14	0.12	0.08

Table 1. Calculated oxide thicknesses for Ge with a range of surface terminations.

Density Functional Theory (DFT) calculations were performed to understand the atomic level details of the role of the carbon chain length of the thiol molecule on the stability of thiol-SAM-passivated Ge(100) surfaces. The Ge(100) surface is modelled with a (2x2) surface supercell expansion with 128 atoms. To simulate the conditions of the bulk, Ge atoms in the bottom layer of the slab are fixed. The top

surface, composed of 8 Ge atoms, was initially fully passivated with Cl atoms. Surface calculations were performed using the slab technique, taking into account the periodically repeating infinite layers separated by vacuum layers along the normal surface. A vacuum thickness of 40 Å is adopted in all cases in order to remove interaction between periodic slabs perpendicular to the surface, while allowing for a range of alkanethiol chain lengths from 4 to 12 C atoms to be explored.

To determine the stable structures and coverages, we calculated the adsorption energy of alkanethiols on the Ge(100) surface for different thiols with an even number of C atoms in the molecule backbone and at various coverages. Coverages from 12.5 to 100% can be constructed in our Ge surface model. We considered the adsorption of the thiols in thiolated form since it is well established that the S–H bond breaks during the adsorption of thiols on Ge surfaces leading to HCl elimination and Ge-S bonding. The adsorption energies (E_{ads}) of the thiols forming the SAMs were computed by the following expression:

$$E_{ad} = E(tot) + E(n \text{ HCl}) - [E (Cl:Ge) + E(n \text{ HS-}C_xH_{2x+1})] \textbf{ (eqn. 1)}$$

where E(tot) is the total energy of the thiol-functionalised Ge surface, with n adsorbed thiol molecules; E(n HCl) is the energy of the isolated HCl molecule multiplied by the number, n, of HCl molecules; E (Cl:Ge) is the energy of the Cl-passivated Ge(100) surface and E (nHS-C_xH_{2x+1}) is the energy of n alkanethiol molecules. All the energies have been computed using the same parameters including the van der Waals corrections. Negative values of the adsorption energies E_{ads} mean energetically favoured adsorption configurations.

The most stable configurations for the thiol SAMs were determined, starting from several initial trial configurations and adsorption sites on the Ge(100) surface, by energy minimisations to sample minima corresponding to equilibrium structures. The results for the computed adsorption energies of Ge(100) passivated by thiols with an even number of –CH_2 units in the chains (C4, C6, C8, C10, C12) are reported in **Figure 3**.

Surface passivation of Ge(100) is favourable for all thiols for coverages above 37.5%. In general, we find that coverages between 75 and 100% are the most favourable, except for the butanethiol (C4) where it is 62.5%, although the higher coverages are still favourable (negative adsorption energy from **eqn. 1**). Referring to computed adsorption energies, the most strongly bound thiol is the hexanethiol (C6), although at the most stable coverages all thiols show high stability, with computed adsorption energies of between -2.0 and -4.5 eV/molecule, which indicates a strong thiol-surface bond. By contrast, in a previous study, on H:Si(111) we found weaker adsorption energies around -1.5 eV.[53] Octane- and decanethiols (C8 and C10) show similar behaviour while butanethiol (C4) appears to show a stronger coverage dependence, with adsorption energies initially comparable with C8 and C10 thiols at low coverage, but being less favourable at high coverages.

These results are comparable to experimental data, in which the Ge passivation with thiols from butanethiol to dodecanethiol are all favourable, while the precise coverage does not have a strong impact on stability.
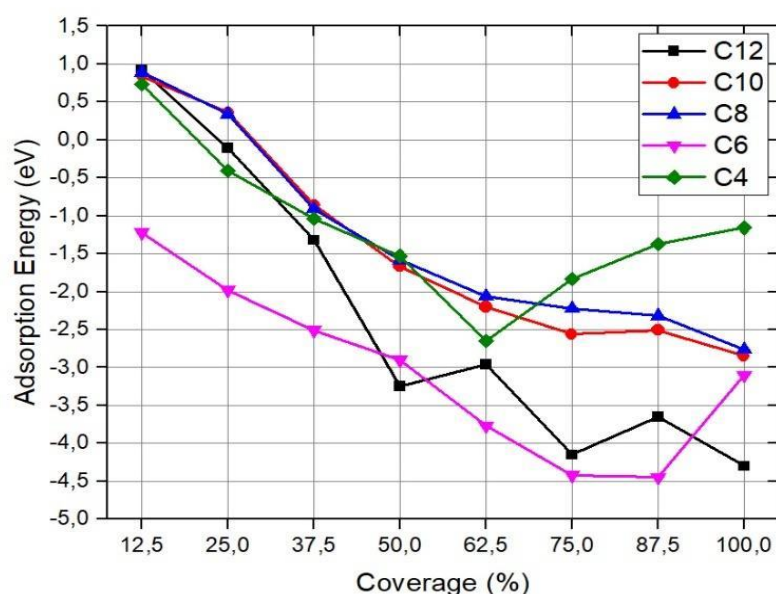
Figure 3. Adsorption energies of Ge(100) passivated by thiols of different lengths as a function of coverage.

In order to understand the E_{ads} values, we have analysed the structural properties of the Ge-SAMs systems. We began our investigation by determining the most favourable configurations for the Ge(100) passivation in which chlorine and sulfur atoms occupy the same Cl–Ge–Cl and S–Ge–S bridge sites.[54, 55] The interatomic distances for the Ge–Cl and Ge–S bonds are 2.4 Å and the distance between Ge atoms is 4.1 Å for both chlorine- and sulfur-passivated Ge(100).

The binding of the alkanethiols induces significant distortions to the surface upon relaxation whereby S atoms move towards the bridge site. In the most favourable configurations, the interatomic distances for the Ge–S bonds in butane- and hexanethiolates on Ge(100) are between 2.2 Å and 2.4 Å and thus vary at most by 0.2 Å. The interatomic distances for the Ge–S bonds in the longer chains, i.e. C8, C10 and C12, are between 2.2 Å and 2.6 Å, varying at most by 0.4 Å. This variation is more

evident in configurations at coverages between 75% and 100%, in which some S atoms bond to only one Ge surface atom.

The corresponding S–C distances for all thiolates at all coverages, vary by only 0.02 Å between 1.82 Å and 1.84 Å. At lower coverages, from 12.5% to 37%, the S–C distance is constant across all thiol chains and assumes a maximum value of 1.84 Å. As the coverage increases, the S–C distance for the thiols assumes different values. Consequently, the interatomic distances within the molecule do not depend significantly on the length of the thiolate chains, but depend on the particular arrangement of thiols on the Ge surface.

Moreover, from structural analysis, we have found that the alkanethiols form a compact monolayer with a non-homogeneous thickness. The thiol chain thickness can be determined as the projection of the length of the chain along the c-axis, denoted by l_c in **Appendix Figure DFT-S5.3**. We have computed the thickness for C4, C6, C8, C10 and C12 alkanethiol SAMs that entirely cover the Ge surface and at the relevant, most stable partial coverages. The difference in the thickness is related to the simultaneous variation of the length and the tilt angle, l and θ, respectively, of each chain forming the monolayer. The tilt angle, defined in **Appendix Figure DFT-S5.3**, corresponds to the angle between the thiol chain and the normal to the surface at the adsorption point. The angles are measured between the c-axis and the straight line joining S and C_n (n = 4, 6, 8, 10, 12). On gold, [41, 56] and silicon [57] surfaces, thiols usually adopt a tilted structure which can promote interactions between the chains and consequent stabilisation of the system.

Alkanethiol molecules in the SAM also exhibit a precession angle (α), which is used to demonstrate the coexistence of differently oriented chains. The precession

angle (α) corresponds to the angle between thiol chain projection into the ab plane (surface) and the a-axis (see **Appendix Figure DFT-S5.3**).[58]

Tilt and precession angles, length and thickness of the thiol chains for the most stable structures of these alkanethiol SAMs on Ge(100) at different coverages are given in **Appendix Table DFT-S5.4**.

The tilt of the chains is more pronounced in the case of short-chain thiol-passivated Ge (butanethiol (C4) and hexanethiol (C6)). Furthermore, an increase of the tilt angles in butanethiol chains up to 35° is found at low coverages; at full coverage, this angle assumes the minimum value of 4°. The precession angles obtained indicate different chain orientations at low coverage. At the most stable coverage and at full coverage, average precession angles of 180° and 220° (for C4 and C6, respectively) indicate that the thiol chains are well ordered. This ordering in the thiol-SAM structure is one origin of enhanced stability at higher coverages where the ordering promotes the interchain vdW interactions.

The tilt angle in octanethiol (C8) chains assumes a maximum value of 36° between coverages of 37.5% and 75% and this angle decreases to 2° at higher coverages. In addition, the precession angle increases from 154° to 230° as the coverage increases from 75% to 100%. In these cases, the chains are oriented in two different directions, with precession angles of 205° and 230°, and assume two values of tilt angle; 9° and 3°, respectively. Long-chain thiols at stable coverages adopt two different directions. We find precession angles of 88° - 226° for C10, and 80° - 226° for C12, while the tilt angles are 4° - 14° and 4° - 12°, respectively.

In **Figure 4**, we present two different views of the most favourable configurations for the thiol molecules. Short-chain thiols tend to assume one

orientation while long-chain thiols tend to be more ordered on the surface and assume two orientations. The role of chain length, angles and coverage on the adsorption characteristics have been examined to elucidate the energetics of the Ge-SAM systems. The difference in energies and especially tilt angles indicates that alkanethiolates with long chains promote the stability of the SAM.
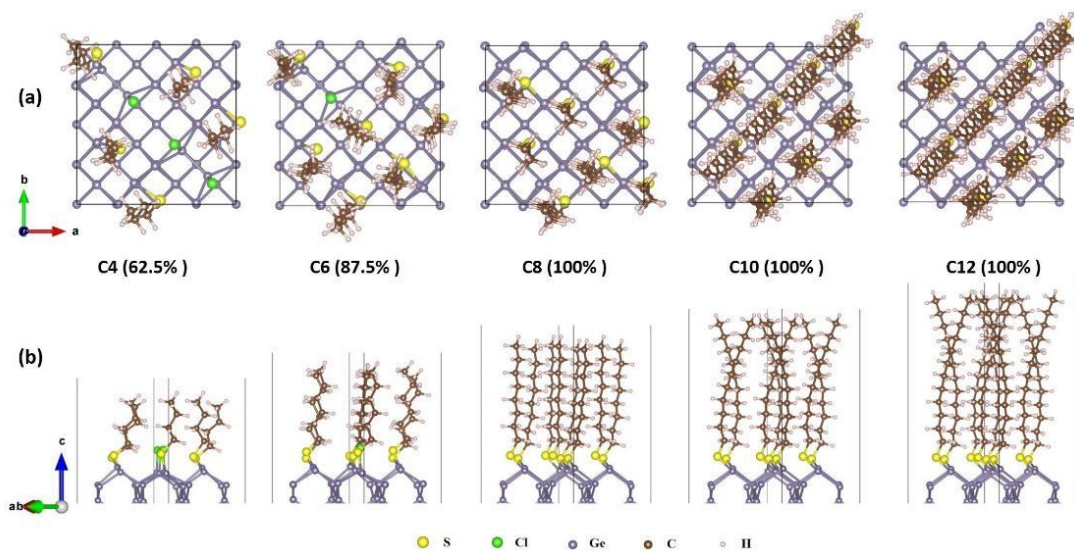
Figure 4. Top **(a)** and side **(b)** views of geometrically-optimised structures of the most stable coverage for each thiol molecule.

In **Figure 5 (i)**, the S 2p peaks for Ge passivated by the thiol molecules (C4, C6, C8, C12) with 0 hours of exposure to ambient conditions are shown and compared with freshly cleaned, as-received Ge (green). ET-passivated Ge is omitted since the authors could not achieve passivation without also causing GeO_2 growth. Sulfur (S) acts as a useful marker when tracking the presence of thiol-SAMs on Ge by XPS. Since the thiols that are used are non-functionalised, the only other atom that is detectable in the thiol molecule by XPS is carbon (C). Hydrogen (H) atoms are not detectable by XPS. C contamination from the environment can easily occur whereas this is less likely to happen with S. Consequently, in the case of the as-received Ge, there is no S peak present at 162.4 eV in **Figure 5 (i)** (green). There is however, a peak

of approximately the same intensity present at 162.4 eV for the four passivated samples. Analysis of this S peak gives qualitative information about the presence of the thiol passivation on the Ge(100) surface. Since each thiol molecule contains only one S atom, irrespective of the number of C atoms present in the backbone of the thiol, a comparable amount of S on the surface indicates that the concentration of the thiol molecules on the Ge surface is similar in all cases. Thus, it can be inferred that the length of the thiol molecule does not have a considerable effect on the level of passivation achieved using the vapour-phase method outlined in the methods section. In **Figure 5 (ii)**, the C 1s peaks are presented for the same sample set. Here, the intensity of the C peak diminishes as the length of the thiol molecule decreases from 12 C to 4 C atoms. In contrast to S, the number of C atoms in each thiol molecule reduces by two from 1-dodecanethiol, with 12 C atoms through to 1-butanethiol with 4 C atoms, which explains the diminishing nature of the C peak from one sample to the next. Although the as-received Ge sample has been degreased using acetone and IPA to remove carbon contamination, C is detectable on the surface – as can be seen by the presence of the C 1s peak at 284.8 eV (green) in **Figure 5 (ii)**. The presence of C is due to unavoidable contamination by adventitious C from the ambient prior to loading into the XPS instrument. The C peak is always present and is used to charge-correct the spectra that are acquired.

Figure 5. Overlaid **(i)** S 2p and **(ii)** C1s spectra for as-received Ge and Ge passivated by BT (black), HT (red), OT (blue) and DT (pink), respectively, with 0 hours exposure to the ambient.

Having exposed the sample set to the ambient for a period of 24 hours, XPS spectra were acquired again. The S 2p and C 1s data are displayed in **Figure 6**. By tracking the changes in intensity of the S 2p, C 1s and Ge 2p peaks, the authors can determine how well each passivating SAM prevents oxidation of the Ge. Again, in all cases, there is an S 2p peak present at 162.4 eV; however, the amount of S has diminished somewhat from the first measurement taken directly after the passivation procedure. The diminishing S 2p signal is likely due to the growth of Ge oxide evidenced by the slight increase in calculated oxide thickness. The Ge 2p data (**Appendix Figure S5.1 & 5.2**) are used to calculate the oxide thicknesses tabulated in **Table 1**.
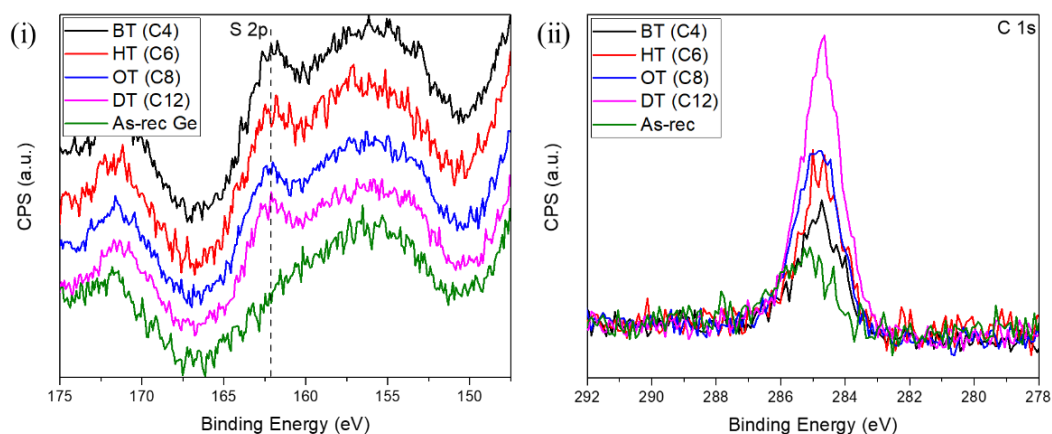
Figure 6. Overlaid **(i)** S 2p and **(ii)** C 1s spectra for as-received Ge and Ge passivated by BT (black), HT (red), OT (blue) and DT (pink) with 24 hours exposure to the ambient.

In **Figure 7 (i)**, a continuation of the trend that has been observed from 0 to 24 hours is evident. After 168 hours of exposure to the ambient conditions, an S signal is still observed for the passivated samples albeit at lower intensity than after 0 and 24 hours. A comparison of the S 2p signals for each sample is displayed in **Figure 8**. In all cases, there is a drop in the intensity of the S signal over 168 hours however, there is less of a drop in intensity of the S 2p peak for the DT-passivated Ge over 168 hours when compared with the other samples. The diminishing nature of the S 2p peak over the course of 168 hours of exposure to ambient conditions can be understood when the growth of the native oxide (**Appendix Figures 5.1 & 5.2**) is considered also. Ge-S bonds are replaced by Ge-O bonds resulting in the appearance of peaks relating to Ge^{+2} (GeO) and Ge^{+4} (GeO_2) in the Ge 2p XPS spectra resulting in thicker calculated oxide thicknesses (**Table 1**) and the reduced intensity of the S 2p peaks.
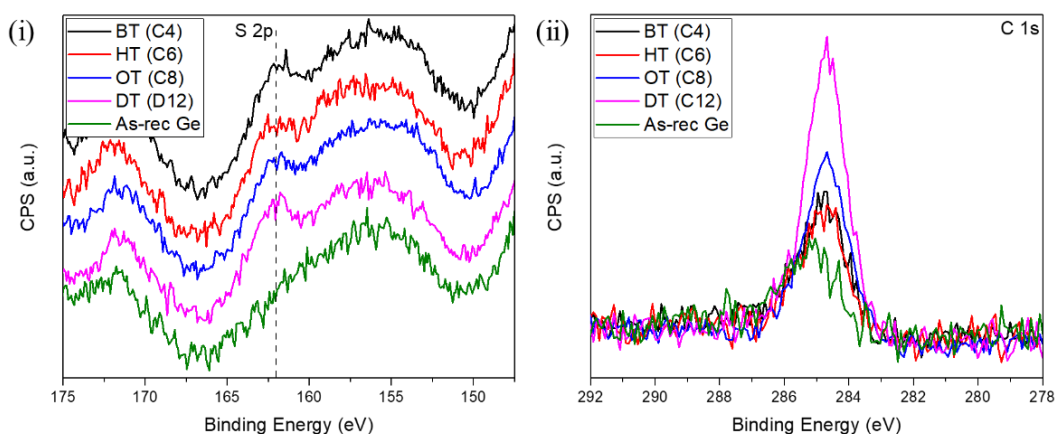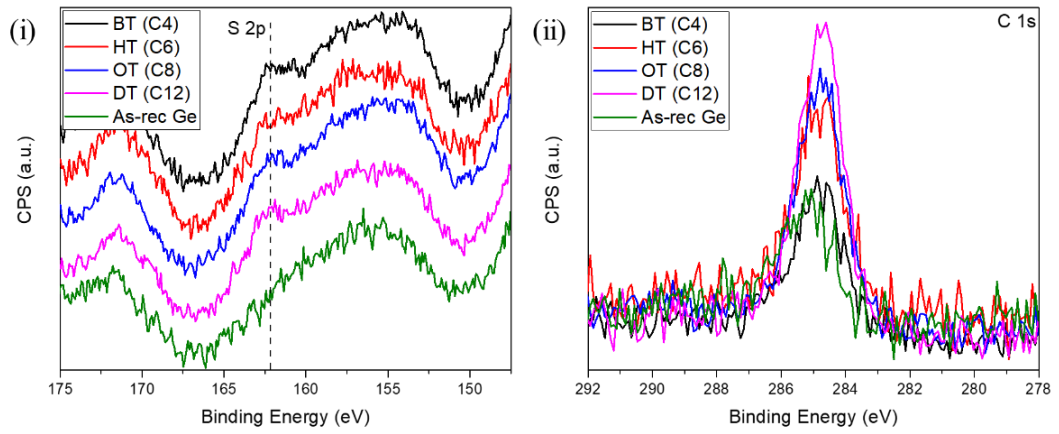
Figure 7. Overlaid **(i)** S 2p and **(ii)** C 1s spectra for as-received Ge and Ge passivated by BT (black), HT (red), OT (blue) and DT (pink) with 168 hours exposure to the ambient.
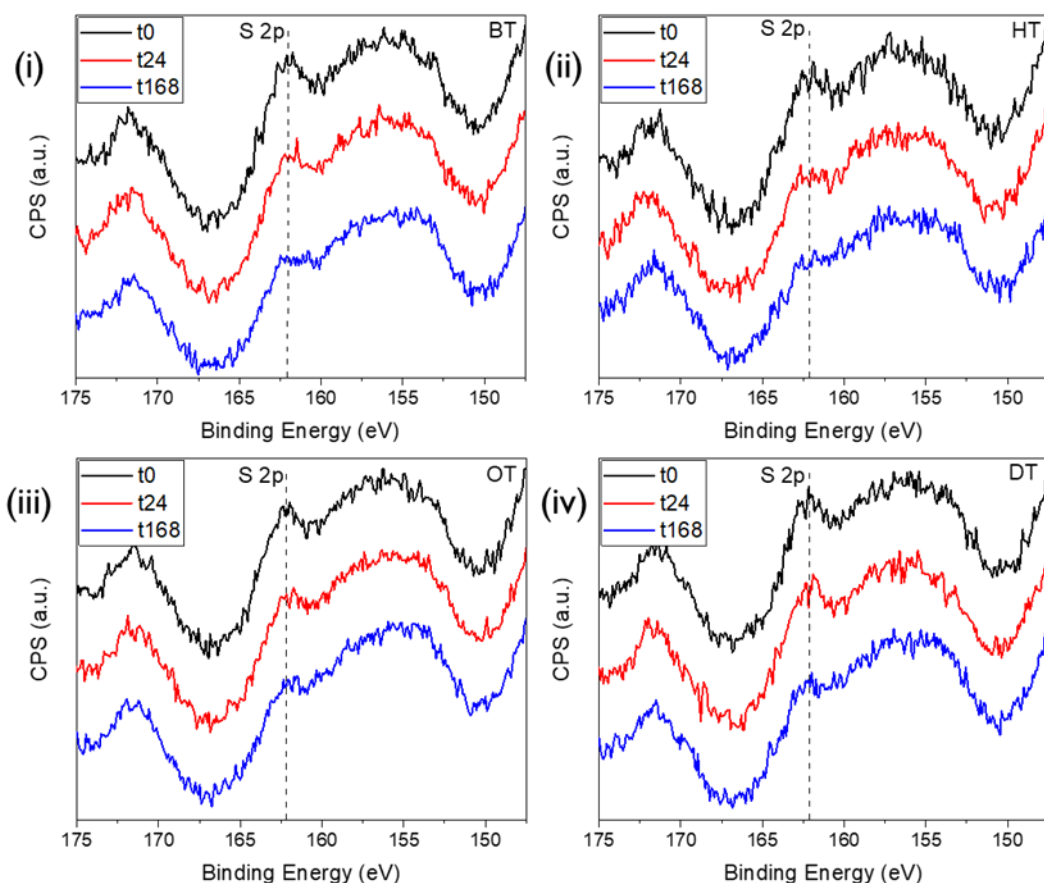
Figure 8. Overlaid S 2p spectra for Ge passivated by **(i)** BT **(ii)** HT **(iii)** OT and **(iv)** DT after 0 (black), 24 (red) and 168 (blue) hours of exposure to the ambient.

Generally, there is a drop in intensity of the C 1s peak from 0 (black) to 24 (red) to 168 (blue) hours as illustrated in **Figure 9**. However, since contamination from the ambient is likely to affect the C data, it is more reliable to follow the S 2p trends, as S is specific to the thiol molecules. With that said, a general trend whereby C concentration on the Ge surface decreases over 168 hours is observed. This indicates that over 168 hours of exposure to ambient conditions, thiol desorption from the Ge surface occurs in all cases, irrespective of thiol chain length.
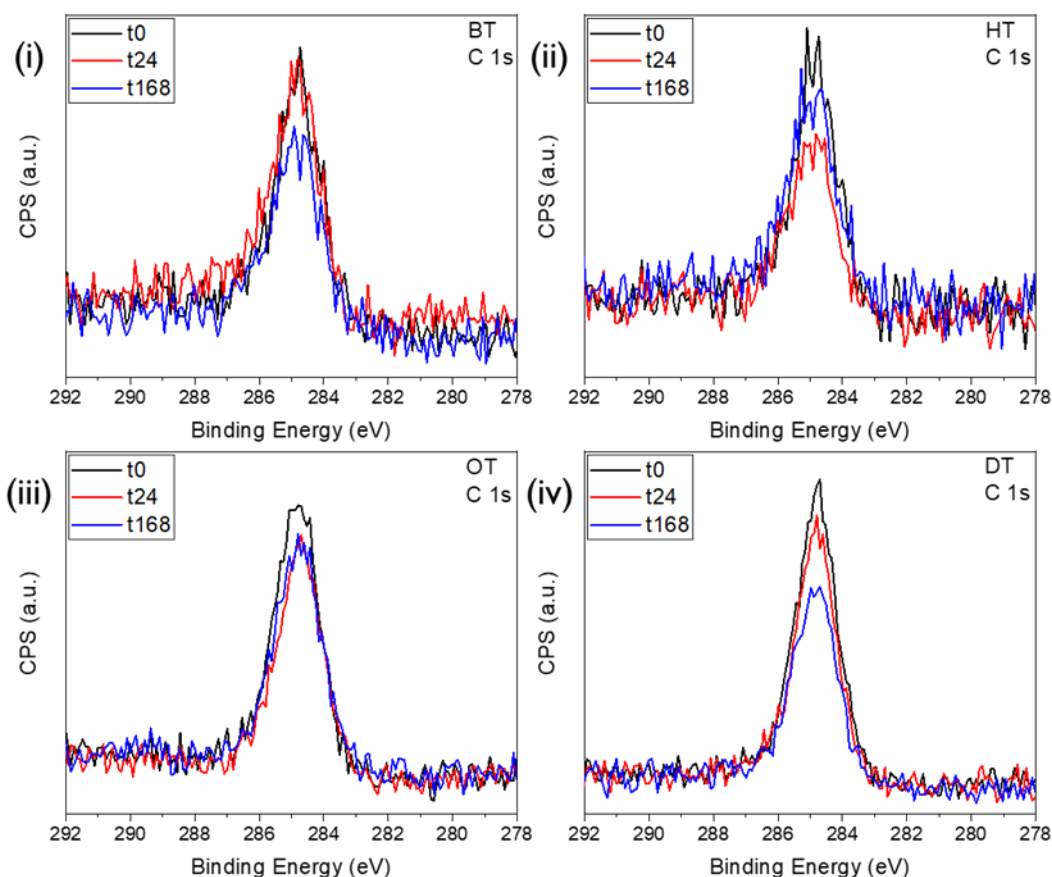
Figure 9. Overlaid C 1s spectra for Ge passivated by **(i)** BT **(ii)** HT **(iii)** OT and **(iv)** DT after 0 (black), 24 (red) and 168 (blue) hours exposure to the ambient.

Water contact angle (WCA) analysis was conducted to give an insight into the wettability of the Ge surfaces directly after passivation. The thiols used in this study are non-functionalised, with each having a non-polar –CH$_3$ termination. Water does not interact favourably with non-polar surfaces and so these kinds of surfaces are said to be hydrophobic in nature. Trends have been observed whereby SAMs consisting of long-chain alkanethiols produce surfaces which are more hydrophobic than those passivated by shorter chain alkanethiols.[43] This trend was generally observed, as can be seen by **Figure 10** whereby hydrophobicity of the passivated Ge surfaces trends with the length of the thiol molecules used to achieve that passivation. SAMs produced

from passivation by ET and BT yield Ge surfaces with approximately the same level of hydrophobicity however, as the chains lengthen, the hydrophobicity of the surface increases to 100° for both OT- and DT-passivated Ge.
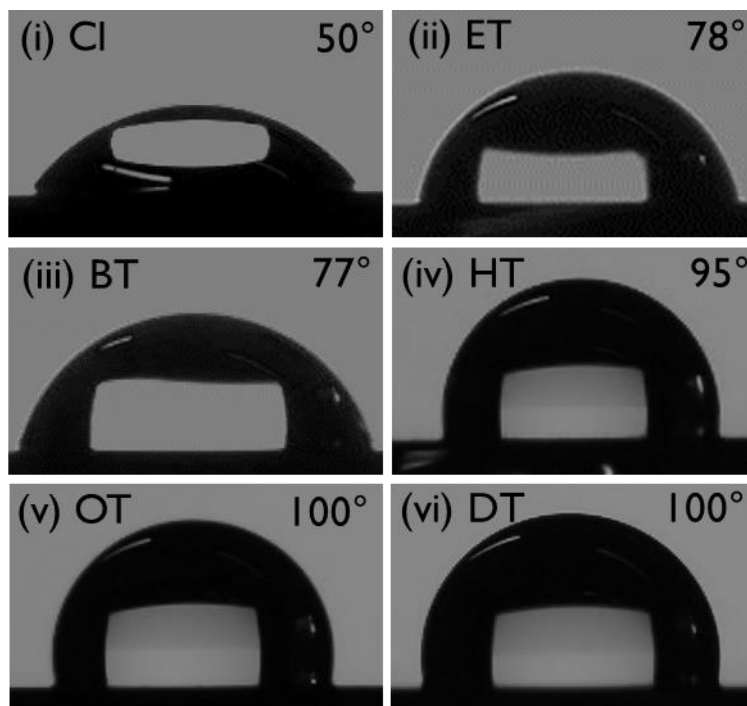
Figure 10. WCA analysis of Ge passivated by **(i)** Cl **(ii)** ET **(iii)** BT **(iv)** HT **(v)** OT **(vi)** DT revealing what effect surface termination has on Ge hydrophobicity.

5.5   Conclusions

The data has shown that resistance to oxidation of thiol-passivated Ge(100) is dependent on the length of the thiol chain. Longer-chain thiols with an even number of $-CH_2$ units in their backbones outperform their shorter-chain counterparts. Calculated adsorption energies confirm that passivation of Ge(100) is more favourable when the number of carbon atoms in the thiol molecule is increased, although even the short-chain butanethiol-SAM is stable. Stability with coverage appears to be

governed by the tilting and orientation of the thiolate chains on the Ge surface. The increased oxide resistance of Ge passivated by the longer-chain thiols is hypothesised to originate from the increased stability of SAMs consisting of long-chain thiols due to the vdW interactions between adjacent thiol molecules in the SAM. The interaction between the thiol molecules stabilises the SAM, which acts as a barrier between the Ge and air. The interaction between the shorter-chain thiols in a SAM is less since there are fewer $-CH_2$ units per thiol. VdW interactions have been shown to play a central role in the stability of thiol SAMs on gold [10] and here it is shown to be an important factor in the oxidation resistance of thiol-passivated Ge.

5.6   References

1.   Bigelow, W.C., D.L. Pickett, and W.A. Zisman, *Oleophobic monolayers: I. Films adsorbed from solution in non-polar liquids.* Journal of Colloid Science, 1946. **1**(6): p. 513-538.

2.   Ulman, A., *Formation and Structure of Self-Assembled Monolayers.* Chemical Reviews, 1996. **96**(4): p. 1533-1554.

3.   Ball, P., *Designing the Molecular World - Chemistry at the Frontier*. 1994, JSTOR: Princeton University Press.

4.   Vericat, C., M.E. Vela, G. Corthey, E. Pensa, E. Cortés, M.H. Fonticelli, F. Ibañez, G.E. Benitez, P. Carro, and R.C. Salvarezza, *Self-Assembled Monolayers of Thiolates on Metals: a Review Article on Sulfur-Metal Chemistry and Surface Structures.* RSC Advances, 2014. **4**(53): p. 27730-27754.

5.   Bain, C.D., H.A. Biebuyck, and G.M. Whitesides, *Comparison of Self-Assembled Monolayers on Gold: Coadsorption of Thiols and Disulfides.* Langmuir, 1989. **5**(3): p. 723-727.

6.   Folkers, J.P., P.E. Laibinis, and G.M. Whitesides, *Self-Assembled Monolayers of Alkanethiols on Gold: the Adsorption and Wetting Properties of Monolayers Derived from Two Components with Alkane Chains of Different Lengths.* Journal of Adhesion Science and Technology, 1992. **6**(12): p. 1397-1410.

7.   Graupe, M., T. Koini, H.I. Kim, N. Garg, Y.F. Miura, M. Takenaga, S.S. Perry, and T.R. Lee, *Self-Assembled Monolayers of CF3-Terminated Alkanethiols on*

Gold. Colloids and Surfaces A: Physicochemical and Engineering Aspects, 1999. **154**(1): p. 239-244.

8. Vericat, C., M.E. Vela, G. Benitez, P. Carro, and R.C. Salvarezza, *Self-Assembled Monolayers of Thiols and Dithiols on Gold: New Challenges for a Well-Known System.* Chemical Society Reviews, 2010. **39**(5): p. 1805-1834.

9. Love, J.C., L.A. Estroff, J.K. Kriebel, R.G. Nuzzo, and G.M. Whitesides, *Self-Assembled Monolayers of Thiolates on Metals as a Form of Nanotechnology.* Chemical Reviews, 2005. **105**(4): p. 1103-1170.

10. Inkpen, M.S., Z.F. Liu, H. Li, L.M. Campos, J.B. Neaton, and L. Venkataraman, *Non-chemisorbed gold–sulfur binding prevails in self-assembled monolayers.* Nature Chemistry, 2019. **11**(4): p. 351-358.

11. Kanukula, D.C.K., A. Boyapati, Y. Md, Iqbal, and S. Bojja, *Corrosion protection of copper by self assembled monolayers.* Indian Journal of Chemical Technology, 2009. **16**: p. 25-31.

12. Cao, X.a., X. Gan, Y. Peng, Y. Wang, X. Zeng, H. Lang, J. Deng, and K. Zou, *An Ultra-Low Frictional Interface Combining FDTS SAMs with Molybdenum Disulfide.* Nanoscale, 2018. **10**(1): p. 378-385.

13. Tao, Y., P. Navaretti, R. Hauert, U. Grob, M. Poggio, and C.L. Degen, *Permanent Reduction of Dissipation in Nanomechanical Si Resonators by Chemical Surface Protection.* Nanotechnology, 2015. **26**(46): p. 465501.

14. Maboudian, R., W.R. Ashurst, and C. Carraro, *Self-assembled monolayers as anti-stiction coatings for MEMS: characteristics and recent developments.* Sensors and Actuators A: Physical, 2000. **82**(1): p. 219-223.

15.   Cullen, G.W., J.A. Amick, and D. Gerlich, *The Stabilization of Germanium Surfaces by Ethylation.* Journal of The Electrochemical Society, 1962. **109**(2): p. 124-127.

16.   He, J., Z.-H. Lu, S.A. Mitchell, and D.D.M. Wayner, *Self-Assembly of Alkyl Monolayers on Ge(111).* Journal of the American Chemical Society, 1998. **120**(11): p. 2660-2661.

17.   Ardalan, P., Y. Sun, P. Pianetta, C.B. Musgrave, and S.F. Bent, *Reaction Mechanism, Bonding, and Thermal Stability of 1-Alkanethiols Self-Assembled on Halogenated Ge Surfaces.* Langmuir, 2010. **26**(11): p. 8419-8429.

18.   Kosuri, M.R., R. Cone, Q. Li, S.M. Han, B.C. Bunker, and T.M. Mayer, *Adsorption Kinetics of 1-Alkanethiols on Hydrogenated Ge(111).* Langmuir, 2004. **20**(3): p. 835-840.

19.   Choi, K. and J.M. Buriak, *Hydrogermylation of Alkenes and Alkynes on Hydride-Terminated Ge(100) Surfaces.* Langmuir, 2000. **16**(20): p. 7737-7741.

20.   Loscutoff, P.W. and S.F. Bent, *Reactivity of the Germanium Surface: Chemical Passivation and Functionalization.* Annual Review of Physical Chemistry, 2006. **57**: p. 467-495.

21.   Cai, Q., B. Xu, L. Ye, Z. Di, S. Huang, X. Du, J. Zhang, Q. Jin, and J. Zhao, *1-Dodecanethiol Based Highly Stable Self-Assembled Monolayers for Germanium Passivation.* Applied Surface Science, 2015. **353**: p. 890-901.

22.   Hohman, J.N., M. Kim, H.R. Bednar, J.A. Lawrence, P.D. McClanahan, and P.S. Weiss, *Simple, Robust Molecular Self-Assembly on Germanium.* Chemical Science, 2011. **2**(7): p. 1334-1343.

23. Collins, G., D. Aureau, J.D. Holmes, A. Etcheberry, and C. O'Dwyer, *Germanium Oxide Removal by Citric Acid and Thiol Passivation from Citric Acid-Terminated Ge(100).* Langmuir, 2014. **30**(47): p. 14123-14127.

24. Collins, G., P. Fleming, S. Barth, C. O'Dwyer, J.J. Boland, M.A. Morris, and J.D. Holmes, *Alkane and Alkanethiol Passivation of Halogenated Ge Nanowires.* Chemistry of Materials, 2010. **22**(23): p. 6370-6377.

25. Yuan, F.W., H.J. Yang, and H.Y. Tuan, *Alkanethiol-Passivated Ge Nanowires as High-Performance Anode Materials for Lithium-Ion Batteries: The Role of Chemical Surface Functionalization.* ACS Nano, 2012. **6**(11): p. 9932-9942.

26. Han, S.M., W.R. Ashurst, C. Carraro, and R. Maboudian, *Formation of Alkanethiol Monolayer on Ge(111).* Journal of the American Chemical Society, 2001. **123**(10): p. 2422-2425.

27. Satta, A., A.R. Peaker, A. Theuwis, A.N. Larsen, B. Depuydt, B. De Jaeger, C. Quaeyhaegens, C.O. Chui, C. Deguet, C. Claeys, D. Esseni, E. Simoen, E. Sangiorgi, E. Kasper, F. Letertre, I. Romandic, J. Vanhellemont, J. Coutinho, K.C. Saraswat, M. De Jonghe, M. Heyns, M. Meuris, M. Caymax, M. Houssa, P. Clauws, P. Palestri, R. Jones, T. Akatsu, V. Markevich, and W. De Baets, *Germanium-Based Technologies. From Materials to Devices*, ed. C. Claeys and E. Simoen. 2007, Oxford: Elsevier. xiv-xvi.

28. Weber, J.R., A. Janotti, and C.G. Van de Walle, *Dangling Bonds and Vacancies in Germanium.* Physical Review B, 2013. **87**(3): p. 035203.

29. Garvey, S., J.D. Holmes, Y.S. Kim, and B. Long, *Vapor-Phase Passivation of Chlorine-Terminated Ge(100) using Self-Assembled Monolayers of Hexanethiol.* ACS Applied Materials & Interfaces, 2020.

30. Kim, J., J. McVittie, K. Saraswat, Y. Nishi, S. Liu, and S. Tan, *Germanium Surface Cleaning with Hydrochloric Acid.* ECS Transactions, 2006. **3**(7): p. 1191-1196.

31. Kim, J.Y., J. McVittie, K. Saraswat, and Y. Nishi, *Passivation Studies of Germanium Surfaces.* Solid State Phenomena, 2008. **134**: p. 33-36.

32. van Dorp, D.H., D. Weinberger, S. Van Wonterghem, S. Arnauts, K. Strubbe, F. Holsteyns, and S. De Gendt, *Nanoscale Etching: Dissolution of III-As and Ge in HCl/H2O2 Solutions.* ECS Transactions, 2015. **69**(8): p. 235-242.

33. Park, K., Y. Lee, J. Lee, and S. Lim, *Oxidation Mechanism of Hydrogen-Terminated Ge(100) Surface.* Applied Surface Science, 2008. **254**(15): p. 4828-4832.

34. Molina, A., J.R. Shallenberger, and S.E. Mohney, *Vapor Phase Passivation of (100) Germanium Surfaces with HBr.* Journal of Vacuum Science & Technology A, 2020. **38**(2): p. 023208.

35. Bodlaki, D., H. Yamamoto, D.H. Waldeck, and E. Borguet, *Ambient Stability of Chemically Passivated Germanium Interfaces.* Surface Science, 2003. **543**(1): p. 63-74.

36. Tao, F. and S.L. Bernasek, *Understanding Odd−Even Effects in Organic Self-Assembled Monolayers.* Chemical Reviews, 2007. **107**(5): p. 1408-1453.

37. Krzykawska, A., M. Szwed, J. Ossowski, and P. Cyganik, *Odd–Even Effect in Molecular Packing of Self-Assembled Monolayers of Biphenyl-Substituted Fatty Acid on Ag(111).* The Journal of Physical Chemistry C, 2018. **122**(1): p. 919-928.

38. Thuo, M.M., W.F. Reus, C.A. Nijhuis, J.R. Barber, C. Kim, M.D. Schulz, and G.M. Whitesides, *Odd−Even Effects in Charge Transport across Self-Assembled Monolayers.* Journal of the American Chemical Society, 2011. **133**(9): p. 2962-2975.

39. Jiang, L., C.S.S. Sangeeth, and C.A. Nijhuis, *The Origin of the Odd–Even Effect in the Tunneling Rates across EGaIn Junctions with Self-Assembled Monolayers (SAMs) of n-Alkanethiolates.* Journal of the American Chemical Society, 2015. **137**(33): p. 10659-10667.

40. Kato, H.S., J. Noh, M. Hara, and M. Kawai, *An HREELS Study of Alkanethiol Self-Assembled Monolayers on Au(111).* The Journal of Physical Chemistry B, 2002. **106**(37): p. 9655-9658.

41. Ramin, L. and A. Jabbarzadeh, *Odd–Even Effects on the Structure, Stability, and Phase Transition of Alkanethiol Self-Assembled Monolayers.* Langmuir, 2011. **27**(16): p. 9748-9759.

42. Yuan, L., D. Thompson, L. Cao, N. Nerngchangnong, and C.A. Nijhuis, *One Carbon Matters: The Origin and Reversal of Odd–Even Effects in Molecular Diodes with Self-Assembled Monolayers of Ferrocenyl-Alkanethiolates.* The Journal of Physical Chemistry C, 2015. **119**(31): p. 17910-17919.

43. Ben Amara, F., E.R. Dionne, S. Kassir, C. Pellerin, and A. Badia, *Molecular Origin of the Odd–Even Effect of Macroscopic Properties of n-Alkanethiolate Self-Assembled Monolayers: Bulk or Interface?* Journal of the American Chemical Society, 2020. **142**(30): p. 13051-13061.

44. Cyganik, P., K. Szelagowska-Kunstman, A. Terfort, and M. Zharnikov, *Odd−Even Effect in Molecular Packing of Biphenyl-Substituted*

Alkaneselenolate Self-Assembled Monolayers on Au(111): Scanning Tunneling Microscopy Study. The Journal of Physical Chemistry C, 2008. **112**(39): p. 15466-15473.

45. Baghbanzadeh, M., F.C. Simeone, C.M. Bowers, K.-C. Liao, M. Thuo, M. Baghbanzadeh, M.S. Miller, T.B. Carmichael, and G.M. Whitesides, *Odd–Even Effects in Charge Transport across n-Alkanethiolate-Based SAMs.* Journal of the American Chemical Society, 2014. **136**(48): p. 16919-16925.

46. Murakami, H., T. Fujioka, A. Ohta, T. Bando, S. Higashi, and S. Miyazaki, *Characterization of Interfaces between Chemically Cleaned or Thermally Oxidized Germanium and Metals.* 2010, ECS.

47. Kresse, G. and J. Furthmüller, *Efficiency of Ab-Initio Total Energy Calculations for Metals and Semiconductors using a Plane-Wave Basis Set.* Computational Materials Science, 1996. **6**(1): p. 15-50.

48. Kresse, G. and J. Furthmüller, *Efficient Iterative Schemes for Ab-Initio Total-Energy Calculations using a Plane-Wave Basis Set.* Physical Review B, 1996. **54**(16): p. 11169-11186.

49. Blöchl, P.E., *Projector augmented-wave method.* Physical Review B, 1994. **50**(24): p. 17953-17979.

50. Perdew, J.P., K. Burke, and M. Ernzerhof, *Generalized Gradient Approximation Made Simple.* Physical Review Letters, 1996. **77**(18): p. 3865-3868.

51. Grimme, S., J. Antony, S. Ehrlich, and H. Krieg, *A Consistent and Accurate Ab-Initio Parametrization of Density Functional Dispersion Correction (DFT-*

D) for the 94 Elements H-Pu. The Journal of Chemical Physics, 2010. **132**(15): p. 154104.

52.   Monkhorst, H.J. and J.D. Pack, *Special Points for Brillouin-Zone Integrations.* Physical Review B, 1976. **13**(12): p. 5188-5192.

53.   Arefi, H.H., M. Nolan, and G. Fagas, *Density Functional Theory with van der Waals Corrections Study of the Adsorption of Alkyl, Alkylthiol, Alkoxyl, and Amino-Alkyl Chains on the H:Si(111) Surface.* Langmuir, 2014. **30**(44): p. 13255-13265.

54.   Hayashi, T., Y. Morikawa, and H. Nozoye, *Adsorption state of dimethyl disulfide on Au(111): Evidence for adsorption as thiolate at the bridge site.* The Journal of Chemical Physics, 2001. **114**(17): p. 7615-7621.

55.   Vargas, M.C., P. Giannozzi, A. Selloni, and G. Scoles, *Coverage-Dependent Adsorption of CH3S and (CH3S)2 on Au(111): a Density Functional Theory Study.* The Journal of Physical Chemistry B, 2001. **105**(39): p. 9509-9513.

56.   Fajín, J.L.C., F. Teixeira, J.R.B. Gomes, and M.N.D.S. Cordeiro, *Effect of van der Waals interactions in the DFT description of self-assembled monolayers of thiols on gold*, in *9th Congress on Electronic Structure: Principles and Applications (ESPA 2014): A Conference Selection from Theoretical Chemistry Accounts*, M.F. Ruiz-Lopez and F.J. Olivares del Valle, Editors. 2016, Springer Berlin Heidelberg: Berlin, Heidelberg. p. 127-139.

57.   Castillo, J.M., M. Klos, K. Jacobs, M. Horsch, and H. Hasse, *Characterization of Alkylsilane Self-Assembled Monolayers by Molecular Simulation.* Langmuir, 2015. **31**(9): p. 2630-2638.

58.   Szefczyk, B., R. Franco, J.A.N.F. Gomes, and M.N.D.S. Cordeiro, *Structure of the interface between water and self-assembled monolayers of neutral, anionic and cationic alkane thiols.* Journal of Molecular Structure: THEOCHEM, 2010. **946**(1): p. 83-87.

Chapter 6
Conclusions & Future Perspectives

6.1   Conclusions

Advanced device architectures and novel materials are being scrutinised in an effort to achieve 'More Moore' and to meet the technological demands of modernity. Improving the channel characteristics of FET devices will involve GAA [1] approaches and the integration of novel high-mobility materials such as Ge, III-V semiconductors and 2D materials, as predicted by the IRDS™. In fact, in 2020 the IRDS™ predicted that Ge will replace SiGe as the channel material of choice by 2028.[2] This is a challenging prospect whereby the level of control over Ge surface chemistry and defect minimisation at the interface between Ge and adjacent materials are essential considerations.[3, 4] The limitations of Ge's native oxide are known and documented in the literature [5-7] and efforts to replace the oxide with more stable passivating layers are well underway.[8-12] SAMs of various kinds of organic molecules have garnered attention as potential methods to achieve Ge passivation owing to the relative ease with which they can be prepared along with the considerable effect they can have on the surface properties of the Ge.[8, 10, 13, 14] Vapour-phase processing of Ge will be an essential step in the production of Ge-based devices since the destructive capillary forces experienced during wet-chemical processing are circumvented. In this body of work, methods to passivate Ge(100) surfaces with aliphatic alkanethiol molecules are explored and insight is gained into the environmental factors that cause SAM-degradation and Ge oxidation.

Chapter 1 introduces key concepts such as the structure and properties of Ge, the issues associated with Ge's native oxide, and a review of the literature on the passivation of Ge surfaces using liquid- and vapour-phase methods.

Chapter 2 details the characterisation and modelling methods that are used throughout this body of work.

Chapter 3 outlines a novel and relatively simple method to achieve the vapour-phase passivation of Ge(100) using 1-hexanethiol. This passivation reaction can be carried out in ~200 minutes whereas the state-of-the-art liquid-phase reactions using 1-dodecanethiol require 24 hours and result in a Ge surface that is less resistant to reoxidation. The motivation to achieve the passivation of Ge using a vapour-phase approach stemmed from the desire to develop a process that is applicable to suspended and tightly pitched arrays of Ge nanostructures. Liquid-phase processing can cause damage to suspended nanostructures due to surface tension and capillary forces can cause arrays of tightly pitched suspended structures to stick together. In addition, since the surface to bulk ratio for nanostructures is high, it was imperative that the developed process had a negligible impact on surface roughness. What may seem like an insignificant increase in roughness on planar Ge would have a considerable affect on 10 nm wide nanowires for example, which are only ~40 atoms wide. The process that was developed caused no meaningful increase in surface roughness of the Ge and served as the bedrock for the rest of the work done in this thesis as it provided a highly reproducible method for the creation of alkanethiol-SAMs on Ge.

Once a robust passivation method had been developed for Ge, an obvious continuation was to determine which environmental factors play a significant role in the degradation of the SAM and the reoxidation of the underlying Ge. In **Chapter 4**,

relative humidity is determined to be one such factor. Alkanethiol-passivated Ge(100) surfaces were exposed to environments with different levels of relative humidity and XPS was used to track the growth of oxide over 168 hours. It was found that alkanethiol-passivated Ge oxidised at a slower rate when stored in a low humidity environment than higher humidity environments. This is a significant finding since it is now understood that the longevity of the SAMs can be increased if relative humidity is controlled. The motivation for this study came from the industry partner who wished to discern for how long the alkanethiol passivation was effective at inhibiting Ge reoxidation and what factors were essential in the reoxidation of the Ge surfaces. In a device fabrication line, relative humidity is easy to control and thus the knowledge acquired is valuable to the industry partner.

A review of the literature on alkanethiol-SAMs on Ge reveals that the vast majority of research has focused on the use of 1-dodecanethiol.[8, 13] This is likely the case as DT-SAMs on Au is a system that has been studied extensively [15-18] and best practices for Au have been applied to Ge. **Chapter 5** outlines a study whereby a series of 1-alkanethiols, with varying carbon chain lengths are used to create SAMs on Ge(100) and a study of the reoxidation of the passivated Ge upon exposure to ambient conditions is undertaken. The authors wished to determine if short-chain thiols were as effective at inhibiting Ge surface reoxidation as their longer chain counterparts. The motivation being that it may be advantageous to achieve passivation with molecules containing fewer C atoms. In device fabrication lines, C is sometimes considered a poison atom as it can cause dopant deactivation during high temperature processing.[19] Furthermore, shorter thiol molecules have higher vapour pressures since their molecular weights (M_w) are lower. Thiols with lower M_w are easier to promote into the vapour necessary to achieve vapour-phase passivation. In this

chapter, the authors observed a trend whereby Ge oxidation resistance improves with the length of the passivating thiol molecules. SAMs consisting of 1-dodecanethiol molecules outperformed those consisting of 1-octanethiol molecules, which outperformed those consisting of 1-hexanethiol molecules and so on. These findings highlight the significance of the vdW interactions between adjacent thiol molecules in the passivating SAM.

In summary, a novel vapour-phase passivation method using alkanethiol SAMs has been developed for Ge(100). The process results in SAMs that are more effective at inhibiting the reoxidation of Ge than the state-of-the-art while taking considerably less time. In addition, the significant role humidity plays in the degradation of the alkanethiol-SAM and the reoxidation of the underlying Ge has been outlined, and the efficacy of alkanethiols of different chain length in relation to inhibition of Ge reoxidation has been elucidated.

6.2   Future Perspectives

As mentioned in the conclusions section, a motivation to develop the vapour-phase passivation method for Ge was to create a non-destructive process that was suitable for Ge nanostructures. Due to difficulties in creating such structures, this goal has not yet been realised. Once Ge nanostructures can be fabricated reliably, an interesting continuation of this work would be to test the developed vapour-phase passivation method (documented in **Chapter 3**) on these structures.

Another topic that warrants exploration is how alkanethiol passivation of Ge affects the electronic properties of Ge-based devices. For example, Ge-MOS

capacitors consist of an oxide layer deposited or grown on Ge after which a metallisation procedure is carried out. Comparing the electronic properties of MOS capacitors with and without thiol-passivation of the Ge prior to oxide deposition may illuminate what effect, if any, the passivation had on the electronic properties of the device. Another potential continuation of this work is to passivate Ge with alkanethiol molecules that have a functionalised tail group in an effort to promote the nucleation of ALD-grown oxides. Growing or depositing oxide layers on Ge is an essential step in making Ge-based devices. The $-CH_3$ tail group of a non-functionalised alkanethiol molecule does not actively promote the nucleation of ALD oxides; however, an amine or hydroxyl group may. This avenue deserves further exploration.

Non-functionalised thiol molecules are used throughout this body of work. In **Chapter 4**, the significant role humidity plays in the degradation of the alkanethiol-SAM and the reoxidation of the underlying Ge is outlined. A topic that warrants further investigation is the use of functionalised alkanethiol molecules to create SAMs on Ge(100). Heavily-fluorinated alkanethiol molecules have previously been shown to form highly-hydrophobic SAMs on Au surfaces.[20] Since water has been shown to be an instrumental factor in the oxidation of SAM-passivated Ge(100) surfaces in **Chapter 4**, efforts to passivate Ge with highly-hydrophobic SAMs may improve the longevity of the SAM and thus the resistance to oxidation of the underlying Ge upon exposure to ambient conditions.

As mentioned in **Chapter 1**, passivation of Ge with organic SAMs is not limited to alkanethiols. Hydrogermylation and Grignard-style chemistry offer alternative routes that result in the formation of Ge-C bonds rather than the Ge-S bonds that alkanethiol passivation yields.[7] These alternative methods warrant exploration

such that they be compared to the alkanethiol-passivated Ge(100) surfaces discussed herein.

Odd-even effects are a widely observed phenomenon across the sciences but in biology, physical chemistry and material science in particular.[21, 22] A contributing factor to the stability of alkanethiol-SAMs on Ge may be the parity of the constituent molecules i.e. whether there is an odd or even number of $-CH_2$ units in the backbone of the passivating molecule. In an effort to avoid such effects, alkanethiol molecules with an odd number of $-CH_2$ units in the C backbone were omitted from the study detailed in **Chapter 5**. An interesting continuation of this work would be to determine what effect, if any, the parity of the passivating thiol molecule has on SAM stability. DFT simulations could help elucidate how the functionalisation of the alkanethiol molecules affects the packing of the SAM and could be used to gain insight into the interaction between water molecules and the SAM-Ge system also.

Ultimately, the scope for further investigations into SAMs on Ge is broad and varied; however, such efforts are necessary if Ge is to gain widespread use in modern CMOS-compatible as predicted by the IRDS™.[2]

6.3 References

1. Witters, L., H. Arimura, F. Sebaai, A. Hikavyy, A.P. Milenin, R. Loo, A.D. Keersgieter, G. Eneman, T. Schram, K. Wostyn, K. Devriendt, A. Schulze, R. Lieten, S. Bilodeau, E. Cooper, P. Storck, E. Chiu, C. Vrancken, P. Favia, E. Vancoille, J. Mitard, R. Langer, A. Opdebeeck, F. Holsteyns, N. Waldron, K. Barla, V.D. Heyn, D. Mocuta, and N. Collaert, *Strained Germanium Gate-All-Around pMOS Device Demonstration Using Selective Wire Release Etch Prior to Replacement Metal Gate Deposition.* IEEE Transactions on Electron Devices, 2017. **64**(11): p. 4587-4593.

2. *International Roadmap for Devices and Systems*. 2020.

3. Binder, J.F., P. Broqvist, and A. Pasquarello, *Charge Trapping in Substoichiometric Germanium Oxide.* Microelectronic Engineering, 2011. **88**(7): p. 1428-1431.

4. Heyns, M. and W. Tsai, *Ultimate Scaling of CMOS Logic Devices with Ge and III–V Materials.* MRS Bulletin, 2011. **34**(7): p. 485-492.

5. Ardalan, P., C.B. Musgrave, and S.F. Bent, *Formation of Alkanethiolate Self-Assembled Monolayers at Halide-Terminated Ge Surfaces.* Langmuir, 2009. **25**(4): p. 2013-2025.

6. Ardalan, P., Y. Sun, P. Pianetta, C.B. Musgrave, and S.F. Bent, *Reaction Mechanism, Bonding, and Thermal Stability of 1-Alkanethiols Self-Assembled on Halogenated Ge Surfaces*, in *Langmuir*. 2010. p. 8419-8429.

7.   Loscutoff, P.W. and S.F. Bent, *Reactivity of the Germanium Surface: Chemical Passivation and Functionalization.* Annual Review of Physical Chemistry, 2006. **57**: p. 467-495.

8.   Cai, Q., B. Xu, L. Ye, Z. Di, S. Huang, X. Du, J. Zhang, Q. Jin, and J. Zhao, *1-Dodecanethiol Based Highly Stable Self-Assembled Monolayers for Germanium Passivation.* Applied Surface Science, 2015. **353**: p. 890-901.

9.   Chabal, S.R.A.Y.J., *Passivation and Characterization of Germanium Surfaces*, in *Advanced Gate Stacks for High-Mobility Semiconductors*. 2008, Springer, Berlin, Heidelberg. p. 73-113.

10.   Collins, G., D. Aureau, J.D. Holmes, A. Etcheberry, and C. O'Dwyer, *Germanium Oxide Removal by Citric Acid and Thiol Passivation from Citric Acid-Terminated Ge(100).* Langmuir, 2014. **30**(47): p. 14123-14127.

11.   Rojas Delgado, R., R.M. Jacobberger, S.S. Roy, V.S. Mangu, M.S. Arnold, F. Cavallo, and M.G. Lagally, *Passivation of Germanium by Graphene.* ACS Applied Materials & Interfaces, 2017. **9**(20): p. 17629-17636.

12.   Xie, Q., S. Deng, M. Schaekers, D. Lin, M. Caymax, A. Delabie, X.-P. Qu, Y.-L. Jiang, D. Deduytsche, and C. Detavernier, *Germanium Surface Passivation and Atomic Layer Deposition of High-k Dielectrics—a Tutorial Review on Ge-Based MOS Capacitors.* Semiconductor Science and Technology, 2012. **27**(7): p. 074012.

13.   Hohman, J.N., M. Kim, H.R. Bednar, J.A. Lawrence, P.D. McClanahan, and P.S. Weiss, *Simple, Robust Molecular Self-Assembly on Germanium.* Chemical Science, 2011. **2**(7): p. 1334-1343.

14. Collins, G., P. Fleming, S. Barth, C. O'Dwyer, J.J. Boland, M.A. Morris, and J.D. Holmes, *Alkane and Alkanethiol Passivation of Halogenated Ge Nanowires.* Chemistry of Materials, 2010. **22**(23): p. 6370-6377.

15. Bain, C.D., H.A. Biebuyck, and G.M. Whitesides, *Comparison of Self-Assembled Monolayers on Gold: Coadsorption of Thiols and Disulfides.* Langmuir, 1989. **5**(3): p. 723-727.

16. Folkers, J.P., P.E. Laibinis, and G.M. Whitesides, *Self-Assembled Monolayers of Alkanethiols on Gold: the Adsorption and Wetting Properties of Monolayers Derived from Two Components with Alkane Chains of Different Lengths.* Journal of Adhesion Science and Technology, 1992. **6**(12): p. 1397-1410.

17. Inkpen, M.S., Z.F. Liu, H. Li, L.M. Campos, J.B. Neaton, and L. Venkataraman, *Non-chemisorbed gold–sulfur binding prevails in self-assembled monolayers.* Nature Chemistry, 2019. **11**(4): p. 351-358.

18. Vericat, C., M.E. Vela, G. Benitez, P. Carro, and R.C. Salvarezza, *Self-Assembled Monolayers of Thiols and Dithiols on Gold: New Challenges for a Well-Known System.* Chemical Society Reviews, 2010. **39**(5): p. 1805-1834.

19. Kennedy, N., S. Garvey, B. Maccioni, L. Eaton, M. Nolan, R. Duffy, F. Meaney, M. Kennedy, J.D. Holmes, and B. Long, *Monolayer Doping of Germanium with Arsenic: A New Chemical Route to Achieve Optimal Dopant Activation.* Langmuir, 2020. **36**(34): p. 9993-10002.

20. Parvate, S., P. Dixit, and S. Chattopadhyay, *Superhydrophobic Surfaces: Insights from Theory and Experiment.* The Journal of Physical Chemistry B, 2020. **124**(8): p. 1323-1360.

21. Ben Amara, F., E.R. Dionne, S. Kassir, C. Pellerin, and A. Badia, *Molecular Origin of the Odd–Even Effect of Macroscopic Properties of n-Alkanethiolate Self-Assembled Monolayers: Bulk or Interface?* Journal of the American Chemical Society, 2020. **142**(30): p. 13051-13061.

22. Tao, F. and S.L. Bernasek, *Understanding Odd−Even Effects in Organic Self-Assembled Monolayers.* Chemical Reviews, 2007. **107**(5): p. 1408-1453.

Chapter 7

Appendix

7.1 Additional Figures
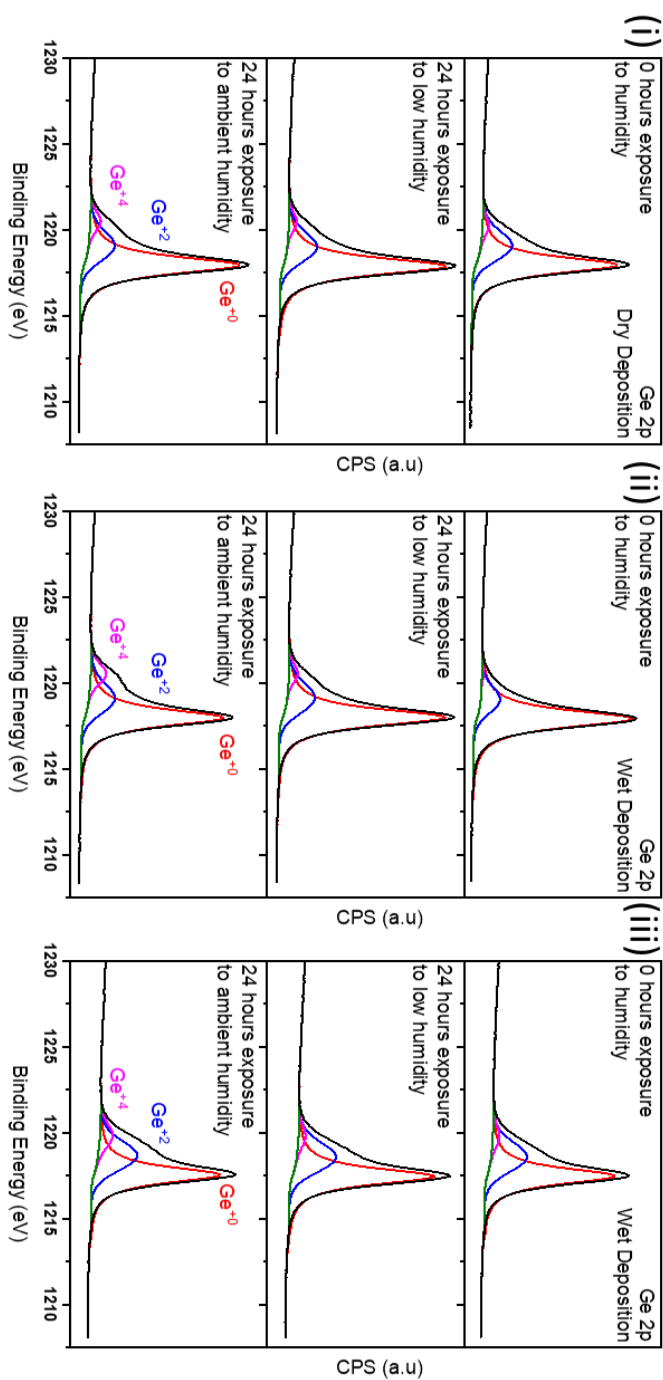
Figure S4.1. (i) Ge 2p spectra for OT-vapour-phase passivated Ge, showing what effect 24 hours of exposure to low and ambient humidity has on the intensity of the fitted Ge peaks. **(ii)** Ge 2p spectra for DT-liquid-phase passivation of on Ge, showing what effect 24 hours of exposure to low and ambient humidity has on the intensity of the fitted Ge peaks. **(iii)** Ge 2p spectra for DT-liquid-phase passivated $Si_{0.25}Ge_{0.75}$, showing what effect 24 hours of exposure to low and ambient humidity has on the intensity of the fitted Ge peaks.
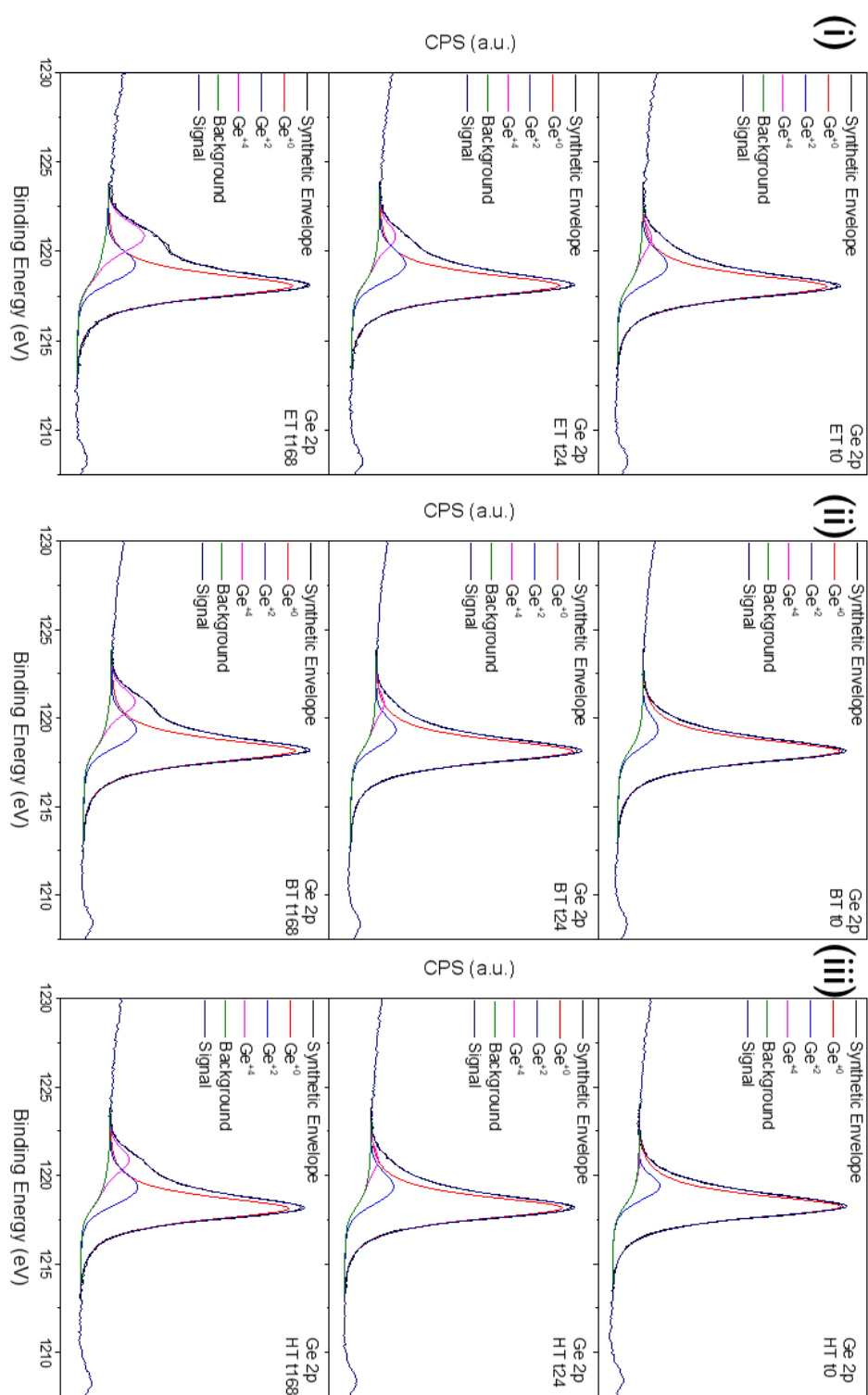
Figure S5.1. Ge 2p spectra for **(i)** ET-, **(ii)** BT-, **(iii)** HT-passivated Ge(100) with Ge^{+0} (red), Ge^{+2} (blue) and Ge^{+4} (pink) peaks fitted illustrating what effect 0, 24 and 168 hours of exposure to the ambient has on the Ge 2p spectra.
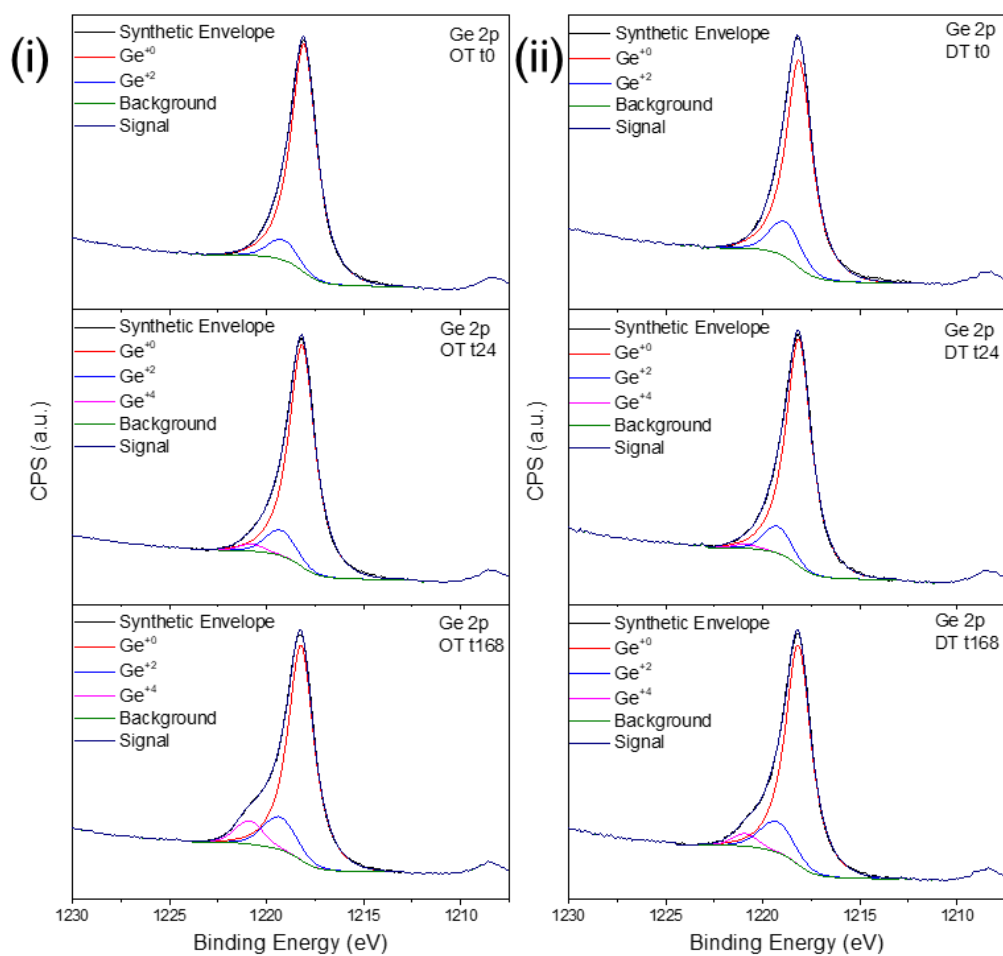
Figure S5.2. Ge 2p spectra for (**i**) OT-, (**ii**) DT-passivated Ge(100) with Ge^{+0} (red), Ge^{+2} (blue) and Ge^{+4} (pink) fitted illustrating what effect 0, 24 and 168 hours of exposure to the ambient has on the Ge 2p spectra.
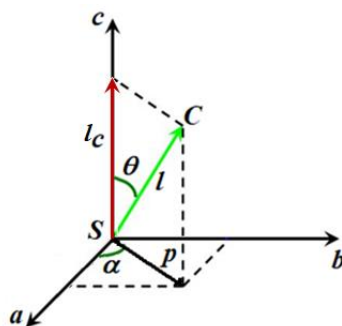
Figure DFT-S5.3. Schematic illustrating the tilt angle (θ), precession angle (α), thiol chain length (l), thiol chain thickness (l_c) and thiol chain projection (p) in ab-plane. Where 'S' and 'C' denote the sulfur and carbon atoms at the end of the thiol chain. The tilt and the precession angles are measured between the c-axis and the S-C bond, and between the a-axis and the projection line, respectively.

%	C4 α(°)	C4 θ(°)	C4 I	C4 I(c)	C6 α(°)	C6 θ(°)	C6 I	C6 I(c)	C8 α(°)	C8 θ(°)	C8 I	C8 I(c)	C10 α(°)	C10 θ(°)	C10 I	C10 I(c)	C12 α(°)	C12 θ(°)	C12 I	C12 I(c)
12.5	179	19	5.30	5.01	193	15	7.87	7.60	210	10	10.37	10.21	164	9	12.91	12.76	172	9	15.49	15.31
25.0	173	25	5.28	4.79	172	21	7.81	7.30	210	9	10.37	10.23	137	3	12.85	12.84	150	6	15.33	15.25
	162	29	5.29	4.61	173	10	7.92	7.80	207	11	10.45	10.27	137	3	12.85	12.84	188	3	15.39	15.37
37.5	160	35	5.28	4.31	150	10	7.81	7.70	154	22	10.36	9.58	78	1	12.82	12.81	170	9	15.43	15.24
	167	33	5.28	4.44	184	18	7.84	7.46	161	18	10.43	9.92	114	3	12.88	12.86	130	2	15.32	15.31
	154	31	5.29	4.54	166	9	7.91	7.81	172	15	10.48	10.12	105	4	12.73	12.70	240	6	15.40	15.30
50.0	222	17	5.31	5.06	158	7	7.82	7.75	163	30	10.46	9.10	129	18	12.88	12.26	159	12	15.30	14.94
	187	21	5.32	4.98	131	18	7.60	7.22	163	30	10.46	9.10	129	18	12.87	12.26	166	4	15.27	15.24
	179	34	5.30	4.38	193	16	7.85	7.55	163	30	10.46	9.10	129	18	12.87	12.26	220	5	15.43	15.38
	210	26	5.31	4.77	180	8	7.91	7.84	163	30	10.46	9.10	129	18	12.87	12.26	252	3	15.08	15.06
62.5	164	19	5.20	4.91	168	18	7.73	7.37	158	26	10.20	9.18	133	15	12.90	12.44	164	8	15.26	15.12
	200	25	5.36	4.87	188	12	7.78	7.61	162	36	10.39	8.44	162	11	12.74	12.52	172	6	15.35	15.26
	155	9	5.29	5.22	176	19	7.85	7.43	170	29	10.45	9.18	132	16	12.87	12.37	152	4	15.58	15.54
	207	25	5.35	4.85	173	17	7.94	7.59	168	29	10.46	9.15	134	11	12.92	12.70	219	3	15.45	15.42
	155	9	5.29	5.22	175	8	7.91	7.83	164	36	10.46	8.48	136	12	12.92	12.65	259	2	15.01	15.00
75.0	233	19	5.28	5.01	176	17	7.77	7.41	163	14	10.45	10.13	218	8	12.96	12.83	160	9	15.66	15.46
	117	13	5.30	5.17	215	15	7.80	7.54	180	15	10.29	9.93	131	6	12.94	12.87	147	6	15.06	14.99
	185	19	5.30	5.01	182	19	7.89	7.46	156	20	10.48	9.86	217	8	12.96	12.83	182	6	15.55	15.45
	169	22	5.24	4.88	180	17	7.94	7.60	153	22	10.44	9.69	291	1	12.96	12.96	221	6	15.54	15.46
	130	9	5.36	5.29	174	10	7.92	7.81	161	16	10.45	10.06	194	0	12.92	12.92	144	10	14.91	14.70
	205	20	5.34	5.03	183	26	7.80	6.99	163	14	10.38	10.09	141	6	12.91	12.84	184	9	15.49	15.30
87.5	101	6	5.30	5.27	239	10	7.79	7.67	251	2	10.44	10.43	224	12	12.99	12.68	226	11	15.48	15.22
	151	24	5.31	4.84	220	15	7.91	7.64	199	9	10.46	10.32	100	4	12.84	12.81	102	3	15.33	15.30
	192	12	5.38	5.26	202	11	7.75	7.62	187	2	10.38	10.37	224	12	12.92	12.62	224	11	15.42	15.15
	233	16	5.33	5.13	170	15	7.89	7.63	212	9	10.47	10.35	79	2	12.77	12.76	225	11	15.50	15.23
	183	23	5.39	4.96	227	12	7.96	7.80	191	9	10.47	10.35	103	4	12.82	12.79	90	4	15.37	15.34

	C4				C6				C8				C10				C12			
	183	7	5.29	5.25	236	7	7.94	7.88	198	9	10.49	10.37	117	4	12.81	12.78	77	2	15.29	15.28
	177	22	5.38	5.00	263	12	7.72	7.57	213	3	10.41	10.40	226	12	12.98	12.68	94	4	15.35	15.31
100	247	4	5.36	5.35	234	3	7.93	7.92	230	3	10.42	10.41	226	14	12.98	12.60	226	12	15.49	15.16
	189	13	5.42	5.27	125	6	8.02	7.97	205	9	10.49	10.37	88	4	12.78	12.74	80	4	15.32	15.29
	189	13	5.42	5.27	197	12	7.98	7.80	231	3	10.42	10.41	226	14	12.98	12.60	226	12	15.49	15.16
	189	13	5.42	5.27	196	12	7.93	7.76	230	3	10.42	10.41	226	14	12.97	12.59	226	12	15.49	15.16
	189	13	5.42	5.27	238	14	7.76	7.53	205	9	10.49	10.37	89	4	12.78	12.74	81	4	15.32	15.28
	188	13	5.42	5.27	194	12	8.00	7.82	205	9	10.49	10.37	89	4	12.78	12.74	80	4	15.32	15.29
	248	4	5.36	5.35	174	4	7.97	7.95	205	9	10.49	10.37	89	4	12.78	12.74	81	4	15.32	15.28
	247	4	5.36	5.35	226	2	7.91	7.90	230	3	10.42	10.41	226	14	12.98	12.59	226	12	15.49	15.16

Table DFT-S5.4. Structural properties, i.e. precession (α) and tilt angles (θ), length (l) and thickness l(c) of C4, C6, C8, C10 and C12 alkanethiols on Ge(100).

7.2 List of Publications

7.2.1 Publications Arising Directly from this Thesis

1. **S. Garvey**, J.D. Holmes, Y.S. Kim, and B. Long, *Vapor-Phase Passivation of Chlorine-Terminated Ge(100) using Self-Assembled Monolayers of Hexanethiol.* ACS Applied Materials & Interfaces, **2020**.

2. **S. Garvey**, A. Serino, B. Maccioni, J.D. Holmes, M. Nolan, N. Draeger, E. Gurer, B. Long, *Humidity-Mediated Oxidation of Thiol-SAM Passivated Ge(100).* ACS Applied Materials & Interfaces, **(in review)**.

3. **S. Garvey**, A. Serino, B. Maccioni, J.D. Holmes, M. Nolan, N. Draeger, E. Gurer, B. Long, *Effect of Thiol Chain Length on Oxidation Resistance of Thiol-*

SAM-Passivated Ge(100) Surfaces. ACS Applied Materials & Interfaces, **(in review)**.

7.2.2 Co-authored Publications

1. Curley, R., R.A. Banta, **S. Garvey**, J.D. Holmes, and E.J. Flynn, *Spherical Silica Particle Production by Combined Biomimetic-Stöber Synthesis using Renewable Sodium Caseinate without Petrochemical Agents.* Applied Nanoscience, **2021**.

2. Kennedy, N., **S. Garvey**, B. Maccioni, L. Eaton, M. Nolan, R. Duffy, F. Meaney, M. Kennedy, J.D. Holmes, and B. Long, *Monolayer Doping of Germanium with Arsenic: A New Chemical Route to Achieve Optimal Dopant Activation.* Langmuir, **2020**. **36**(34): p. 9993-10002.

3. McNulty, D., S. Biswas, **S. Garvey**, C. O'Dwyer, and J.D. Holmes, *Directly Grown Germanium Nanowires from Stainless Steel: High-performing Anodes for Li-Ion Batteries.* ACS Applied Energy Materials, **2020**. **3**(12): p. 11811-11819.

4. Kennedy, N., R. Duffy, L. Eaton, D. O'Connell, S. Monaghan, **S. Garvey**, J. Connolly, C. Hatem, J.D. Holmes, and B. Long, *Phosphorus Monolayer Doping (MLD) of Silicon on Insulator (SOI) Substrates.* Beilstein J. Nanotechnol., **2018**. **9**: p. 2106-2113.

5. McNulty, D., H. Geaney, E. Carroll, **S. Garvey**, A. Lonergan, and C. O'Dwyer, *The Effect of Particle Size, Morphology and C-rates on 3D structured Co3O4 Inverse Opal Conversion Mode Anode Materials.* Materials Research Express, **2017**. **4**(2): p. 025011.

7.3 List of Talks & Posters

1. **<u>S. Garvey</u>**, B. Long, J.D. Holmes. '*Vapour-Phase Passivation of Germanium using Aliphatic Thiols for Integration into Silicon-Based Systems*', 2019 EMRS Spring Meeting, Nice, France, 27-31 May, **2019** (**Talk**).

2. **<u>S. Garvey</u>**, B. Long, J.D. Holmes. '*Supercomputers for Super Problems*', 2019 Pint of Science Festival, Cork, Ireland, 21 May, **2019** (**Talk**).

3. **<u>S. Garvey</u>**, B. Long, J.D. Holmes. '*Germanium Passivation Using Thiols*', Lam University Collaboration Showcase, Portland, Oregon, USA, 9 August, **2018** (**Poster**).

7.4 Internships Undertaken

1. April – October 2018 at Lam Research Corp., Fremont, USA.